SELF-CONSISTENT MEAN FIELD THEORY OF THE LAMELLAR MORPHOLOGY OF BINARY COPOLYMER-HOMOPOLYMER BLENDS

Jeffrey David Vavasour

B.Sc. (Hons.), Memorial University of Newfoundland, 1992

A THESIS SUBMITTED IN PARTIAL FULFILLMENT OF

THE REQUIREMENTS FOR THE DEGREE OF

MASTER OF SCIENCE

in

THE FACULTY OF GRADUATE STUDIES

DEPARTMENT OF PHYSICS AND ASTRONOMY

We accept this thesis as conforming

to the required standard

THE UNIVERSITY OF BRITISH COLUMBIA

January 2000

Abstract

The mean field theory of neat copolymers [1] has been extended to consider binary copolymer-homopolymer blends. A set of self-consistent equations was derived describing the most-probable configuration of the system for a given set of parameters. Numerical techniques yielded the density distributions of the copolymer blocks and homopolymer.

The lamellar microphase-separated state of the copolymer-homopolymer blend was probed over a wide range of system parameters. For blends in which the ratio of homopolymer molecular volume to copolymer molecular volume, f_H, was negligible, the system was found to mimic a copolymer-solvent blend, [2] with a reduction in the domain thickness analogous to that seen in the dilution approximation of neutral solvents.

When $f_H \simeq 0.5$, the homopolymer was found to reside preferentially at the centre of the copolymer's subdomain of like-species. This localisation enlarged the subdomain appropriately for the homopolymer volume and, as a by-product, enlarged the total domain thickness of the lamellar unit cell relative to the neat case.

At intermediate f_H, a balance was struck in which the domain thickness was largely unaffected by the addition of homopolymer. Unlike the prior fourth-order Many-Wave Approximation (MWA) result, [3] this effect seemed to manifest after an initial stabilising quantity of homopolymer localised at the interphase. The value of f_H at which the domain thickness was most stable was roughly $4.50(\chi r_C)^{-1.36}$, where χr_C is the product of the Flory parameter and the copolymer molecular volume in appropriate dimensionless units. As expected, the MWA and the current result's weak-segregation limit were in agreement.

Our results suggest that an experimental investigation into homopolymer localisation is warranted.

Table of Contents

List of Tables

List of Figures

List of Symbols

Symbol	*Description*
κ	Subscript representing one of the three species of monomer in the system: copolymer block A ($\kappa = A$), copolymer block B ($\kappa = B$) or homopolymer ($\kappa = H$). The subscript C may also be used to denote the whole copolymer molecule (i.e. blocks A and B combined).
$\chi_{\kappa\kappa'}$	Flory interaction parameter between species κ and species κ'.
$\rho_{0\kappa}$	Monomer density of species κ. $1/\rho_{0\kappa}$ is the volume of the monomer.
ρ_{ref}	Reference density used in the definition of $\chi_{\kappa\kappa'}$. Typically, $\rho_{ref} \equiv \rho_{0H}$.
b_κ	Statistical segment length (i.e. *rms* separation) in a polymer chain of species κ.
ϵ_κ	Conformational asymmetry parameter for species κ with respect to the homopolymer. $\epsilon_\kappa \equiv \rho_{0\kappa} b_\kappa^2 / \rho_{0H} b_H^2$.
r_κ	Volume of the copolymer block (if $\kappa = A$ or B), homopolymer (if $\kappa = H$) or total copolymer (if $\kappa = C$), in units of $1/\rho_{ref}$.
f_κ	Equivalent to the ratio r_κ / r_C.
Z_κ	Degree of polymerisation (i.e. number of monomers in a polymer chain) of a copolymer block or homopolymer.
$\bar{\phi}_\kappa$	Average volume fraction of species κ in the system.
N_κ	Number of copolymer molecules (if $\kappa = C$) or homopolymer molecules (if $\kappa = H$) in the system.
$\mathbf{Z}$	Partition function

$\boldsymbol{r}_\kappa(\cdot)$	A parameterised space curve, representing a polymer as a Gaussian chain.
$P[\boldsymbol{r}_\kappa(\cdot)]$	The probability of a Gaussian chain having configuration $\boldsymbol{r}_\kappa(\cdot)$, known as the Wiener measure.
$\phi_\kappa(\boldsymbol{r})$	Local volume fraction of species κ at $\boldsymbol{r}$.
$\rho_\kappa(\boldsymbol{r})$	Local monomer density of species κ at $\boldsymbol{r}$, equivalent to $\rho_{0\kappa}\phi_\kappa(\boldsymbol{r})$.
$\omega_\kappa(\boldsymbol{r})$	Potential acting on species κ at $\boldsymbol{r}$.
$\eta(\boldsymbol{r})$	Contribution to potential due to the incompressibility condition $\phi_A(\boldsymbol{r}) + \phi_B(\boldsymbol{r}) + \phi_H(\boldsymbol{r}) = 1$.
$Q_\kappa(\boldsymbol{r}, \tau\|\boldsymbol{r}')$	Propagator defining the probability of a monomer in a chain of species κ being at $\boldsymbol{r}$, given that another monomer in the same chain τ steps away is at $\boldsymbol{r}'$.
$q_\kappa(\boldsymbol{r}, \tau)$	Equivalent to $\int \mathrm{d}\boldsymbol{r}'\ Q_\kappa(\boldsymbol{r}, \tau\|\boldsymbol{r}')$.
$q'_A(\boldsymbol{r}, \tau)$	Equivalent to $\int \mathrm{d}\boldsymbol{r}'\mathrm{d}\boldsymbol{r}''\ Q_A(\boldsymbol{r}, \tau\|\boldsymbol{r}')Q_B(\boldsymbol{r}', Z_B\|\boldsymbol{r}'')$.
$q'_B(\boldsymbol{r}, \tau)$	Equivalent to $\int \mathrm{d}\boldsymbol{r}'\mathrm{d}\boldsymbol{r}''\ Q_B(\boldsymbol{r}, \tau\|\boldsymbol{r}')Q_A(\boldsymbol{r}', Z_A\|\boldsymbol{r}'')$.
$q'_H(\boldsymbol{r}, \tau)$	Equivalent to $q_H(\boldsymbol{r}, \tau)$.
Q_C	Equivalent to $\int \mathrm{d}\boldsymbol{r}\ q_A(\boldsymbol{r}, 1)q_B(\boldsymbol{r}, 1)$.
Q_H	Equivalent to $\int \mathrm{d}\boldsymbol{r}\ q_H(\boldsymbol{r}, 1)$.
$\mathcal{F}$	Free energy of the system.
Δf	Free energy density of an equilibrium structure, relative to the homogeneous phase.
f_{mixing}	Free energy density of mixing.
f_{hom}	Free energy density of homogeneous phase.
L	Homopolymer localisation measure.

d_A	Subdomain A thickness – thickness of a single region dominated by species A, bounded on either side by an interphase plane.
d_B	Subdomain B thickness – thickness of a single region dominated by species B, bounded on either side by an interphase plane.
d	Domain thickness – sum of $d_A + d_B$, equivalent to the lattice parameter of the lamellar structure.
R	Equivalent to $d/2$.
$J(x)$	Probability density of copolymer A-B joints at offset x within the half-cell of thickness R.

The following symbols are specific to the fluorescence decay formalism cited in Section 5.1:

$\varphi(z_0, t)$	Survival probability of an excited donor located at z_0 as a function of time t.
$w(r)$	Decay rate of an excited donor as a function of donor-acceptor separation r.
$C_A(z)$	Concentration of acceptors at z.
$C_D(z)$	Concentration of donors at z.
$\bar{C}_A(z)$	Average concentration of acceptors within a sphere of radius R_{max} centred at z.
$\bar{C}_A$	Average concentration of acceptors in the system.
$\bar{C}_D$	Average concentration of donors in the system.
R_0	Förster radius – characteristic scale parameter used in definition of $w(r)$.

$I_D(t)$	Intensity of donor decay as a function of time.
$I_D^0(t)$	Baseline intensity of donor decay in absence of acceptors, as a function of time.
Φ_{ET}	Integrated quantum efficiency of donor-acceptor energy transfer, equivalent to $1 - \int I_D(t)\mathrm{d}t / \int I_D^0(t)\mathrm{d}t$.
$N_A(z)$	Equivalent to $\frac{2}{3}\pi^{\frac{3}{2}} R_0^3 C_A(z)$.

Acknowledgements

I would like to thank my supervisor, Dr. Birger Bergersen, for his willing interest in this project and his enthusiasm for the exploration of the full diversity of condensed matter theory. I would also like to extend special thanks to Dr. Mark Whitmore for providing the initial motivation for this research, as well as his continued support and contribution throughout this project in his role of unofficial co-supervisor.

Thanks to Dr. Mitch Winnik's polymer research group at the University of Toronto for their interest in our theoretical models in relation to their fluorescence decay experiments, and to John Spiro of that group in particular for his considered and exhaustive effort to bridge the gap between experiment and theory.

Thanks also to Dr. Myer Bloom for his helpful counsel on how I should best negotiate my re-entry into academia after four years in industry, thus making this project a reality.

And finally, I would very much like to express my love and gratitude to my family: Eternal thanks to my wife, *Dr.* Irene Vavasour, for her gentle understanding and unwaivering support, even in my delusional moment of inspiration while waiting in line at Earl's. Irene, you have been the joy and sanity in my world from the moment we met. Thanks also to my parents, Robert and Gail, for keeping the faith. And last-but-not-least, thanks and love to our brand new arrival, Zachary Colin Vavasour, for infusing me with the sense of urgency I needed to finish this thing. This one's dedicated to you!

"A straight line may be the shortest
distance between two points, but it
is by no means the most interesting."
– The Doctor, in the *Doctor Who*
episode "The Time Monster"

Chapter 1

Introduction

Polymer dynamics has been a rich source of both experimental and theoretical study within the field of condensed matter physics. This interest is driven by the ubiquitous industrial and commercial applications of polymer materials. As advances in amalgams fulfilled a demand for metals of unique properties, so too do advances in polymers satisfy a demand for specialised synthetic materials.

A polymer itself is termed a *macromolecule*. It is essentially a composite molecule constructed from several repeated *monomer* building blocks, strung together into one or more chains. Complex extended molecular structures can result from polymerisation. The monomers may be connected into a single linear chain (a "linear polymer"), several chains connected to a common hub (a "star polymer") or chains with sporadic forking ("graft polymers").

Typically there can be several hundred to several thousand monomer units in a polymer. The number of monomer units which make up a polymer chain is called the *degree of polymerisation*, which we denote here by the symbol Z. These long chains tend to be fairly flexible at the monomer joints. In absence of interactions, these chains would distribute throughout a system according to a collection of discrete randoms walk of Z steps.

When the monomers that build a chain are all of the same chemical structure or "species", the polymer is termed a *homopolymer*. When one bonds together two or more homopolymers of different species, the result is called a *copolymer*.

In our current investigation, we will be considering two types of polymer molecules: a linear *diblock* copolymer, and a homopolymer. A linear diblock copolymer is a polymer constructed by attaching one end of a linear homopolymer of one species to the end of another linear homopolymer of a distinct species creating a longer but still linear molecule. Symbolically, this is written as an A-b-B copolymer where A and B denote the distinct species. If one species were *polystyrene* (PS) and the other *polyisoprene* (PI), this would then be written PS-b-PI. The portion of the chain which is of species A is referred to as the A block, and likewise the portion of the chain which is of species B is referred to as the B block. Hence, diblock copolymer refers to a copolymer comprised of two blocks of distinct species.

Ensembles of diblock copolymers exhibit some well-known and interesting thermodynamic behaviour. [4] Typically, when one has two distinct species of monomer, there exists a net repulsive interaction between the monomers. That is, their dissimilar molecular properties result in an immisicibility, in analogy to oil and water.

This repulsive interaction is traditionally quantified by the Flory parameter, χ. [5] To first order, this energy is independent of T. However, the free energy of the system is generally expressed as a dimensionless free energy, $\mathcal{F}/k_BT$, and so, to first order, this energy behaves as H/T where H is a constant. Experimentally, χ is found to behave as

$$\chi \simeq K + \frac{H}{T}. \tag{1.1}$$

K is a corrective term which contains entropic effects that are not included in the Flory-Huggins entropy of mixing. The temperature dependence in χ gives experimentalists a way to vary χ dynamically, and thus a way to probe the impact the magnitude of χ has on the system.

So, with a diblock copolymer, one has a molecule in which the monomers in block A will be repulsed by the monomers in block B. The chemical bonds in the polymer

are sufficiently strong that the molecule will not break up and dissociate. However, the flexibility of the molecule is such that the repulsion between A and B blocks will bias the molecule's random walk so as to minimise contact between dissimilar species.

In a system of many copolymer molecules, copolymer molecules will also attempt to orient so as to minimise the contact between their block A and their neighbours' block B, and vice versa. When this tendency is strong enough to overcome natural entropy and diffusion effects in the system, this drive toward alignment induces a spontaneous ordering of the system. Just as free-spinning magnets might orient along a common axis to eliminate contact between like poles, copolymers can align along a common axis to eliminate contact between dissimilar blocks. This ordering is called *microphase separation*. Several ordered structures are possible which minimise exposure of dissimilar blocks to each other. The most common of these are the lamellar, cylindrical, and spherical morphologies.

In the lamellar structure, the copolymers tend to orient so that block A lies to one side of a dividing plane while block B lies to the other. The dividing plane is called the interphase. The chemical joint between block A and block B typically lies roughly within this dividing plane. Symbolically, one might write this as A|B with A indicating a region dominated by species A, B a region dominated by species B, and | the interphase where the A-B joints would reside. In a typical three-dimensional system, this layering would repeat several times in the mirroring pattern A|BB|AA|BB|A....

The space between two consecutive interphase planes is called a subdomain. Each subdomain is either dominated by species A or species B. (N.B. blocks enter the subdomain from both bounding interphase planes.) The perpendicular distance between two interphase planes is called the subdomain thickness. The thickness of species A's subdomain may be different than that of species B, depending on the relative sizes of the A and B blocks in the copolymer as well as other geometric factors. The total domain

thickness is the sum of the A and B subdomain thicknesses.

The cylindrical and spherical morphologies are similar in concept, except that instead of the interphase being a plane, the A-B junction centres on a cylindrical or spherical surface – with block A penetrating inside and block B extending outside, or vice versa. (The smaller block will be the species on the inside of the cylinder or sphere. [1]) As with the lamellar case, in an extended three-dimensional system several such domains will form. In the case of cylinders, they will organise on a hexagonal lattice. In the spherical case, the spherical domains will repeat on a body-centred cubic lattice. [4] Other, more exotic structures are also possible such as the gyroid. [6]

Extensive experimental and theoretical study has been aimed toward quantifying these various morphologies and also determining the circumstances under which they occur. In order to reduce the complexity of the system for the purposes of modelling, early theory made certain assumptions about the distribution of species A and B. In their "narrow-interphase approximation", [7] Helfand and Wasserman considered the situation where the interphase thickness – the transitional region between A-dominance and B-dominance – was negligible. When there is little overlap between block A and block B, this is known as "strong segregation". Experimentally, this is known to occur for large χ and/or degree of polymerisation, Z. From this assumption, they were able to draw conclusions about the strong segregation limit.

Complementary to this was the work of Leibler, [8] who probed the weak segregation regime. The weak segregation regime is accepted to be roughly as

$$10.5 \lesssim \chi Z \lesssim 14, \tag{1.2}$$

where χ is the aforementioned Flory interaction parameter and Z is the total degree of polymerisation of the copolymer molecule. [1] In weak segregation, there is much intermixing between the A and B blocks, and so the variations in species density can

be approximated as *sine* waves. In such a situation, the smooth transition between A subdomain and B subdomain would result in an extended interphase. This model was successful in making key predictions in the weak-segregation limit, such as the fact that ideal copolymers – ones in which the A monomers and B monomers had the same size and step length – would not microphase separate below the lower bound on χZ in Eq. 1.2. However, this first-order approximation had a very limited range of validity, and quickly diverged from expectations above $\chi Z \simeq 14$. [1]

The two extremal approximations were required to reduce the formalism to something manageable at the time of investigation. With the advent of economic high-powered computing, it became possible to obtain numerical solutions from the more complex "self-consistent mean field" formalism where such approximations were absent. The efforts of Whitmore and Noolandi in this direction considered a copolymer system diluted by a neutral solvent (i.e. one that interacted equally with species A and B), and then the limit as solvent density $\rho_S \to 0$ was considered. [2] This formalism was later refined to consider the full spectrum of segregation (i.e. full range of χZ), covering all common morphologies both with and without the presence of solvent. [1, 9, 10]

Further refinement to the self-consistent formalism was achieved by Matsen and Schick, [11] when they disposed of the "unit cell approximation" (UCA) that was still inherent in the formalism of Refs. [1, 2, 9, 10]. In the UCA, the hexagonal and *bcc* lattices were probed using a cylindrical or spherical unit cell rather than the proper Wigner-Seitz unit cell. [12] The UCA had been employed to effect symmetries which would reduce the variations in density to purely radial ones, thus effectively reducing the problem to one dimension. Having the system of equations in 1-D was necessary for realistic efforts at numerical solution in these works. [1]

For the present investigation, we considered a parallel effort in copolymer theory. Namely, we considered systems of binary copolymer-homopolymer blends. Such a blend

consists of taking a system comprised solely of copolymers (a "neat copolymer system") and introducing homopolymers to the system. The homopolymers in our case are also of species A, the same species as block A of the copolymer, but of different length. Since A and B are simply non-specific labels, we are considering a blend of copolymers and homopolymers where the homopolymer is of the same species as one of the copolymer blocks.

Works in copolymer-homopolymer blend formalism have largely been an extension of the work of Leibler. In Banaszak and Whitmore's "Many-Wave Approximation" (MWA), [3] the density distributions are represented as a fundamental *sine* wave plus several integral harmonics, and the free energy is represented by a fourth-order expansion in these fields. Effectively, the MWA considers the Fourier transform of the density distribution, truncated to some finite order. While the inclusion of higher-order terms than that of the Leibler formalism does extend its range of applicability, there is still cause for concern regarding its validity out of the weak segregation regime.

More recent advances such as the work of Matsen consider solutions with a very large number of harmonic terms in the density variations, and without any approximation on free energy. [13] These investigations have thus been far limited in the scope and mainly have considered the phase diagram of competing equilibrium morphologies.

In our present investigation, we have extended the self-consistent mean field formalism of Refs. [1] and [14] to the case of copolymer-homopolymer blends, and have used this formalism to probe blend morphologies and behaviour in both the weak and strong segregation regime. By concentrating exclusively on the lamellar morphology, the shortcomings of the unit-cell approximation used in the early self-consistent efforts were avoided while maintaining a manageable numerical task.

The results of Banaszak and Whitmore's MWA formalism were compared and contrasted with the current effort, and new insight into cell and sub-cell properties was

gained.

Chapter 2 covers the underlying formalism of the blend-extended self-consistent mean field theory. Chapter 3 provides a systematic study of domain and subdomain thickness dependencies on common system parameters. Chapter 4 provides a brief foray into phase behaviour, both in the microphase context and elsewhere. Chapter 5 provides insight into experimentally-discernible inhomogeneities in the distribution of homopolymer within the lamellar unit cell. Finally, in Chapter 6 we summarise the key insights drawn from these various investigations. For reference, the C-based computer program used to implement the formalism from Chapter 2 is included in Appendix A.

Chapter 2

Theory

2.1 Formalism

The goal is to construct a model of a copolymer-homopolymer system from which its thermodynamic properties can be studied. The traditional starting point for describing a thermodynamic system is the construction of a partition function. [15] In a partition function we have to sum over all possible configurations of the system, weighted by the probability of each configuration. In order to describe the configuration of an ensemble of N_C copolymers and N_H homopolymers, we must first construct a mathematical description of a polymer chain.

A polymer chain consists of a number of chemically-bonded, repeating monomer units. The separation between consecutive monomers – the bond length – is generally approximated as a Gaussian distribution. [16] And so, the probability of separation $\boldsymbol{r}$ is given by

$$\psi(\boldsymbol{r}) = [\frac{3}{2\pi b^2}]^{\frac{3}{2}} \exp[-\frac{3|\boldsymbol{r}|^2}{2b^2}], \tag{2.1}$$

where b is a characteristic length parameter called the *statistical segment length*, representing the most-probable separation. There is no bias in the orientation of this bond, and so no angular variation of probability.

By extension, for a chain consisting of Z monomers with each monomer's location given by $\boldsymbol{R}_i$ where $i = \{1, 2, \ldots, Z\}$, the probability of a configuration would be the

product of the probabilities for each individual bond length given by Eq. 2.1

$$\begin{aligned}\Psi(\{\boldsymbol{R}_i\}) &= \prod_{i=1}^{Z-1} \psi(|\boldsymbol{R}_{i+1} - \boldsymbol{R}_i|) \\ &= [\frac{3}{2\pi b^2}]^{3(Z-1)/2} \exp[-\sum_{i=1}^{Z-1} \frac{3|\boldsymbol{R}_{i+1} - \boldsymbol{R}_i|^2}{2b^2}]. \end{aligned} \tag{2.2}$$

Typical polymer chains have a relatively large degree of polymerisation, Z, and so in the typical formalism we replace Eq. 2.2 with its continuous equivalent [17]

$$P[\boldsymbol{r}(\cdot)] \propto \exp[-\frac{3}{2b^2}\int_0^Z \mathrm{d}\tau\ \dot{\boldsymbol{r}}^2(\tau)], \tag{2.3}$$

where the polymer chain is represented by an arbitrary space-curve, $\boldsymbol{r}(\tau)$, parameterised by the monomer position along the chain, τ. Here we have defined $\dot{\boldsymbol{r}}(\tau)$ as $\mathrm{d}\boldsymbol{r}/\mathrm{d}\tau$. The standard notation, $\boldsymbol{r}(\cdot)$, expresses the fact that $P[\boldsymbol{r}(\cdot)]$ is a functional evaluating the probability of the entire space-curve's configuration, rather than just the probability of one point along the curve, e.g., being at some specific $\boldsymbol{r}(\tau)$. Eq. 2.3 is known as the Wiener measure.

With the probability for a given configuration of a polymer chain known, we can now construct our partition function. For a copolymer-homopolymer blend, we want all configurations of N_C copolymers and N_H homopolymers weighted by their probability. A copolymer is the concatenation of two polymer chains or "blocks" of dissimilar physical characteristics. As such, it should be represented by two separate polymer chains, each with a probability given by Eq. 2.3, but with different Z and b. These two blocks will be designated block A and block B. Only configurations where block A and block B are joined should be considered, so the partition function will be restricted to include only those cases.

An additional restriction on configurations is the incompressibility condition. Monomers occupy fixed volumes and so the partition function must exclude configurations where monomers overlap or where vacuum is left in the system.

Finally, in addition to being weighted by the probabilities given by the Wiener measure, each polymer chain is subject to net interactions with other chains. This results in it being less probable that two dissimilar species be close together than far apart. And so this interaction potential must be introduced as a Boltzmann factor for the configuration.

Combining all of these contributions, we have a partition function of the form

$$\begin{aligned}
\mathbf{Z} \;=\; & \frac{\mathcal{Z}_H^{N_C}}{N_C!}\frac{\mathcal{Z}_H^{N_H}}{N_H!} \times \\
& \int \prod_{i=1}^{N_C}\prod_{j=1}^{N_H} \delta\boldsymbol{r}_{Ai}(\cdot)\delta\boldsymbol{r}_{Bi}(\cdot)\delta\boldsymbol{r}_{Hj}(\cdot) \times \\
& P_A[\boldsymbol{r}_{Ai}(\cdot)]P_B[\boldsymbol{r}_{Bi}(\cdot)]P_H[\boldsymbol{r}_{Hj}(\cdot)] \times \\
& \delta[\boldsymbol{r}_{Ai}(Z_A) - \boldsymbol{r}_{Bi}(Z_B)] \times \\
& \delta[[1 - \frac{\hat{\rho}_A(\cdot)}{\rho_{0A}} - \frac{\hat{\rho}_B(\cdot)}{\rho_{0B}} - \frac{\hat{\rho}_H(\cdot)}{\rho_{0H}}] \times \\
& \exp[-\hat{V}(\cdot)/k_BT]. \qquad (2.4)
\end{aligned}$$

The $\mathcal{Z}_C$ and $\mathcal{Z}_H$ terms are the kinetic contributions to the partition function. The integral is a functional integral evaluated over all continuous space curves $\boldsymbol{r}_{Ai}(\cdot)$ and $\boldsymbol{r}_{Bi}(\cdot)$ representing blocks A and B of each of the N_C copolymer molecules, and over all space curves $\boldsymbol{r}_{Hj}(\cdot)$ representing each of the N_H homopolymer molecules. The third line of Eq. 2.4 provides the Wiener measure weighting for the probability of each polymer chain's configuration. The fourth line is a second delta functional that restricts the functional integral to only those configurations where $\boldsymbol{r}_{Ai}(\cdot)$ and $\boldsymbol{r}_{Bi}(\cdot)$ meet end-to-end, creating a copolymer molecule. The fifth line is a delta functional representing the incompressibility of the system. Here, $\hat{\rho}_\kappa(\boldsymbol{r})$ represents the total number density of monomers of type κ =A, B, or H passing through $\boldsymbol{r}$. The constant $\rho_{0\kappa}$ is the bulk monomer density for that type. That is, $1/\rho_{0\kappa}$ would be the exclusion volume of a single monomer of species κ. The final line is a Boltzmann distribution weighing the configuration by a factor due to interactions among all components of the system.

The goal is to transform this partition function into a functional integration over all configurations weighted only by a free energy. The mathematic procedure to accomplish this is quite involved, however. The process ultimately leads to the self-consistent field (SCF) equations utilised in Section 2.4. What follows in the remainder of this section and Section 2.2 is a rigourous derivation of the SCF equations. For those wishing to consider only the final form of the equations defining the system, one may skip to Section 2.3.

The first stage in this derivation requires eliminating all delta functionals from the partition function and collecting all probabilities into a single $\exp[-\mathcal{F}]$ free energy term. To do this, we first define $\hat{\rho}_\kappa(\boldsymbol{r})$. The monomer density $\hat{\rho}_\kappa(\boldsymbol{r})$ is a count of the number of monomers of species κ which pass through $\boldsymbol{r}$. This may be obtained by enumerating the number of space curves $\boldsymbol{r}_{\kappa i}(\tau)$ passing through $\boldsymbol{r}$, via

$$\hat{\rho}_\kappa(\boldsymbol{r}) \;=\; \sum_{i=1}^{N_\kappa} \int_0^{Z_\kappa} \mathrm{d}\tau \; \delta[\boldsymbol{r} - \boldsymbol{r}_{\kappa i}(\tau)]. \tag{2.5}$$

The monomer density $\hat{\rho}_\kappa(\boldsymbol{r})$ is effectively a piecewise definition of a continuous function, $\rho_\kappa(\boldsymbol{r})$. We can replace occurrences of $\hat{\rho}_\kappa(\boldsymbol{r})$ in Eq. 2.4 with its continuous equivalent by invoking the identity

$$\begin{aligned} \delta[1 - \frac{\hat{\rho}_A(\cdot)}{\rho_{0A}} - \frac{\hat{\rho}_B(\cdot)}{\rho_{0B}} - \frac{\hat{\rho}_H(\cdot)}{\rho_{0H}}] e^{-\hat{V}[\{\hat{\rho}_\kappa(\cdot)\}]/k_B T} \;=\; & \int \prod_\kappa \delta\rho_\kappa(\cdot) \; \delta[\rho_\kappa(\cdot) - \hat{\rho}_\kappa(\cdot)] \times \\ & \delta[1 - \frac{\rho_A(\cdot)}{\rho_{0A}} - \frac{\rho_B(\cdot)}{\rho_{0B}} - \frac{\rho_H(\cdot)}{\rho_{0H}}] \times \\ & e^{-V[\{\rho_\kappa(\cdot)\}]/k_B T}. \end{aligned} \tag{2.6}$$

Like the delta function, the delta functionals in Eq. 2.6 may be expressed as a functional integral of the form

$$\delta[\rho_\kappa(\cdot) - \hat{\rho}_\kappa(\cdot)] \;\propto\; \int \delta\omega_\kappa(\cdot) \exp\Big\{ \int \mathrm{d}\boldsymbol{r} \; \omega_\kappa(\boldsymbol{r})[\rho_\kappa(\boldsymbol{r}) - \hat{\rho}_\kappa(\boldsymbol{r})] \Big\}, \tag{2.7}$$

and

$$\delta[1 - \frac{\rho_A(\cdot)}{\rho_{0A}} - \frac{\rho_B(\cdot)}{\rho_{0B}} - \frac{\rho_H(\cdot)}{\rho_{0H}}] \;\propto\; \int \delta\eta(\cdot) \exp\Big\{ \int \mathrm{d}\boldsymbol{r} \; \eta(\boldsymbol{r}) \times$$

$$[1 - \frac{\rho_A(\boldsymbol{r})}{\rho_{0A}} - \frac{\rho_B(\boldsymbol{r})}{\rho_{0B}} - \frac{\rho_H(\boldsymbol{r})}{\rho_{0H}}]\Big\}, \quad (2.8)$$

where the bounds on integration of $\omega_\kappa(\boldsymbol{r})$ and $\eta(\boldsymbol{r})$ are $\pm i\infty$. Though $\omega_\kappa(\boldsymbol{r})$ and $\eta(\boldsymbol{r})$ appear here as dummy integrations, they do take on a physical significance which will become apparent later.

Substituting these identities into the partition function, it becomes

$$\begin{aligned}
\mathbf{Z} \;\propto\; & \frac{\mathcal{Z}_H^{N_C}}{N_C!}\frac{\mathcal{Z}_H^{N_H}}{N_H!} \times \\
& \int \prod_\kappa \delta\rho_\kappa(\cdot)\delta\omega_\kappa(\cdot)\delta\eta(\cdot) \times \\
& \exp\Big\{ \int \mathrm{d}\boldsymbol{r}\ \eta(\boldsymbol{r})[1 - \frac{\rho_A(\boldsymbol{r})}{\rho_{0A}} - \frac{\rho_B(\boldsymbol{r})}{\rho_{0B}} - \frac{\rho_H(\boldsymbol{r})}{\rho_{0H}}]\Big\} \times \\
& \exp\Big\{ \int \mathrm{d}\boldsymbol{r}\ [\omega_A(\boldsymbol{r})\rho_A(\boldsymbol{r}) + \omega_B(\boldsymbol{r})\rho_B(\boldsymbol{r}) + \omega_H(\boldsymbol{r})\rho_H(\boldsymbol{r})]\Big\} \times \\
& Q_C^{N_C} Q_H^{N_H} \exp[-V[\{\rho_\kappa(\cdot)\}]/k_B T], \qquad (2.9)
\end{aligned}$$

where

$$\begin{aligned}
Q_C^{N_C} \;=\; & \int \prod_{i=1}^{N_C} \delta\boldsymbol{r}_{Ai}(\cdot)\delta\boldsymbol{r}_{Bi}(\cdot) P_A[\boldsymbol{r}_{Ai}(\cdot)] P_B[\boldsymbol{r}_{Bi}(\cdot)] \delta[r_{Ai}(Z_A) - r_{Bi}(Z_B)] \times \\
& \exp\Big\{ - \int \mathrm{d}\boldsymbol{r}\ [\omega_A(\boldsymbol{r})\hat{\rho}_A(\boldsymbol{r}) + \omega_B(\boldsymbol{r})\hat{\rho}_B(\boldsymbol{r})]\Big\}, \qquad (2.10)
\end{aligned}$$

and

$$Q_H^{N_H} \;=\; \int \prod_{i=1}^{N_H} \delta\boldsymbol{r}_{Hi}(\cdot) P_H[\boldsymbol{r}_{Hi}(\cdot)] \exp[- \int \mathrm{d}\boldsymbol{r}\ \omega_H(\boldsymbol{r})\hat{\rho}_H(\boldsymbol{r})]. \qquad (2.11)$$

Substituting Eq. 2.5 into Eq. 2.10 and 2.11 we find that they can be reduced to

$$\begin{aligned}
Q_C \;=\; & \int \delta\boldsymbol{r}_A(\cdot)\delta\boldsymbol{r}_B(\cdot) P_A[\boldsymbol{r}_A(\cdot)] P_B[\boldsymbol{r}_B(\cdot)] \delta[r_A(Z_A) - r_B(Z_B)] \times \\
& \exp\Big\{ - \int_0^{Z_A} \mathrm{d}\tau\ \omega_A[\boldsymbol{r}_A(\tau)] - \int_0^{Z_B} \mathrm{d}\tau\ \omega_B[\boldsymbol{r}_B(\tau)]\Big\}, \qquad (2.12)
\end{aligned}$$

and

$$Q_H \;=\; \int \delta\boldsymbol{r}_H(\cdot) P_H[\boldsymbol{r}_A(\cdot)] \exp\Big\{ - \int_0^{Z_H} \mathrm{d}\tau\ \omega_H[\boldsymbol{r}_H(\tau)]\Big\}. \qquad (2.13)$$

Q_C and Q_H now contain all the discrete structure of the polymers, with the partition function in Eq. 2.9 now being evaluated over all possible density distributions rather than all possible configurations of N_C discrete copolymers and N_H discrete homopolymers.

Using traditional notation, Q_C and Q_H can be expressed in terms of a "propagator" function, [17] defined for each species κ as

$$\begin{aligned} Q_\kappa(\boldsymbol{R},\tau|\boldsymbol{R}') &= \int \delta\boldsymbol{r}_\kappa(\cdot)\ \delta[\boldsymbol{r}_\kappa(\tau)-\boldsymbol{R}]\delta[\boldsymbol{r}_\kappa(0)-\boldsymbol{R}'] \times \\ &\qquad \exp\Big\{-\int_0^\tau \mathrm{d}\tau'\ \Big\{\frac{3}{2b_\kappa^2}\dot{\boldsymbol{r}}^2(\tau')+\omega_\kappa[\boldsymbol{r}_\kappa(\tau')]\Big\}\Big\}. \end{aligned} \tag{2.14}$$

Conceptually, the propagator $Q_\kappa(\boldsymbol{R},\tau|\boldsymbol{R}')$ is an integration over all configurations of a block's space-curve which originate at $\boldsymbol{r}(0)=\boldsymbol{R}'$ and terminate at $\boldsymbol{r}(\tau)=\boldsymbol{R}$. The integrand is weighted by the probability of each configuration. The propagator may be interpreted as being proportional to the probability that a block starting at $\boldsymbol{R}'$ will arrive at $\boldsymbol{R}$ after τ monomer steps. Both mathematically and conceptually, then, it follows that Eq. 2.14 satisfies

$$Q_\kappa(\boldsymbol{R},\tau|\boldsymbol{R}') = Q_\kappa(\boldsymbol{R}',\tau|\boldsymbol{R}). \tag{2.15}$$

Furthermore, it can be shown that $Q_\kappa(\boldsymbol{R},\tau|\boldsymbol{R}')$ satisfies the diffusion equation, [17]

$$\Big[\frac{b_\kappa^2}{6}\nabla^2-\omega_\kappa(\boldsymbol{r})\Big]Q_\kappa(\boldsymbol{r},\tau|\boldsymbol{r}') = \frac{\partial}{\partial\tau}Q_\kappa(\boldsymbol{r},\tau|\boldsymbol{r}'), \tag{2.16}$$

with the initial condition,

$$Q_\kappa(\boldsymbol{r},0|\boldsymbol{r}') = \delta(\boldsymbol{r}-\boldsymbol{r}'). \tag{2.17}$$

Since our polymer chains are represented by the continuous limit of a random walk, it is natural that we should find that the propagation is subject to the diffusion process. And so, Eqs. 2.16 and 2.17 could be accepted intuitively. Note that in 2.16 the $\omega_\kappa(\boldsymbol{r})$'s are playing the role of a potential, biasing the random walk. It will be shown that $\omega_\kappa(\boldsymbol{r})$ is related to the interaction potential, V, from Eq. 2.4.

Using the definition in Eq. 2.14, Eqs. 2.12 and 2.13 can be restated as

$$\begin{aligned} Q_C &= \int \mathrm{d}\boldsymbol{R}_1\mathrm{d}\boldsymbol{R}_2\mathrm{d}\boldsymbol{R}_3\mathrm{d}\boldsymbol{R}_4 \times \\ &\quad Q_A(\boldsymbol{R}_2, Z_A|\boldsymbol{R}_1)\delta(\boldsymbol{R}_2 - \boldsymbol{R}_4)Q_B(\boldsymbol{R}_4, Z_B|\boldsymbol{R}_3) \\ &= \int \mathrm{d}\boldsymbol{R}_1\mathrm{d}\boldsymbol{R}_2\mathrm{d}\boldsymbol{R}_3 \; Q_A(\boldsymbol{R}_2, Z_A|\boldsymbol{R}_1)Q_B(\boldsymbol{R}_2, Z_B|\boldsymbol{R}_3), \end{aligned} \tag{2.18}$$

and

$$Q_H = \int \mathrm{d}\boldsymbol{R}_1\mathrm{d}\boldsymbol{R}_2 \; Q_H(\boldsymbol{R}_2, Z_H|\boldsymbol{R}_1). \tag{2.19}$$

We now have that Q_C and Q_H can be obtained exclusively from the potentials $\omega_\kappa(\boldsymbol{r})$ and so we are ready to state the partition function as

$$\mathbf{Z} \propto \int \prod_\kappa \delta\rho_\kappa(\cdot)\delta\omega_\kappa(\cdot)\delta\eta(\cdot) \exp\Big\{ - \mathcal{F}[\{\rho_\kappa(\cdot)\}, \{\omega_\kappa(\cdot)\}, \eta(\cdot)]\Big\}, \tag{2.20}$$

where

$$\begin{aligned} \mathcal{F}[\{\rho_\kappa(\cdot)\}, \{\omega_\kappa(\cdot)\}, \eta(\cdot)] &= -N_C \ln \mathcal{Z}_C + \ln N_C! - N_C \ln Q_C - \\ &\quad -N_H \ln \mathcal{Z}_H + \ln N_H! - N_H \ln Q_H - \\ &\quad \int \mathrm{d}\boldsymbol{r} \; \eta(\boldsymbol{r})[1 - \frac{\rho_A(\boldsymbol{r})}{\rho_{0A}} - \frac{\rho_B(\boldsymbol{r})}{\rho_{0B}} - \frac{\rho_H(\boldsymbol{r})}{\rho_{0H}}] - \\ &\quad \int \mathrm{d}\boldsymbol{r} \; [\omega_A(\boldsymbol{r})\rho_A(\boldsymbol{r}) + \omega_B(\boldsymbol{r})\rho_B(\boldsymbol{r}) + \omega_H(\boldsymbol{r})\rho_H(\boldsymbol{r})] + \\ &\quad V[\{\rho_\kappa(\cdot)]/k_BT. \end{aligned} \tag{2.21}$$

Applying Stirling's approximation [15] to $\ln N_\kappa!$ for a large numbers of copolymers, and combining all of the logarithmic terms, this becomes

$$\begin{aligned} \mathcal{F}[\{\rho_\kappa(\cdot)\}, \{\omega_\kappa(\cdot)\}, \eta(\cdot)] &= N_C(\ln \frac{N_C}{\mathcal{Z}_C Q_C} - 1) + N_H(\ln \frac{N_H}{\mathcal{Z}_H Q_H} - 1) - \\ &\quad \int \mathrm{d}\boldsymbol{r} \; \eta(\boldsymbol{r})[1 - \frac{\rho_A(\boldsymbol{r})}{\rho_{0A}} - \frac{\rho_B(\boldsymbol{r})}{\rho_{0B}} - \frac{\rho_H(\boldsymbol{r})}{\rho_{0H}}] - \\ &\quad \int \mathrm{d}\boldsymbol{r} \; [\omega_A(\boldsymbol{r})\rho_A(\boldsymbol{r}) + \omega_B(\boldsymbol{r})\rho_B(\boldsymbol{r}) + \omega_H(\boldsymbol{r})\rho_H(\boldsymbol{r})] + \\ &\quad V[\{\rho_\kappa(\cdot)\}]/k_BT. \end{aligned} \tag{2.22}$$

We now have the partition function in the desired form, with a configuration's probability given by a single Boltzmann-weighted probability which depends on the configuration of the fields $\rho_\kappa(\boldsymbol{r})$, $\omega_\kappa(\boldsymbol{r})$, and $\eta(\boldsymbol{r})$.

2.2 The Mean Field Approximation

To find the most probable density distributions $\rho_\kappa(\boldsymbol{r})$ for a system, one would employ the saddle-function approximation. The minimum value of $\mathcal{F}$ would correspond to the most probable configuration according to the $\exp[-\mathcal{F}]$ weighting in Eq. 2.20. To find this minimum, we employ the functional equivalent to Lagrange multipliers, where we have

$$\int \mathrm{d}\boldsymbol{r}\ \rho_\kappa(\boldsymbol{r}) = N_\kappa, \tag{2.23}$$

with $N_A \equiv N_B \equiv N_C$. (i.e. The number of A blocks and number of B blocks in the system are each equal to the number of copolymers, since there is one A block and one B block per copolymer.) Eq. 2.23 represents a conservation of number.

The functional Lagrange multiplier method identifies the minimum of $\mathcal{F}$ from Eq. 2.22 with respect to some field configuration $\xi(\boldsymbol{r})$ as

$$\frac{\delta\mathcal{F}}{\delta\xi(\boldsymbol{r})} = \lambda_A\frac{\delta\mathcal{C}_A}{\delta\xi(\boldsymbol{r})} + \lambda_B\frac{\delta\mathcal{C}_B}{\delta\xi(\boldsymbol{r})} + \lambda_H\frac{\delta\mathcal{C}_H}{\delta\xi(\boldsymbol{r})}, \tag{2.24}$$

where $\mathcal{C}_\kappa$ is the constraint surface given by Eq. 2.23. Evaluating Eq. 2.24 with respect to the configurations of the fields $\rho_\kappa(\boldsymbol{r})$, $\omega_\kappa(\boldsymbol{r})$, and $\eta(\boldsymbol{r})$ produces the relations

$$\frac{\eta(\boldsymbol{r})}{\rho_{0\kappa}} - \omega_\kappa(\boldsymbol{r}) + \frac{\delta}{\delta\rho_\kappa(\boldsymbol{r})}V[\{\rho_\kappa(\cdot)\}]/k_BT = \lambda_\kappa, \tag{2.25}$$

$$-\rho_\kappa(\boldsymbol{r}) - \frac{N_\kappa}{Q_\kappa}\frac{\delta Q_\kappa}{\delta\omega_\kappa(\boldsymbol{r})} = 0, \tag{2.26}$$

$$1 - \frac{\rho_A(\boldsymbol{r})}{\rho_{0A}} - \frac{\rho_B(\boldsymbol{r})}{\rho_{0B}} - \frac{\rho_H(\boldsymbol{r})}{\rho_{0H}} = 0, \tag{2.27}$$

where $Q_A \equiv Q_B \equiv Q_C$. As promised, these equations give solutions for the most probable configurations of the fields.

Of course, to consider the *mean field* solution of $\rho_\kappa(\boldsymbol{r})$ one should evaluate

$$\begin{aligned} <\hat{\rho}_\kappa(\boldsymbol{r})> \ = \ & \int\prod_{\kappa'}\delta\rho_{\kappa'}(\cdot)\delta\omega_{\kappa'}(\cdot)\delta\eta(\cdot)\ \rho_\kappa(\boldsymbol{r})\times \\ & \exp\Big\{-\mathcal{F}[\{\rho_{\kappa'}(\cdot)\},\{\omega_{\kappa'}(\cdot)\},\eta(\cdot)]\Big\}. \end{aligned} \tag{2.28}$$

To the extent that $\mathcal{F}$ is sharply peaked about the most probable configuration, we will have $< \hat{\rho}_\kappa(\boldsymbol{r}) >$ equal to the most probable configuration of $\rho_\kappa(\boldsymbol{r})$. This is the mean field approximation.

To the extent that mean field approximation is valid, we would also have that Eq. 2.20 reduces to

$$\mathbf{Z} \quad \propto \quad \exp -\mathcal{F}. \tag{2.29}$$

And so, in the mean field approximation, $\mathcal{F}$ represents the free energy of the system.

A chief source of ambiguity remains in the definition of the potential $V[\{\rho_\kappa(\cdot)\}]$. As it happens, a very simple relation is sufficient to provide a meaningful definition of $V[\{\rho_\kappa(\cdot)\}]$. Many preceding studies [2, 9, 18] have found that long-range repulsive interactions between monomers have a negligible effect on the system. Thus, for a monomer of species κ at $\boldsymbol{r}$ it suffices to consider only point-wise interactions. In these terms, a valid form for the interaction potential $V[\{\rho_\kappa(\cdot)\}]$ would be

$$V[\{\rho_\kappa(\cdot)\}]/k_BT \quad = \quad \sum_{\kappa\kappa'} \int \mathrm{d}\boldsymbol{r} \ \rho_\kappa(\boldsymbol{r}) W_{\kappa\kappa'} \rho_{\kappa'}(\boldsymbol{r}), \tag{2.30}$$

where $W_{\kappa\kappa'}$ represents the strength of the repulsive interaction between species κ and κ'. The sum notation over κ and κ' here represent the six *unique* combinations of two species chosen from A, B, or H.

It is useful to define coefficients

$$U_{\kappa\kappa'} = W_{\kappa\kappa'} - \tfrac{1}{2}\frac{\rho_{0\kappa}}{\rho_{0\kappa'}} W_{\kappa\kappa'} - \tfrac{1}{2}\frac{\rho_{0\kappa'}}{\rho_{0\kappa}} W_{\kappa'\kappa'}. \tag{2.31}$$

For like monomers, where $\kappa = \kappa'$, this relation reduces to

$$U_{\kappa\kappa} = 0. \tag{2.32}$$

Substituting Eq. 2.31 into Eq. 2.30 and taking advantage of the relations in Eqs. 2.23

and 2.27 yields

$$V[\{\rho_\kappa(\cdot)\}]/k_BT \;=\; \sum_{\kappa\kappa'}\int \mathrm{d}\boldsymbol{r}\;\rho_\kappa(\boldsymbol{r})U_{\kappa\kappa'}\rho_{\kappa'}(\boldsymbol{r}) + \sum_\kappa \rho_{0\kappa}N_\kappa W_{\kappa\kappa}. \tag{2.33}$$

The final sum term is an additive constant to the free energy which may be neglected as it will not affect the minimum in $\mathcal{F}$. It represents the contribution to the free energy from a species interacting with itself.

By convention, the $U_{\kappa\kappa'}$ coefficient is expressed in terms of the Flory interaction parameter, $\chi_{\kappa\kappa'}$, defined as [19]

$$\chi_{\kappa\kappa'} \;\equiv\; \frac{\rho_{0\kappa}\rho_{0\kappa'}}{\rho_{ref}}U_{\kappa\kappa'}. \tag{2.34}$$

As can be seen, the Flory interaction parameter is defined with respect to a reference number density, ρ_{ref}. Furthermore, $\chi_{\kappa\kappa}$, the Flory parameter for the interaction between species κ and itself, is 0.

Applying the definitions in Eqs. 2.33 and 2.34 to Eq. 2.25, we obtain an explicit expression for the potentials $\omega_\kappa(\boldsymbol{r})$,

$$\omega_\kappa(\boldsymbol{r}) \;=\; \frac{\rho_{ref}}{\rho_{0\kappa}}\Big\{\sum_{\kappa'\neq\kappa}\frac{\chi_{\kappa\kappa'}}{\rho_{0\kappa'}}\rho_\kappa(\boldsymbol{r}) + \frac{\eta(\boldsymbol{r})}{\rho_{ref}}\Big\} - \lambda_\kappa. \tag{2.35}$$

It remains to obtain the density distributions from Eq. 2.26. We calculate these in terms of the normalised local volume fractions,

$$\phi_\kappa(\boldsymbol{r}) \;\equiv\; \frac{\rho_\kappa(\boldsymbol{r})}{\rho_{0\kappa}}, \tag{2.36}$$

which leads to the incompressibility condition Eq. 2.27 restated as

$$\phi_A(\boldsymbol{r}) + \phi_B(\boldsymbol{r}) + \phi_H(\boldsymbol{r}) \;=\; 1. \tag{2.37}$$

In order to evaluate Eq. 2.26, we need to know how to evaluate the functional derivative $\delta Q_\kappa/\delta\omega_\kappa(\boldsymbol{r})$. Using the relation

$$\omega_\kappa[\boldsymbol{r}_\kappa(\tau')] \;=\; \int \mathrm{d}\boldsymbol{r}\;\omega_\kappa(\boldsymbol{r})\delta[\boldsymbol{r}_\kappa(\tau') - \boldsymbol{r}], \tag{2.38}$$

we find that

$$\frac{\delta}{\delta\omega_\kappa(\boldsymbol{r})}\omega_\kappa[\boldsymbol{r}_\kappa(\tau')] \;\; = \delta[\boldsymbol{r}_\kappa(\tau') - \boldsymbol{r}]. \tag{2.39}$$

Using the functional equivalent of the chain rule, we can use Eq. 2.39 to evaluate the functional derivative of Eq. 2.14, yielding

$$\begin{aligned}\frac{\delta Q_\kappa}{\delta\omega_\kappa(\boldsymbol{r})} &= -\int_0^{Z_\kappa} \mathrm{d}\tau \int \delta\boldsymbol{r}_\kappa(\cdot)\delta[\boldsymbol{r}_\kappa(\tau) - \boldsymbol{r}]\delta[\boldsymbol{R}_1 - \boldsymbol{r}_\kappa(0)]\delta[\boldsymbol{R}_2 - \boldsymbol{r}_\kappa(Z_\kappa)] \times \\ &\qquad \exp\Big\{ -\int_0^{Z_\kappa} \mathrm{d}\tau' \, \Big\{ \frac{3}{2b_\kappa^2}\dot{\boldsymbol{r}}_\kappa^2(\tau') + \omega_\kappa[\boldsymbol{r}_\kappa(\tau')] \Big\} \Big\}. \\ &= -\int_0^{Z_\kappa} \mathrm{d}\tau \; Q_\kappa(\boldsymbol{r}, \tau|\boldsymbol{R}) Q_\kappa(\boldsymbol{r}, Z_\kappa - \tau|\boldsymbol{R}'). \end{aligned} \tag{2.40}$$

Evaluating Eq. 2.26 requires the evaluation of the functional derivatives of Q_C and Q_H which, by Eqs. 2.18 and 2.19, can be expressed in terms of the functional derivatives of $Q_\kappa(\boldsymbol{R}, \tau|\boldsymbol{R}')$. Thus, by use of Eqs. 2.26 and 2.36 we have

$$\phi_H(\boldsymbol{r}) \;\; \propto \;\; \int_0^{Z_H} \mathrm{d}\tau \;\; \int \mathrm{d}\boldsymbol{R}\mathrm{d}\boldsymbol{R}' \; Q_H(\boldsymbol{r}, \tau|\boldsymbol{R}) Q_H(\boldsymbol{r}, Z_H - \tau|\boldsymbol{R}'). \tag{2.41}$$

By requiring that

$$\frac{1}{\Omega}\int \mathrm{d}\boldsymbol{r} \; \phi_H(\boldsymbol{r}) \;\; = \;\; \overline{\phi}_H, \tag{2.42}$$

where Ω is the system volume, we have a prefactor on Eq. 2.41 of $\overline{\phi}_H\Omega/Z_H Q_H$.

We can obtain an expression for $\overline{\phi}_H$ by recalling that $1/\rho_{0H}$ is the volume of a monomer. Thus the homopolymer has volume Z_H/ρ_{0H}, and N_H homopolymers would occupy a volume $N_H Z_H/\rho_{0H}$. This is a volume fraction $N_H Z_H/\rho_{0H}\Omega$ of the system volume Ω. The quantity $\overline{\phi}_H$ represents the system-averaged volume fraction of homopolymer, and so these two quantities should be equal. This relation also holds for the two copolymer blocks and so we have, in general,

$$\bar{\phi}_\kappa \;\; = \;\; \frac{N_\kappa Z_\kappa}{\rho_{0\kappa}\Omega}. \tag{2.43}$$

Going through a parallel process to that which derived Eq. 2.41 for the homopolymer, we find for the copolymer blocks A and B that

$$\phi_\kappa(\boldsymbol{r}) = \frac{\bar{\phi}_\kappa}{Z_\kappa}\frac{\Omega}{Q_C}\int_0^{Z_\kappa} \mathrm{d}\tau \int \mathrm{d}\boldsymbol{R}\mathrm{d}\boldsymbol{R}'\mathrm{d}\boldsymbol{R}''\; Q_\kappa(\boldsymbol{r},\tau|\boldsymbol{R}) \times Q_\kappa(\boldsymbol{r}, Z_\kappa-\tau|\boldsymbol{R}')Q_{\kappa'}(\boldsymbol{R}', Z_{\kappa'}|\boldsymbol{R}''), \tag{2.44}$$

where, here, κ =A or B and κ' is the opposite block of the copolymer, B or A respectively.

One last step of simplification remains in the expressions of $\phi_\kappa(\boldsymbol{r})$ which will aid in the numerical solution of these equations. We note that $\phi_\kappa(\boldsymbol{r})$ can be re-expressed as

$$\phi_\kappa(\boldsymbol{r}) = \frac{\bar{\phi}_\kappa}{Z_\kappa}\frac{\Omega}{Q_\kappa}\int_0^{Z_\kappa} \mathrm{d}\tau\; q_\kappa(\boldsymbol{r},\tau)q'_\kappa(\boldsymbol{r}, Z_\kappa-\tau), \tag{2.45}$$

where

$$q_\kappa(\boldsymbol{r},\tau) = \int \mathrm{d}\boldsymbol{r}'\; Q_\kappa(\boldsymbol{r},\tau|\boldsymbol{r}'), \tag{2.46}$$

$$q'_\kappa(\boldsymbol{r},\tau) = \begin{cases} \int \mathrm{d}\boldsymbol{r}'\mathrm{d}\boldsymbol{r}''\; Q_A(\boldsymbol{r},\tau|\boldsymbol{r}')Q_B(\boldsymbol{r}', Z_B|\boldsymbol{r}'') & \text{if } \kappa = \text{A} \\ \int \mathrm{d}\boldsymbol{r}'\mathrm{d}\boldsymbol{r}''\; Q_B(\boldsymbol{r},\tau|\boldsymbol{r}')Q_A(\boldsymbol{r}', Z_A|\boldsymbol{r}'') & \text{if } \kappa = \text{B} \\ \int \mathrm{d}\boldsymbol{r}'\; Q_H(\boldsymbol{r},\tau|\boldsymbol{r}') & \text{if } \kappa = \text{H} \end{cases} \tag{2.47}$$

These functions $q_\kappa(\boldsymbol{r},\tau)$ and $q'_\kappa(\boldsymbol{r},\tau)$ also satisfy the diffusion equation, Eq. 2.16, except with the initial conditions

$$q_\kappa(\boldsymbol{r},0) = 1, \tag{2.48}$$

$$q'_\kappa(\boldsymbol{r},0) = \begin{cases} q_B(\boldsymbol{r}, Z_B) & \text{if } \kappa = \text{A} \\ q_A(\boldsymbol{r}, Z_A) & \text{if } \kappa = \text{B} \\ 1 & \text{if } \kappa = \text{H} \end{cases} \tag{2.49}$$

In terms of these new functions, Q_C and Q_H are

$$Q_C = \int \mathrm{d}\boldsymbol{r}\; q_A(\boldsymbol{r}, Z_A)q_B(\boldsymbol{r}, Z_B), \tag{2.50}$$

and

$$Q_H = \int \mathrm{d}\boldsymbol{r}\; q_H(\boldsymbol{r}, Z_H). \tag{2.51}$$

Closing off the system of equations, the potentials $\omega_\kappa(\boldsymbol{r})$ can be expressed in terms of the local volume fractions $\phi_\kappa(\boldsymbol{r})$ as

$$\omega_\kappa(\boldsymbol{r}) = \frac{\rho_{ref}}{\rho_{0\kappa}}\Big\{ \sum_{\kappa' \neq \kappa} \chi_{\kappa\kappa'}\phi_\kappa(\boldsymbol{r}) + \frac{\eta(\boldsymbol{r})}{\rho_{ref}} \Big\} - \lambda_\kappa. \tag{2.52}$$

Taking advantage of the fact that the diffusion equation 2.16 will obtain the same result regardless of any additive constant applied to $\omega_\kappa(\boldsymbol{r})$, we choose the convention

$$\omega_\kappa(\boldsymbol{r}) = \frac{\rho_{ref}}{\rho_{0\kappa}}\Big\{ \sum_{\kappa' \neq \kappa} \chi_{\kappa\kappa'}[\phi_\kappa(\boldsymbol{r}) - \bar{\phi}_\kappa] + \frac{\eta(\boldsymbol{r})}{\rho_{ref}} \Big\}. \tag{2.53}$$

We now have the core of a self-consistent set of equations which determine the most probable configuration of the system: Eq. 2.16 applied to $q_\kappa(\boldsymbol{r}, \tau)$ and $q'_\kappa(\boldsymbol{r}, \tau)$ with initial conditions from Eqs. 2.48 and 2.49 give these propagators in terms of the potentials $\omega_\kappa(\boldsymbol{r})$. Eq. 2.45 gives the volume fractions $\phi_\kappa(\boldsymbol{r})$ – the normalised equivalent of $\rho_\kappa(\boldsymbol{r})$ – in terms of these propagators. Eq. 2.53 gives the potentials $\omega_\kappa(\boldsymbol{r})$ in terms of these volume fractions. The remaining field, $\eta(\boldsymbol{r})$, represents the contribution to the potential due to incompressibility, and is determined implicitly, chosen so that Eq. 2.27 will be satisfied.

From here, we may move forward to define a numerical process whereby these self-consistent field (SCF) equations may be solved.

2.3 Dimensionless Self-Consistent Field Equations

We are interested in obtaining the solution to the SCF equations in which the normalised density distributions, $\phi_\kappa(\boldsymbol{r})$ reflect a lamellar morphology. In this symmetry, $\phi_\kappa(\boldsymbol{r})$ varies only along one axis, and exhibits a periodic variation built from symmetric unit cells, symbolically represented by A|BB|A. Thus, $\phi_\kappa(\boldsymbol{r})$ can be reduced to a function of only one co-ordinate, x, and be periodic.

The remaining fields that have to be evaluated in the SCF equations will have the same symmetry. Since $\eta(\boldsymbol{r})$ enforces incompressibility on $\phi_\kappa(\boldsymbol{r})$ it will be constant along axes along which $\phi_\kappa(\boldsymbol{r})$ is constant. The potentials, $\omega_\kappa(\boldsymbol{r})$, are a direct function of $\phi_\kappa(\boldsymbol{r})$ and $\eta(\boldsymbol{r})$. The $q_\kappa(\boldsymbol{r},\tau)$ and $q'_\kappa(\boldsymbol{r},\tau)$ functions have initial conditions which satisfy the symmetry and are subject to the potentials $\omega_\kappa(\boldsymbol{r})$ which also satisfy the symmetry, and so can easily be shown to be one-dimensional as well.

Furthermore, the periodicity of these functions mean that we need only evaluate them over a single period or unit cell. The free energy can also be determined using only one period. In a periodic system, the free energy density of the system, $\mathcal{F}/\Omega$ is equivalent to the free energy density over one unit cell. In fact, we need only evaluate the fields over half the unit cell since the second half of the cell is the mirror image of the first.

Let us define R to be this half-period of the cell. We have that $R = d/2$ where d is the domain thickness defined in Chapter 1. To solve the SCF equations, we enforce mirrored boundary conditions on the diffusion equation, Eq. 2.16, at $x = 0$ and $x = R$ (i.e. at the centre of each subdomain). One would determine the equilibrium value of R by solving the SCF equations in this symmetry for a range of candidate R's and finding the one which minimises the free energy.

To do this, we need a practical form for the free energy. Substituting Eqs. 2.27 and

2.33 into Eq. 2.22, the free energy density becomes

$$\begin{aligned}\frac{f}{k_BT} &\equiv \frac{\mathcal{F}}{\Omega} \\ &= \frac{N_C}{\Omega}(\ln\frac{N_C}{\mathcal{Z}_C Q_C}-1)+\frac{N_H}{\Omega}(\ln\frac{N_H}{\mathcal{Z}_H Q_H}-1)- \\ &\quad \frac{1}{\Omega}\int \mathrm{d}\boldsymbol{r}\ \sum_{\kappa}\rho_{0\kappa}\omega_\kappa(\boldsymbol{r})\phi_\kappa(\boldsymbol{r})+ \\ &\quad \frac{1}{\Omega}\int \mathrm{d}\boldsymbol{r}\ \sum_{\kappa\kappa'}\rho_{ref}\chi_{\kappa\kappa'}\phi_\kappa(\boldsymbol{r})\phi_{\kappa'}(\boldsymbol{r}). \end{aligned} \tag{2.54}$$

To evaluate the minimum in Eq. 2.54, it is convenient to consider its relative value, Δf, compared to that of a homogeneous system where $\phi_\kappa(\boldsymbol{r}) = \bar{\phi}_\kappa$. This reference energy will be independent of R and so only provides a constant offset to Eq. 2.54. Thus, a minimum in Δf vs. R will correspond to a minimum in f vs. R. The condition for homogeneity requires that the potentials $\omega_\kappa(\boldsymbol{r})$ be zero. Thus, evaluating Eq. 2.54 in this trivial case we have

$$\begin{aligned}\frac{f_{hom}}{k_BT} &= \frac{N_C}{\Omega}(\ln\frac{N_C}{\mathcal{Z}_C\Omega}-1)+\frac{N_H}{\Omega}(\ln\frac{N_H}{\mathcal{Z}_H\Omega}-1)+ \\ &\quad \frac{1}{\Omega}\int \mathrm{d}\boldsymbol{r}\sum_{\kappa\kappa'}\rho_{ref}\chi_{\kappa\kappa'}\bar{\phi}_\kappa\bar{\phi}'_\kappa. \end{aligned} \tag{2.55}$$

And so, the relative free energy density, Δf, is

$$\begin{aligned}\frac{\Delta f}{\rho_{ref}k_BT} &= \frac{f-f_{hom}}{\rho_{ref}k_BT} \\ &= \frac{1}{\Omega}\int \mathrm{d}\boldsymbol{r}\Big\{\sum_{\kappa\kappa'}\chi_{\kappa\kappa'}[\phi_\kappa(\boldsymbol{r})\phi_{\kappa'}(\boldsymbol{r})-\bar{\phi}_\kappa\bar{\phi}_{\kappa'}]- \\ &\quad \sum_\kappa\frac{\rho_{0\kappa}}{\rho_{ref}}\omega_\kappa(\boldsymbol{r})\phi_\kappa(\boldsymbol{r})\Big\}-\frac{N_C}{\rho_{ref}\Omega}\ln\frac{Q_C}{\Omega}-\frac{N_H}{\rho_{ref}\Omega}\ln\frac{Q_H}{\Omega}. \end{aligned} \tag{2.56}$$

In considering a single unit cell, then, one can make the substitution $(1/\Omega)\int \mathrm{d}\boldsymbol{r}\ldots \rightarrow (1/R)\int_0^R \mathrm{d}x\ldots$. From Eqs. 2.50 and 2.51, one can see that Q_C and Q_H are extrinsic quantities (i.e. measured over the system volume Ω). Yet, in the equation above and in the expression in Eq. 2.45 for $\phi_\kappa(\boldsymbol{r})$ we only ever require the intrinsic quantity $\mathcal{Q}_\kappa \equiv Q_\kappa/\Omega$. $\mathcal{Q}_\kappa$ also has the form $(1/\Omega)\int \mathrm{d}\boldsymbol{r}\ldots$ and so the same reduction can be applied.

Quantities such as N_κ/Ω represent the average number density of chains of type κ in the system. From Eq. 2.43 this is simply $\phi_\kappa \rho_{0\kappa}/Z_\kappa$.

Thus we have eliminated all occurrences of Ω in the SCF equations and the free energy density, and are now free to evaluate the equations over a single unit cell.

In Ref. [1], it was found most useful to do further remapping of system parameters so as to make the distance scales and polymer sizes dimensionless. Note that our spacial integrals now consider $(1/R)\int_0^R \mathrm{d}x$. Similarly, our monomer step τ in Eq. 2.45 considers $(1/Z_\kappa)\int_0^{Z_\kappa} \mathrm{d}\tau$. This invites the remapping of x and τ via $x \to x/R$ and $\tau \to \tau/Z_\kappa$. The only occurrences of x and τ which are not in this integral form are in the diffusion equation, Eq. 2.16. To compensate for these new dimensionless scales, then, we recast the diffusion equation as

$$\left[\frac{b_\kappa^2}{6R^2}\nabla^2 - \omega_\kappa(\boldsymbol{r})\right] q_\kappa(\boldsymbol{r},\tau) = \frac{1}{Z_\kappa}\frac{\partial}{\partial\tau} q_\kappa(\boldsymbol{r},\tau), \tag{2.57}$$

with an equivalent diffusion equation for $q'_\kappa(\boldsymbol{r},\tau)$.

A useful quantity in the next step of the remapping is r_κ, which is the dimensionless volume of a polymer chain of species κ. It is the volume of a polymer chain defined with respect to a reference volume, $1/\rho_{ref}$, where ρ_{ref} is the reference density used in the definition of the Flory parameter, χ. (See Eq. 2.34.) Since the volume of a polymer chain is given by the number of monomers, Z_κ, multiplied by the size of a monomer, $1/\rho_{0\kappa}$, we have

$$\begin{aligned} r_\kappa &\equiv \rho_{ref}\frac{Z_\kappa}{\rho_{0\kappa}} \\ &= \frac{\rho_{ref}}{\bar{\phi}_\kappa}\frac{N_\kappa}{\Omega}. \end{aligned} \tag{2.58}$$

Additionally, we define the size of the copolymer molecule which is simply the sum of the dimensionless volumes of the molecule's A and B blocks, i.e.

$$r_C = r_A + r_B. \tag{2.59}$$

For convenience, we also define the quantity $\overline{\phi}_C$ which is equal to $\overline{\phi}_A + \overline{\phi}_B$ and equivalent to $1 - \overline{\phi}_H$ by the incompressibility condition.

With these quantities considered, the final stage of the remapping is to rescale $\omega_\kappa(\boldsymbol{r})$ in Eq. 2.53 by a factor of $r_C\rho_{0\kappa}/\rho_{ref}$, and place compensating factors in the SCF equations wherever $\omega_\kappa(\boldsymbol{r})$ is referenced. In a similar manner, the incompressibility field $\eta(\boldsymbol{r})$ is also rescaled by a factor of $1/\rho_{ref}$.

We can now restate the SCF equations. The recast potential from 2.53 becomes

$$\omega_\kappa(x) \;=\; \sum_{\kappa' \neq \kappa} \chi_{\kappa\kappa'} r_C [\phi_\kappa(x) - \bar{\phi}_\kappa] + \eta(x). \tag{2.60}$$

The diffusion equation becomes

$$\Big[\frac{r_C\rho_{0\kappa}b_\kappa^2}{6\rho_{ref}R^2}\frac{\partial^2}{\partial x^2} - \omega_\kappa(x)\Big] q_\kappa(x,\tau) = \frac{r_C}{r_\kappa}\frac{\partial}{\partial\tau} q_\kappa(x,\tau), \tag{2.61}$$

with initial conditions for $q_\kappa(x,\tau)$ still as given in Eq. 2.48 but $q'_\kappa(x,\tau)$'s parameters rescaled from Eq. 2.49 so that

$$q'_\kappa(x,0) \;=\; \begin{cases} q_B(x,1) & \text{if } \kappa = \text{A} \\ q_A(x,1) & \text{if } \kappa = \text{B} \\ 1 & \text{if } \kappa = \text{H} \end{cases} \tag{2.62}$$

The local volume fractions, $\phi_\kappa(\boldsymbol{r})$, from Eq. 2.45 become

$$\phi_\kappa(x) \;=\; \frac{\bar{\phi}_\kappa}{\mathcal{Q}_\kappa}\int_0^1 \mathrm{d}\tau\; q_\kappa(x,\tau) q'_\kappa(x,1-\tau), \tag{2.63}$$

and the free energy becomes

$$\begin{aligned}\frac{r_C\Delta f}{k_BT} \;=\; \int_0^1 \mathrm{d}x \Big\{ &\sum_{\kappa\kappa'} \chi_{\kappa\kappa'} r_C [\phi_\kappa(x)\phi_{\kappa'}(x) - \bar{\phi}_\kappa\bar{\phi}_{\kappa'}] \\ &- \sum_\kappa \omega_\kappa(x)\phi_\kappa(x)\Big\} - \overline{\phi}_C \ln \mathcal{Q}_C - \overline{\phi}_H \frac{r_C}{r_H}\ln \mathcal{Q}_H. \end{aligned} \tag{2.64}$$

We have several parameters in this set of equations. The coefficient preceding the spacial derivative in Eq. 2.61 can be written as $\beta\epsilon_\kappa$ where

$$\beta \equiv \frac{r_C \rho_{0H} b_H^2}{6\rho_{ref} R^2}, \tag{2.65}$$

and

$$\epsilon_\kappa \equiv \frac{\rho_{0\kappa} b_\kappa^2}{\rho_{0H} b_H^2}. \tag{2.66}$$

The ϵ_κ parameter is a generalisation of the asymmetry parameter defined for neat copolymers. [1, 20] Here, it is defined with respect to the homopolymer, and so $\epsilon_H = 1$ by definition.

As it stands, we have a β parameter, two non-trivial ϵ_κ parameters, three species giving three $\bar{\phi}_\kappa$ parameters and three unique $\chi_{\kappa\kappa'} r_C$ parameters ($\chi_{AH} r_C$, $\chi_{BH} r_C$ and $\chi_{AB} r_C$), and the ratio r_H/r_C for a daunting total of 10 parameters for our copolymer-homopolymer blend.

We can eliminate one parameter by defining f_κ via

$$f_\kappa \equiv \frac{r_\kappa}{r_C}. \tag{2.67}$$

Physically, f_A is the fraction of the copolymer molecule's volume which is of species A, while f_B is the complement – the fraction that is of species B. From this definition, trivially we have $f_A + f_B = 1$. From Eqs. 2.43 and 2.58 we have $\overline{\phi}_A = f_A \overline{\phi}_C$ and $\overline{\phi}_B = f_B \overline{\phi}_C$. We also have by incompressibility that $\overline{\phi}_H = 1 - \overline{\phi}_C$. Thus, all $\bar{\phi}_\kappa$ are expressible in terms of two parameters, f_A and $\overline{\phi}_C$.

The parameter f_H does not have the same interpretation. It is the ratio r_H/r_C, which has already been identified as a parameter in the SCF equations. Thus, f_H defines the ratio of a homopolymer's molecular volume to a copolymer's molecular volume.

From Eq. 2.65, we see that the parameter β contains the lamellar structure's half-period, R. R is not an external parameter, but rather one that is determined by locating

the value which minimises the relative free energy, Δf. By extension, then, β is determined by minimising Δf and should not be regarded as an external parameter.

Thus, the total number of independent external parameters needed to describe a copolymer-homopolymer blend has been identified as eight – ϵ_A, ϵ_B, $\chi_{AB}r_C$, $\chi_{AH}r_C$, $\chi_{BH}r_C$, f_A, $\overline{\phi}_C$, and f_H. The reference density, ρ_{ref}, does *not* represent an external parameter as it is cancelled out in all occurrences, including the product $\chi_{\kappa\kappa'}r_C$. As such, it is convenient to define the reference density as $\rho_{ref} \equiv \rho_{0H}$.

This conclusion that a binary blend can be characterised by eight parameters does not rely on the system exhibiting a lamellar symmetry. The reduction to eight parameters is valid so long as the morphology can be characterised by a single lattice parameter, as would also be the case in the spherical, cylindrical, or gyroidal morphologies. [18]

For the present theoretical investigation, we have chosen to trim down the number of system parameters considered to a more respectable number. As the characteristic parameters that go into the definition of ϵ_κ in Eq. 2.66 are in dispute for even the more commonly studied polymers and are never very dissimilar, [20] for the bulk of our theoretical investigation – specifically, when not comparing against experiment – we chose $\epsilon_A = \epsilon_B = 1$.

Further, we chose to investigate systems wherein the species of monomer in the homopolymer was the same as the species in one of the two blocks in the copolymer. We chose block A to represent the like species. As such, $\chi_{AH} = 0$ and $\chi_{AB} = \chi_{BH} \equiv \chi$. This condition is of particular importance as it gives us a method wherein an explicit expression for $\eta(x)$ may be obtained. In particular, the potentials reduce to

$$\begin{aligned} \omega_A(x) &= \omega_H(x) \\ &= \chi r_C[\phi_B(x) - \overline{\phi}_B] + \eta(x), \end{aligned} \tag{2.68}$$

and

$$\omega_B(x) \;=\; \chi r_C[\phi_A(x) + \phi_H(x) - \overline{\phi}_A - \overline{\phi}_H] + \eta(x). \tag{2.69}$$

Adding Eqs. 2.68 and 2.69 and taking advantage of the incompressibility condition in Eq. 2.27, we have

$$\eta(x) \;=\; \frac{\omega_A(x) + \omega_B(x)}{2}. \tag{2.70}$$

As will be seen in Section 2.4, an explicit SCF equation for $\eta(x)$ is crucial to the numerical solution of this system of equations.

Finally, we chose to restrict the investigation to symmetric copolymers with $f_A = f_B$. These are typical of copolymer-homopolymer blend experiments and are helpful in optimising the likelihood that a lamellar structure will form. [1]

So, the systems investigated encompass $f_A = f_B = \frac{1}{2}$, $\epsilon_A = \epsilon_B = 1$, $\chi_{AH} = 0$, and $\chi_{AB} = \chi_{BH} = \chi$ for a selection of χr_C, f_H, and $\overline{\phi}_C$ except when comparisons were made with experiment, wherein the correct ϵ_κ and f_κ values were used to the extent that they were known.

2.4 Iterative Solution and Numerical Methods

The SCF equations are represented by Eqs. 2.61, 2.63, 2.68, 2.69 and 2.70. Each of these equations gives one of the fields, $\phi_\kappa(x)$, $\omega_\kappa(x)$, etc. in terms of the others. There is no evident means by which they may be decoupled, and no analytic solution presents itself.

What one may do, however, is attempt an iterative "trial and error" approach. For our investigation we started with the following zeroth order approximation for $\phi_\kappa(x)$ and $\eta(x)$:

$$\phi_A(x) = \overline{\phi}_A(1 + \cos \pi x), \tag{2.71}$$

$$\phi_B(x) = \overline{\phi}_B(1 - \cos \pi x), \tag{2.72}$$

$$\phi_H(x) = \overline{\phi}_H, \tag{2.73}$$

$$\eta(x) = 0. \tag{2.74}$$

This initial trial was motivated by the fact that weakly-segregated neat copolymer systems and copolymer-homopolymer blends have a cosine-like variation in their density distributions, [3, 8] and that homopolymer, to the extent that it resembles selective solvent, [10] would distribute fairly evenly throughout the system. The incompressibility field, $\eta(x)$, was chosen to be zero for lack of guiding evidence otherwise.

Eqs. 2.68 and 2.69 were then employed to generate an initial trial solution for $\omega_\kappa(x)$. It was from here that the iterative process began. The process was as follows:

1. Using the trial $\omega_\kappa(x)$'s, the diffusion equation, Eq. 2.61, was solved for each of the initial conditions in Eqs. 2.48 and 2.62.

2. The solutions from Step 1 were used to generate new $\mathcal{Q}_\kappa \equiv Q_\kappa/\Omega$ via Eqs. 2.18 and 2.19.

3. Using the results of these two steps new $\phi_\kappa(x)$'s were generated using Eq. 2.63.

4. A new $\eta(x)$ was generated via Eq. 2.70.

5. New potentials, $\omega_\kappa(x)$, were generated from the results of steps 3 and 4 using Eqs. 2.68 and 2.69.

6. If, for some preselected convergence parameter, δ, the condition

$$|\omega_\kappa^{(n)}(x) - \omega_\kappa^{(n-1)}(x)| < \delta$$

was satisfied for all x, we had a converged solution and stopped iterating here.

7. If the condition in step 6 was violated, we selected a new potential

$$\omega_\kappa^{(n+1)} = s\omega_\kappa^{(n)}(x) + (1-s)\omega_\kappa^{(n-1)}(x)$$

and returned to step 1.

8. Iteration ceased when the solution satisfied the condition in Step 6, or else when a preset maximum number of iterations was reached.

Typically, the convergence parameter, δ, was on the order of 10^{-7}, the ratio s was typically 1/10, and the maximum number of iterations attempted before giving up was 10^4, although these parameters were sometimes varied when convergence proved difficult.

The above iterative process has a physical analogy. It is essentially the dynamic evolution of a system to equilibrium. The initial conditions on $\phi_\kappa(x)$ and $\eta(x)$ represented the initial state of a system out of equilibrium. This state produced a potential due to the repulsive interactions between monomers. Taking a snapshot of that potential, we then calculated a new configuration of the polymer chains in that potential. We then allowed the system to evolve, partially, to that state. The degree to which the system evolved to the new state was controlled by s.

If the iteration was successful, when the system was "released" (i.e. when the iterations were started) it would spring out of the initial state and oscillate toward an equilibrium. Convergence was not guaranteed, of course, and if s was chosen to be too large, the system would persistently overshoot equilibrium. A selection of too small an s would slow the system's progress toward equilibrium. (N.B. a small value of s would not give a false sense of stability as the stability condition was tested in Step 6 before the ratio s came into play.)

The numerical self-consistent field (NSCF) equations were very straightforward to evaluate. The diffusion equation, Eq. 2.61 was solved using the Crank-Nicholson method, [21] with a discretised grid of $\Delta x = 1/100$ and $\Delta\tau = 1/400$, where both x and τ ranged from 0 to 1. These values were found quite adequate for the bulk of the investigation. Only when $\phi_\kappa(x)$ was extremely step-like in the strong-segregation limit did convergence problems become apparent.

Integrals, including those found in $\phi_\kappa(x)$ and the evaluation of the relative free energy, Δf, were carried out using Simpson's Rule, which gives fourth-order accuracy. [22] For the integrals, steps of $\Delta x = 1/100$ and $\Delta\tau = 1/40$ were used.

Utilising Eq. 2.65, a natural distance scale exists for R. If we define a new R' such that

$$\beta \;=\; \frac{1}{6(R')^2}, \tag{2.75}$$

then we have a simple definition of β and a dimensionless definition of R in units of $\sqrt{r_C}b_H$. To minimise Δf with respect to R, we selected a trial value guided by the results for neat copolymer systems, [1] typically found in the range 0.7 to 1.2. Then R was stepped up and down from the original selected value in increments of 0.1, solving the NSCF equations each time to obtain a free energy, until a minimum was found. From that minimum, we then stepped in increments of 0.01 to pin-point the minimum

with refined accuracy. The process was repeated for increments of 0.001 and 0.0001, ultimately locating the R yielding the minimum Δf to as much as five significant figures. The dimensionless domain thickness, d, was then simply given by $d = 2R$.

Appendix A includes the program listing in C which implemented the numerical solution of the above iterative algorithm.

Chapter 3

Domain and Subdomain Sizes

3.1 Comparison of Initial Results

Systems of copolymer-homopolymer blends have previously been studied in the so-called *weak-segregation* and near-weak-segregation regime using the mean field formalism. [3, 23, 24]. In these prior investigations, the density distributions $\phi_\kappa(\boldsymbol{r})$, potential distributions $\omega_\kappa(\boldsymbol{r})$, and incompressibility field $\eta(\boldsymbol{r})$ were expanded in terms of their Fourier components, and the system's free energy evaluated only to the fourth order in these fields.

Early investigations considered only the single dominate term of this expansion – the "one-wave approximation". [23, 24] This was found to have a very restricted range of applicability and neglected one of the more notable characteristics of the behaviour of the lamellar morphology in blends. [3] Namely, it is found in experiment [25, 26] that the domain thickness of the lamellar structure may either increase or decrease with the addition of homopolymer, depending on the value of f_H. The one-wave approximation failed to reproduce this result.

A refined "Many-Wave Approximation" (MWA), [3] which used several terms in the Fourier expansion, was successful in qualitatively reproducing this phenomenon. Figures 3 and 4 of Ref. [3] represent the domain thickness, d, for an ideal system wherein $\chi r_C = 12$, $f_H = 0.0025$, 0.1, 0.2, and 0.3, $\overline{\phi}_C = 0.8$, 0.85, 0.9, 0.95, and 1, $f_A = 0.5$, and $\epsilon = 1$.

In Figures 3.1 and 3.2, we redo these calculations for these systems using the full

(a)

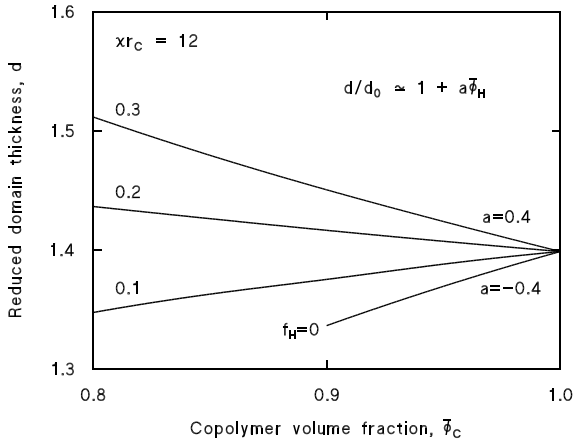

(b)

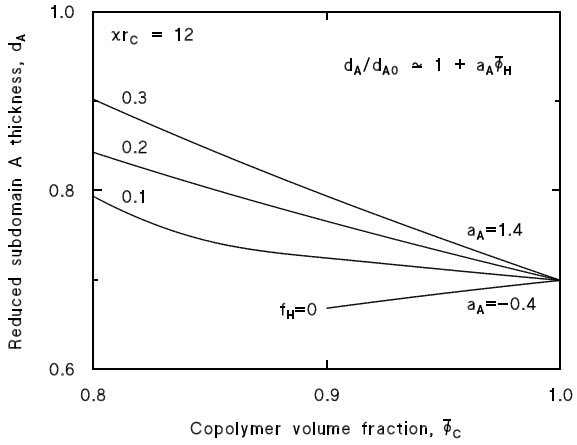

(c)

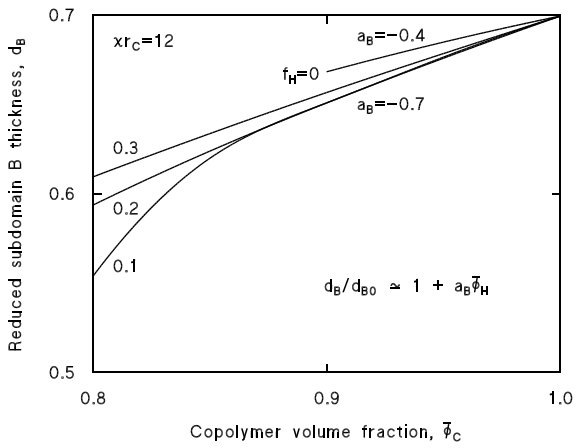

Figure 3.1: Reduced domain and subdomain thicknesses as a function of $\overline{\phi}_C$ using NSCF, for comparison with "Many-Wave Approximation's" ideal test case. These graphs can be compared with the calculations in Banaszak and Whitmore's [3] Figure 3 for (a) domain thickness d vs. copolymer volume fraction $\overline{\phi}_C$, (b) the thickness of subdomain A, d_A, vs. $\overline{\phi}_C$, and (c) the thickness of subdomain B, d_B vs. $\overline{\phi}_C$. All thicknesses are expressed in units of $b_H {r_C}^{\frac{1}{2}}$. To convert to the units of Ref. [3], multiply by ${r_C}^{\frac{1}{2}}$=20.

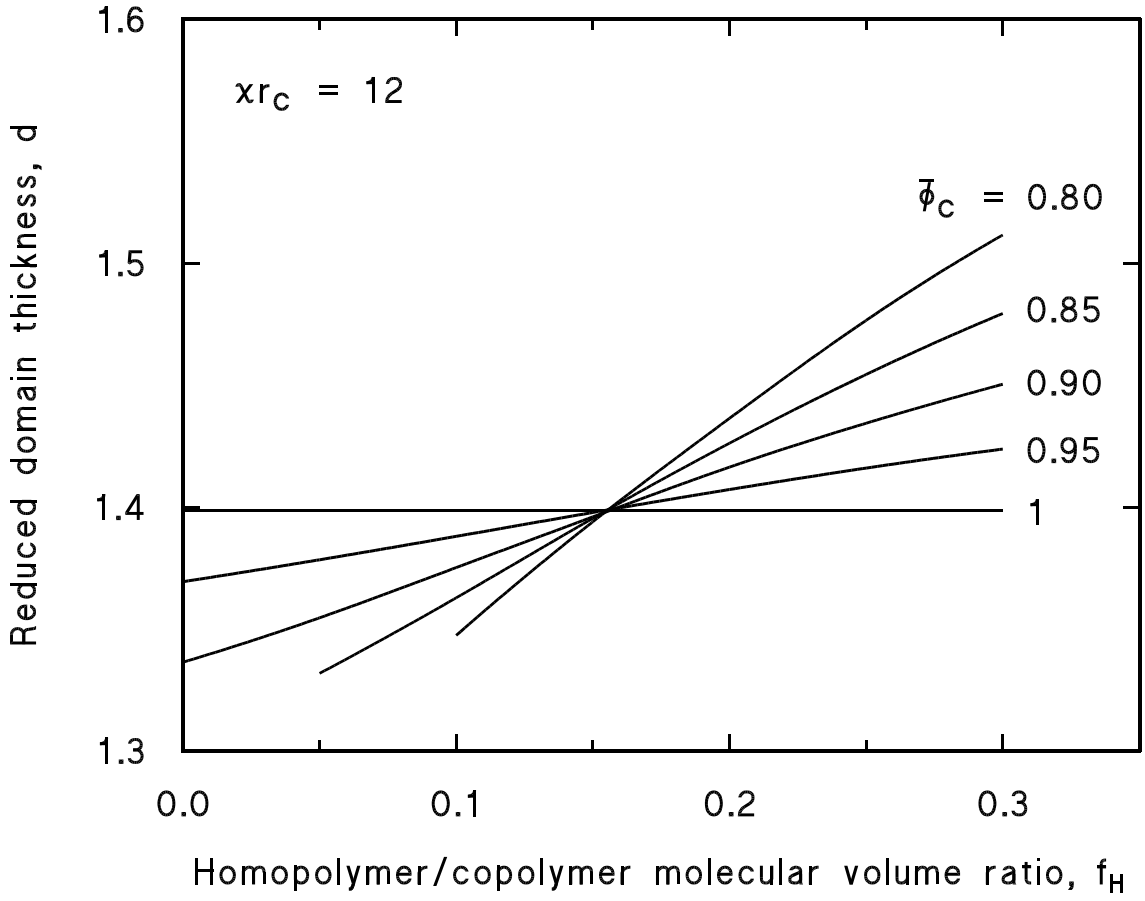

Figure 3.2: Reduced domain thickness as a function of f_H using NSCF, for comparison with "Many-Wave Approximation's" ideal test case. This graph can be compared directly with the calculations in Banaszak and Whitmore's [3] Figure 4. Units are as for our Figure 3.1.

NSCF formalism. In considering Figure 3.1 first, the $\overline{\phi}_C = 1$ limit corresponds to a system composed entirely of neat copolymer. In absence of homopolymer, the parameter f_H, which expresses a characteristic of the homopolymer, has no effect on the result. Hence, all curves converge to the same domain and subdomain thicknesses at $\overline{\phi}_C = 1$. As homopolymer is added (i.e. as $\overline{\phi}_C$ decreases), the effects of the various homopolymers develop.

As with the MWA, NSCF predicts that for the relatively large homopolymer molecules (e.g. $f_H = 0.3$) the domain thickness, d, increases with the addition of homopolymer (i.e. as $\overline{\phi}_C$ decreases). Similarly, with the addition of small homopolymer molecules (e.g. $f_H \to 0$), domain thickness decreases. A similar effect may be witnessed on the thickness of subdomain A, d_A. For subdomain B, the thickness d_B decreases for all considered cases of f_H. All of these results are qualitatively consistent with the MWA.

Differences, however, appear in the details. At the basic level, it is found that the domain thickness, d_0, in the neat copolymer limit (where $\overline{\phi}_C = 1$) differs between the results of MWA and our NSCF study. Ref. [3] gives $d_0/(b_H {r_C}^{\frac{1}{2}}) \approx 1.45$. Our study gives the value to be approximately 1.40, which is, to precision, in agreement with the quantitative result of the earlier NSCF investigation of neat copolymer systems. [18] These values represent a mere 4% discrepancy between MWA and NSCF, which may be considered a respectable discrepancy for a truncated approximation of density distributions and a fourth-order free energy as in the MWA.

More striking differences exist, however. First, in considering Figure 3.1(a), one notices that the $f_H = 0.2$ line experiences a more linear ascent with decreasing $\overline{\phi}_C$; whereas in Banaszak and Whitmore's MWA investigation, there is a mild non-linear downward curve with decreasing $\overline{\phi}_C$. Also of particular note is the fact that the $f_H \to 0$ line has a slope of 0.4 in our graph while it has a slope of 1.0 in the MWA result.

Similarly, in Figure 3.1(b), the $f_H = 0.1$ line increases as $\overline{\phi}_C$ decreases, with a clear

upwards curvature. The equivalent line in Ref. [3] has a clear downward curvature in the neighbourhood of $\overline{\phi}_C = 0.8$.

In the case of Figure 3.1(c), there is again a quantitative difference with our result having a more modest slope as $f_H \to 0$ and again, like Figure 3.1(b), the $f_H = 0.1$ case having a more pronounced downward curvature in the neighbourhood of $\overline{\phi}_C = 0.8$.

To begin understanding these discrepancies, one may first wish to establish some confidence in the newer NSCF result in situations where it disagrees with the MWA. An ideal place to start is in the consideration of the slope of d vs. $\overline{\phi}_C$ for the $f_H \to 0$ limit in Figure 3.1(a). This limit represents the situation where the homopolymer molecule is "very small" with respect to the size of the copolymer molecule. For our case of $\epsilon = 1$, this is the limit where $Z_H \ll Z_C$. That is, the degree of polymerisation of the homopolymer is negligible on the scale of the copolymer. A molecule with negligible polymerisation is effectively a monomer – a simple molecule. In fact, in the situation Banaszak and Whitmore consider, they explicitly have $Z_H = 1$ and $Z_C \gg 1$.

So, in the limit of $f_H \to 0$ we are considering a system of neat copolymers diluted by the introduction of simple monomers of species A. This is precisely the selective solvent case. [10] In the limit of large Z_C, good solvents – whether selective or neutral [2, 9] – tend to distribute evenly throughout the system. Even though a selective solvent such as ours should preferentially gather in the A subdomain, the relatively low value of χr_H makes the repulsion insufficient to overcome entropy considerations. Selective solvents are generally expected to be good solvents when $\chi r_H \ll 0.5$. [27] (N.B. for a solvent molecule of $Z_H = 1$ and using the convention $\rho_{ref} = \rho_{0H}$, we have $r_H = 1$, reducing the condition to $\chi \ll 0.5$.) This limit of homogeneously distributed homopolymer resembles the dilution approximation in neutral solvents. [2, 9, 18]

In the dilution approximation, a system may be represented by an equivalent neat

copolymer system (i.e. one without solvent) via the substitution of χ with

$$\chi_{eff} = \overline{\phi}_C \chi. \tag{3.1}$$

It is known from the study of neat copolymer systems that domain thickness scales roughly as [1]

$$d = (\chi r_C)^p {r_C}^{\frac{1}{2}}. \tag{3.2}$$

Considering that r_C is fixed in this exercise, in the dilution approximation we thus have

$$\begin{aligned} d/d_0 &= (\chi_{eff}/\chi)^p \\ &= {\overline{\phi}_C}^p \\ &= (1-\overline{\phi}_H)^p. \end{aligned} \tag{3.3}$$

Using the binomial expansion for small $\overline{\phi}_H$, this becomes roughly

$$d/d_0 \approx 1 - p\overline{\phi}_H, \tag{3.4}$$

illustrating a roughly linear scaling of d in the limit of small $\overline{\phi}_H$, with the slope given by p. In the weak-segregation regime where $\chi r_C = 12$, Figure 4(b) of Ref. [1] gives that $p \approx 0.4$. Thus, we would expect that d vs. $\overline{\phi}_C$ in the $f_H \to 0$ case would have a rough linear dependence with slope of 0.4, which is, in fact, the value obtained here. And so, we have independent evidence that in the comparison of NSCF vs. MFA approaches to copolymer-homopolymer blends, the NSCF result is the more realistic one in this case.

On the matter of other differences, they may be better illuminated by looking at the NSCF's results for the d vs. f_H dependence for these systems, reproduced here in Figure 3.2. Like Figure 4 of Banaszak and Whitmore's MWA paper, [3] there is a rough linear dependence present in d vs. f_H for the various values of $\overline{\phi}_C$ considered. Like the MWA result, these d vs. f_H plots all cross $d = d_0$ at roughly the same value of f_H.

This f_H is called the "threshold" value. Banaszak and Whitmore found this value to be roughly 1/5. Here, its value in the NSCF result is roughly 0.16, or 1/6. In Section 3.3, we find that this threshold is not a fixed value but instead has an effective χr_C dependence plus a weaker $\overline{\phi}_C$ dependence. In the limit of $\chi r_C = 10.5$ and $\overline{\phi}_C \to 1$, we also obtain a threshold of 1/5, implying MWA is most successful in this extreme. The cut-off $\chi r_C \gtrsim 10.5$ represents the microphase separation transition (MST) boundary in neat copolymer systems, above which ordering first starts to occur – i.e. the extreme weak segregation. The implication here is that in the detailed balance between energy and entropy which determines whether the domain thickness grows or shrinks with addition of homopolymer, the MWA's applicability may be confined to systems very near the MST limit.

As further groundwork in establishing the NSCF formalism, we consider the predicted results of NSCF in comparison with several experimental cases also considered to test the validity of the MWA. [3]

Figure 3.3 illustrates the comparison between the NSCF results and the experimental systems considered by Winey et al. [25] In these experiments, systems of PS-b-PI (polystyrene-polyisoprene) copolymer blended with several sizes of PS homopolymers were considered. The copolymer utilised corresponded roughly to $\chi r_C = 32$, $f_A = 0.51$. One may evaluate ϵ_{PI} for such a system by referring to the experimental values for the statistical segment length and bulk monomer density of polystyrene and polyisoprene. Unfortunately, these numbers are not precisely known but, following Ref. [20], we have chosen a realistic value of 1.3.

The dependence of domain thickness on the volume fraction of copolymer present in the system, $\overline{\phi}_C$, was plotted for the four PS-b-PI/PS blends in question. In each system, the PS-b-PI characteristics were fixed, and only the homopolymer size was varied. The four homopolymers were designated 2.6hPS, 6hPS, 14hPS, and 37hPS. The molecular

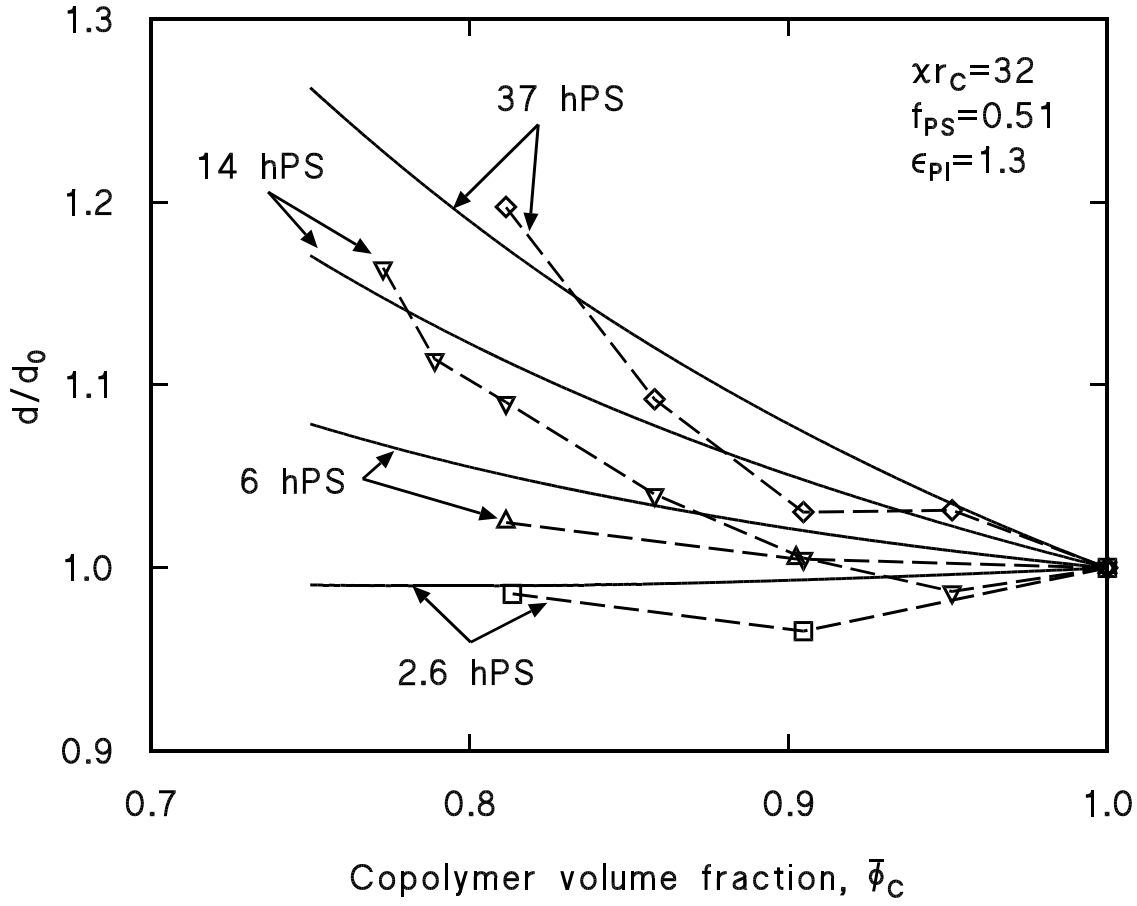

Figure 3.3: Theoretical domain thicknesses vs. Winey et al's experimental results. [25] Four PS-b-PI/PS blends are shown of common $\chi r_C = 32$ and $f_H = 0.0504$, 0.1210, 0.2722, and 0.7158 – designated 2.6hPS, 6hPS, 14hPS, and 37hPS respectively. Dashed lines with markers indicate experiment. Solid lines indicate NSCF predictions. Domain thicknesses are expressed relative to the neat case.

weights for these molecules given in Ref. [25] correspond to f_H values of 0.0504, 0.1210, 0.2722, and 0.7158 respectively.

In Figure 3.3 one can see that the NSCF theory does indeed predict the trends of d/d_0, at least on a qualitative level. The remaining discrepancy is likely attributed to the uncertainty in ϵ_{PI}, or a non-trivial relation between χ and changes in the physical properties of the polymers, as well as experimental uncertainties which would seem to be implied by the sporadic, non-trivial displacements of some of the experimental data points.

Nonetheless, the results in Figure 3.3 do represent an improved agreement between the NSCF theory and Winey et al, when compared to the earlier MWA effort. [3] In particular, the NSCF theory seems to have greater success in predicting the sign and magnitude of the domain thickness vs. $\overline{\phi}_C$ slope than the former MWA effort, with the 6hPS slope have the correct sign, and the $\overline{\phi}_C \lesssim 0.8$ experimental data points more closely matching the corresponding NSCF predictions.

A similar comparison to the experimental effort of Hashimoto et al [26] indicates a similar qualitative agreement in trends of the NSCF results and experiment. Again the agreement, though somewhat lacking in precision, has greater success than the former MWA comparison. [3] (N.B. The scale in our Figure 3.4 is finer than that of Ref. [3], and so our plot emphasises discrepancies more than in the former work.)

It would seem that the NSCF is a step in the right direction toward practical prediction of experiment, but uncertainties in the precise determination of the conformational asymmetry parameter, ϵ, and uncertainties in the experimental procedure may hamper high-precision comparison. Nonetheless, these comparisons do justify an optimism in the NSCF's capacity to predict experimentally-measurable qualitative and crudely-quantitative trends.

(a)

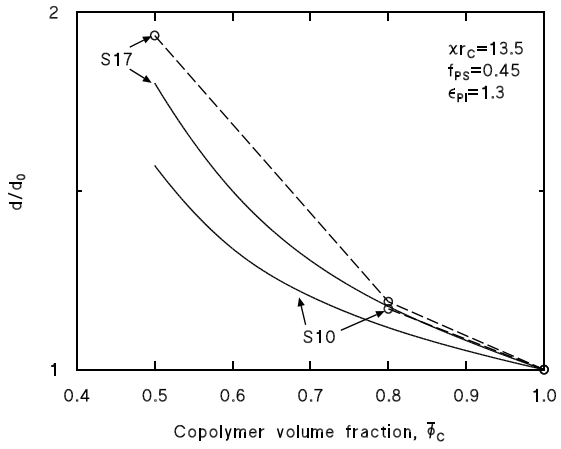

(b)

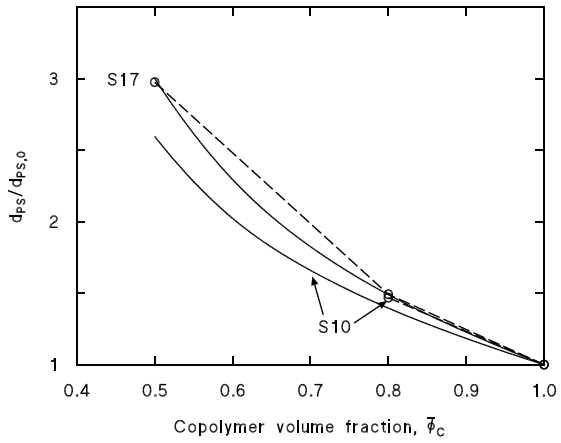

(c)

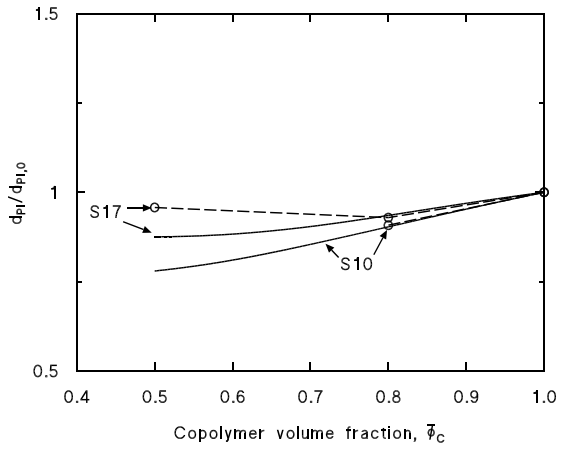

Figure 3.4: Comparison of NSCF results with Hashimoto et al's experimental results. [26] Two PS-b-PI/PS blends are shown of common $\chi r_C = 13.5$ and $f_H = 0.3096$ and 0.4954 – designated S10 and S17 respectively. Dashed lines with markers indicate experiment. Solid lines indicate NSCF predictions. Plotted are (a) domain thickness, (b) PS subdomain thickness, and (c) PI subdomain thickness, all relative to the neat case.

3.2 Domain Thickness vs. Relative Size of Homopolymer

As defined Chapter 2, f_H defines the ratio of the total molecular volume of a homopolymer molecule to the total molecular volume of a copolymer molecule. The definition of f_H is the more rigourous measure of relative homopolymer size within the mean field theory than the conventional ratio of homopolymer to copolymer degree of polymerisation, Z_H/Z_C. [3, 25, 26] The conventional definitions of Z_κ contain some ambiguity. For example, one might define a new "effective monomer" which is comprised of n adjoined monomers from the original definition. In this remapping, one would have

$$Z'_\kappa = \frac{Z_\kappa}{n}, \tag{3.5}$$

$$\rho'_{0\kappa} = n\rho_{0\kappa}, \tag{3.6}$$

$$Z'_\kappa (b'_\kappa)^2 = Z_\kappa b_\kappa^2. \tag{3.7}$$

This relation holds for non-integral values of n. Since the polymer is being represented as a random walk, Eq. 3.7 represents a constant quantity which is the statistical end-to-end separation of the polymer. Thankfully, in this remapping, our fundamental parameters of the dimensionless self-consistent field equations in Section 2.3 remain invariant. Often, in practice, one considers an effective Z where the remapping above is done so that $\rho_{0A} = \rho_{0B} = \rho_{0H}$. In this casting of parameters, Z_κ and r_κ would be equivalent according to Eq. 2.58 and we would have $f_H \equiv Z_H/Z_C$ from the definition, Eq. 2.67.

For the purposes of this investigation, we shall consider copolymer-homopolymer blends where $\epsilon_\kappa = 1$. Since we can define $\rho_{0A} = \rho_{0B} = \rho_{0H}$ via the remapping above, the $\epsilon_\kappa = 1$ condition represents the additional specification that $b_A = b_B = b_H$. As most experimental systems investigated tend to have modest asymmetry (i.e. $\epsilon_\kappa \simeq 1$) and asymmetry effects do not dominate except for extreme values of ϵ_κ, [20] it is reasonable to consider such $\epsilon_\kappa = 1$ systems to be representative of many realistic experimental

Variable	*Value*
χr_C	10, 20, 30, 40, 50
$\overline{\phi}_C$	0.1, 0.2, 0.3, 0.4, 0.5, 0.6, 0.7, 0.8, 0.85, 0.9, 0.95, 1
f_H	0*, 0.0008, 0.002, 0.005, 0.0075, 0.01, 0.015, 0.02, 0.0225, 0.025, 0.03, 0.05, 0.075, 0.1, 0.25, 0.5

Table 3.1: Parameters for investigated hypothetical systems. Systems investigated derived from all combinations of the tabulated parameters, with the additional choices that $f_A = f_B$ and $\epsilon_\kappa = 1$. The $f_H = 0$ case actually represents an evaluation of the dilution approximation wherein a neat copolymer system with $\chi_{eff} r_C = \overline{\phi}_C \chi r_C$ is considered. [9, 18]

systems.

A wide variety of systems was investigated for various values of χr_C, $\overline{\phi}_C$, and f_H, all considering exclusively the case where $f_A = f_B = \frac{1}{2}$ (i.e. configurationally symmetric copolymer) and $\epsilon_A = \epsilon_B = 1$ (i.e. conformationally symmetric copolymer). Table 3.1 summarises the various choices of χr_C, $\overline{\phi}_C$, and f_H.

Figures 3.5 through 3.9 illustrate the dependence of the lamellar repeat distance, d, on the ratio f_H for increasing values of χr_C. Only values of $\overline{\phi}_C \geq 0.3$ have been plotted, as the NSCF calculations for $\overline{\phi}_C = 0.1$ and 0.2 did not achieve a satisfactory convergence, and the resultant numerical noise in the free energy inhibited obtaining reliable equilibrium domain thicknesses.

Several characteristics are common among these results. In the limit of small f_H, the smallest homopolymer considered was $f_H = 0.0008$. In this range, the addition of homopolymer resulted in a *reduction* in the domain thickness.

To understand this, we must recognise that we are considering a limit in which homopolymer molecules are over three orders of magnitude smaller than the copolymer molecules in the system. As discussed in Section 3.1, on such an extremal scale the extended geometry of the homopolymer molecule can be neglected, effectively reducing

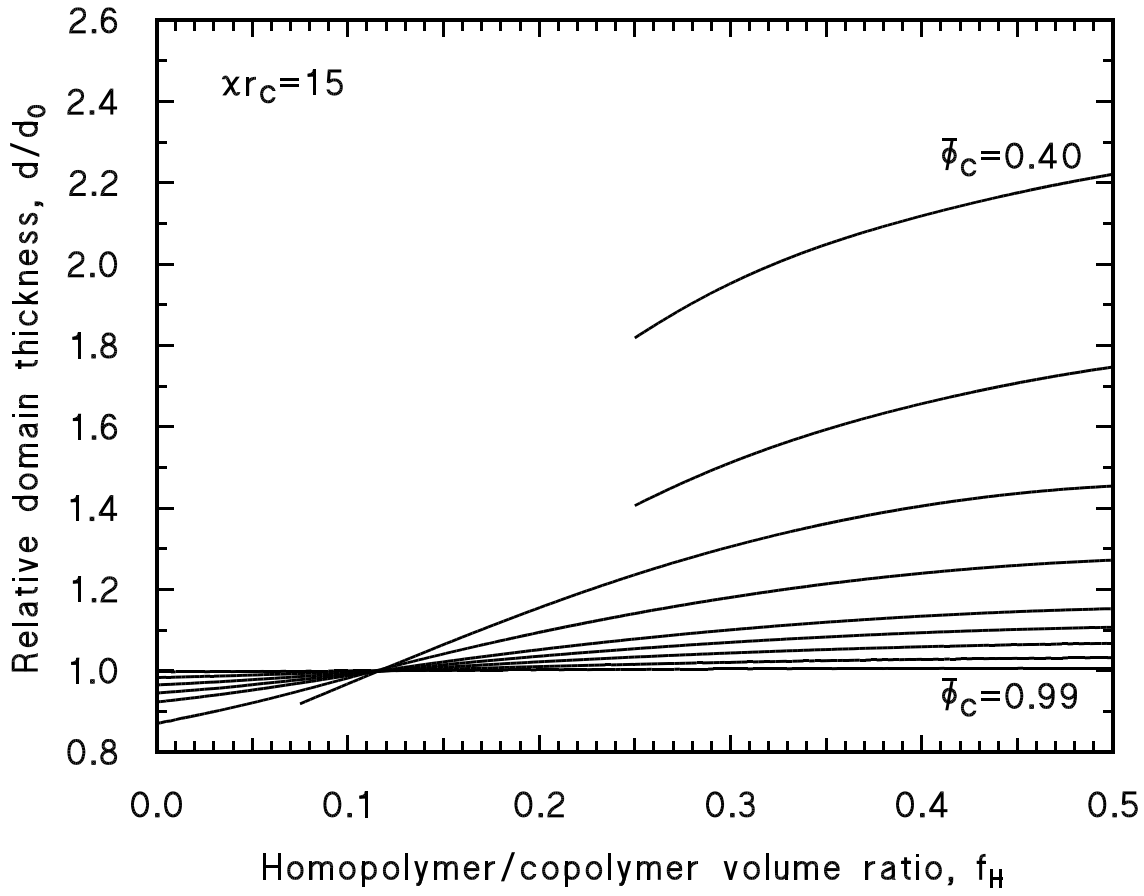

Figure 3.5: Domain thickness as a function of f_H for $\chi r_C = 15$. d_0 represents the domain thickness for the neat copolymer system wherein $\chi r_C = 15$. $\overline{\phi}_C = 0.4$, 0.5, 0.6, 0.7, 0.8, 0.85, 0.9, 0.95, and 0.99 are shown.

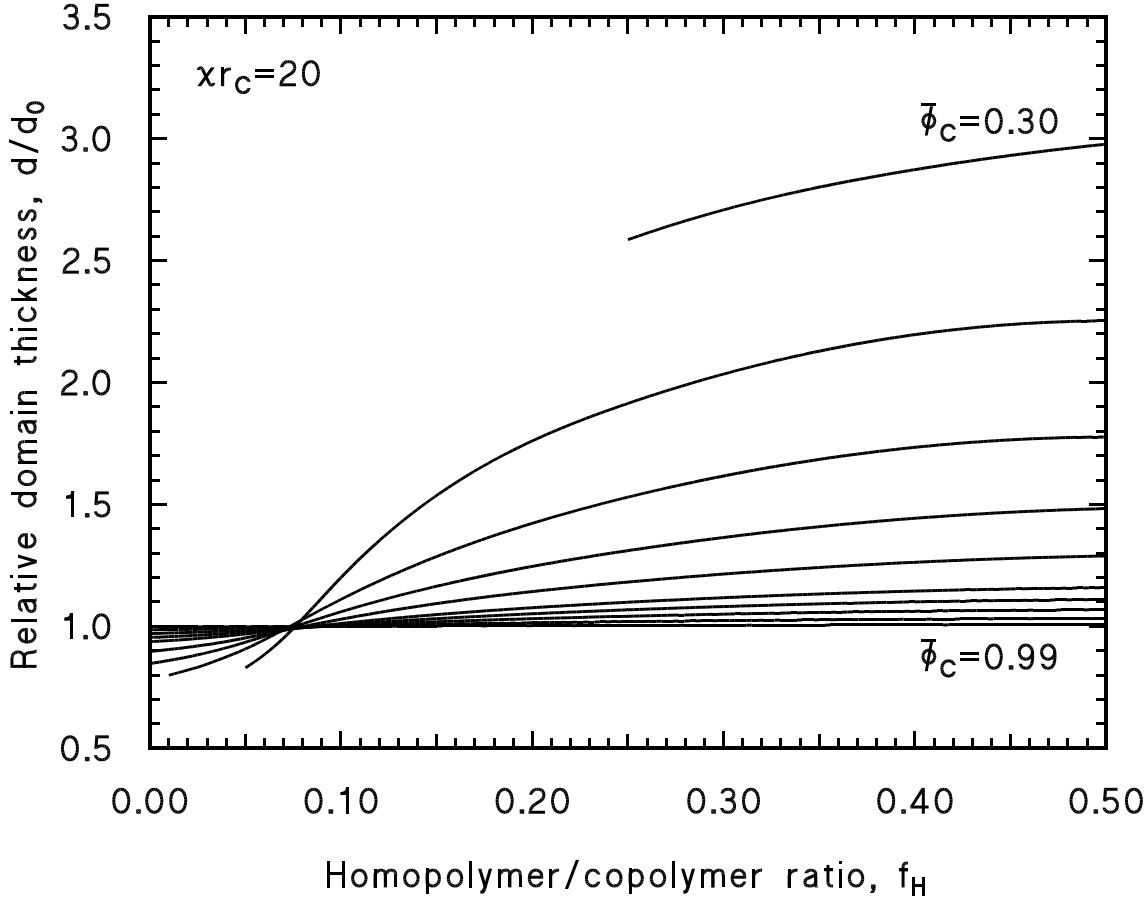

Figure 3.6: Domain thickness as a function of f_H for $\chi r_C = 20$. d_0 represents the domain thickness for the neat copolymer system wherein $\chi r_C = 20$. $\overline{\phi}_C = 0.3$, 0.4, 0.5, 0.6, 0.7, 0.8, 0.85, 0.9, 0.95, and 0.99 are shown.

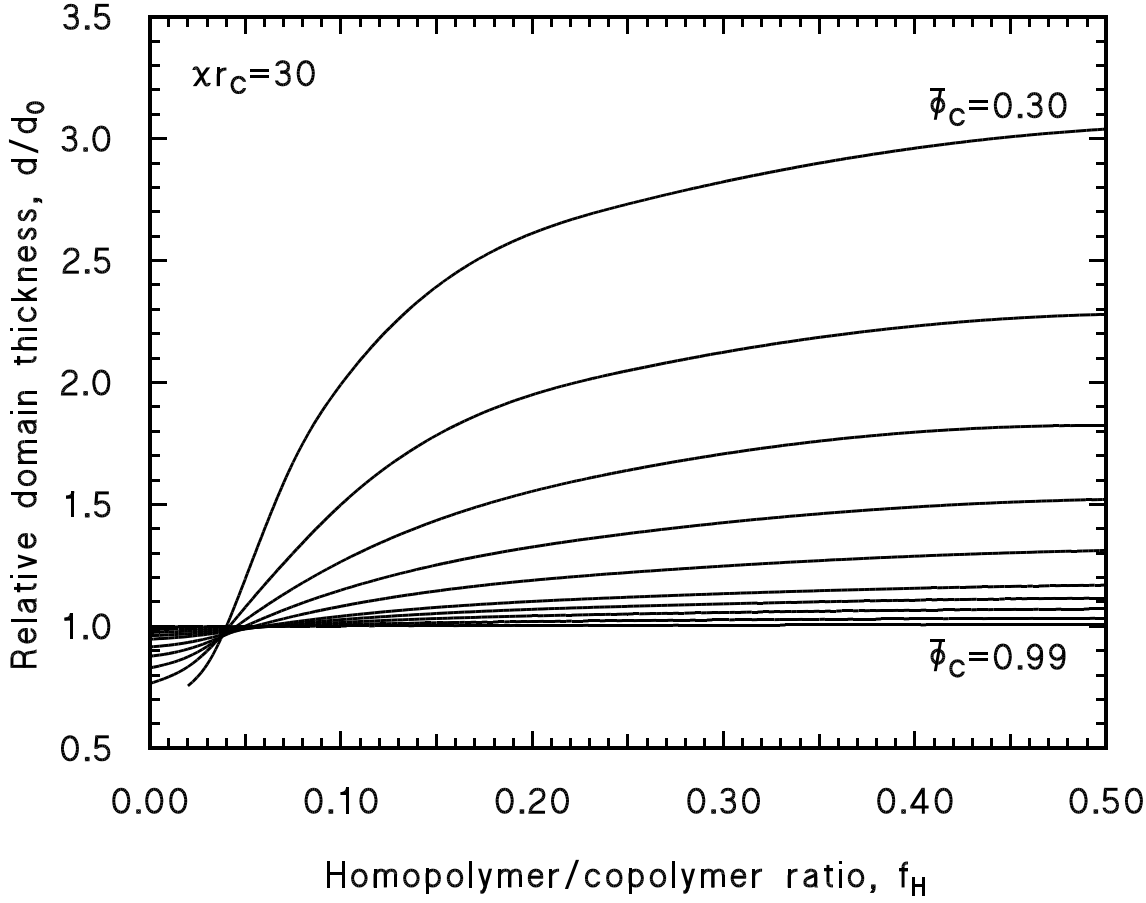

Figure 3.7: Domain thickness as a function of f_H for $\chi r_C = 30$. d_0 represents the domain thickness for the neat copolymer system wherein $\chi r_C = 30$. $\overline{\phi}_C = 0.3$, 0.4, 0.5, 0.6, 0.7, 0.8, 0.85, 0.9, 0.95, and 0.99 are shown.

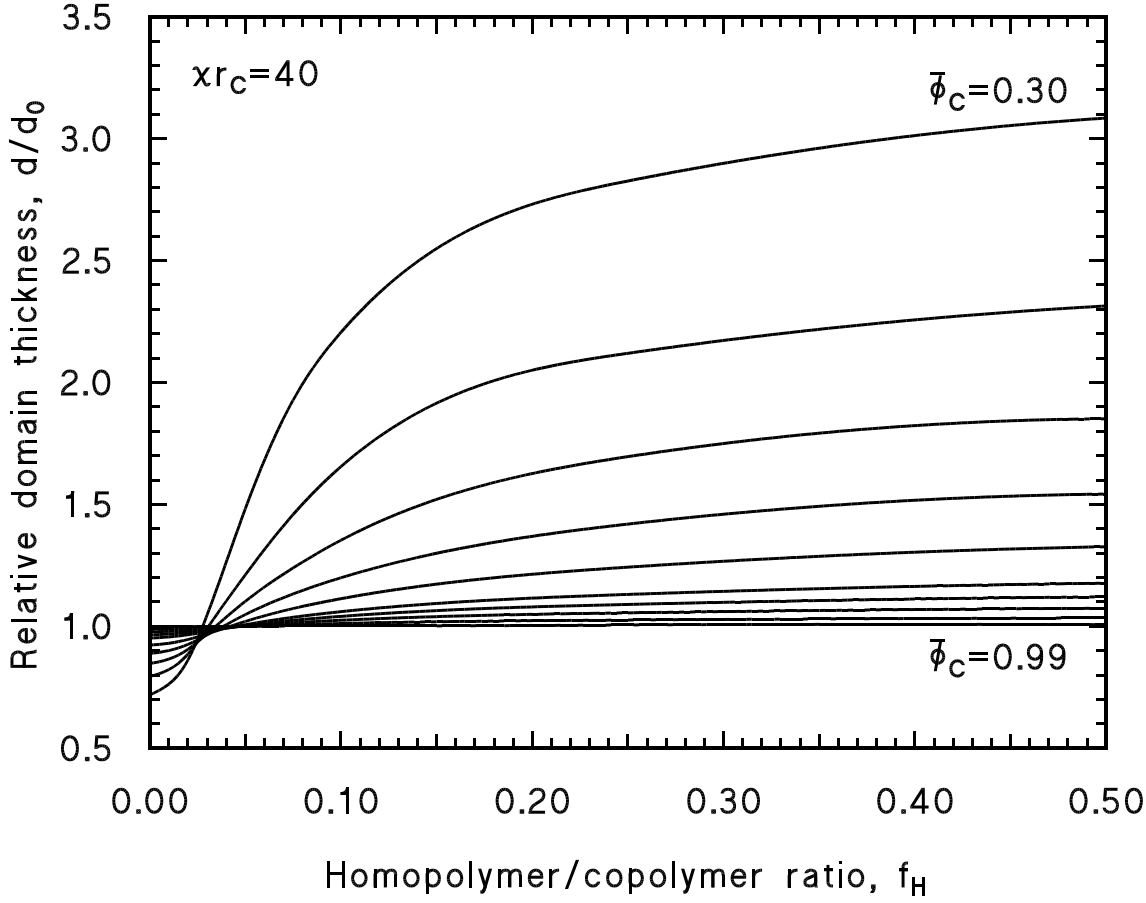

Figure 3.8: Domain thickness as a function of f_H for $\chi r_C = 40$. d_0 represents the domain thickness for the neat copolymer system wherein $\chi r_C = 40$. $\overline{\phi}_C = 0.3$, 0.4, 0.5, 0.6, 0.7, 0.8, 0.85, 0.9, 0.95, and 0.99 are shown.

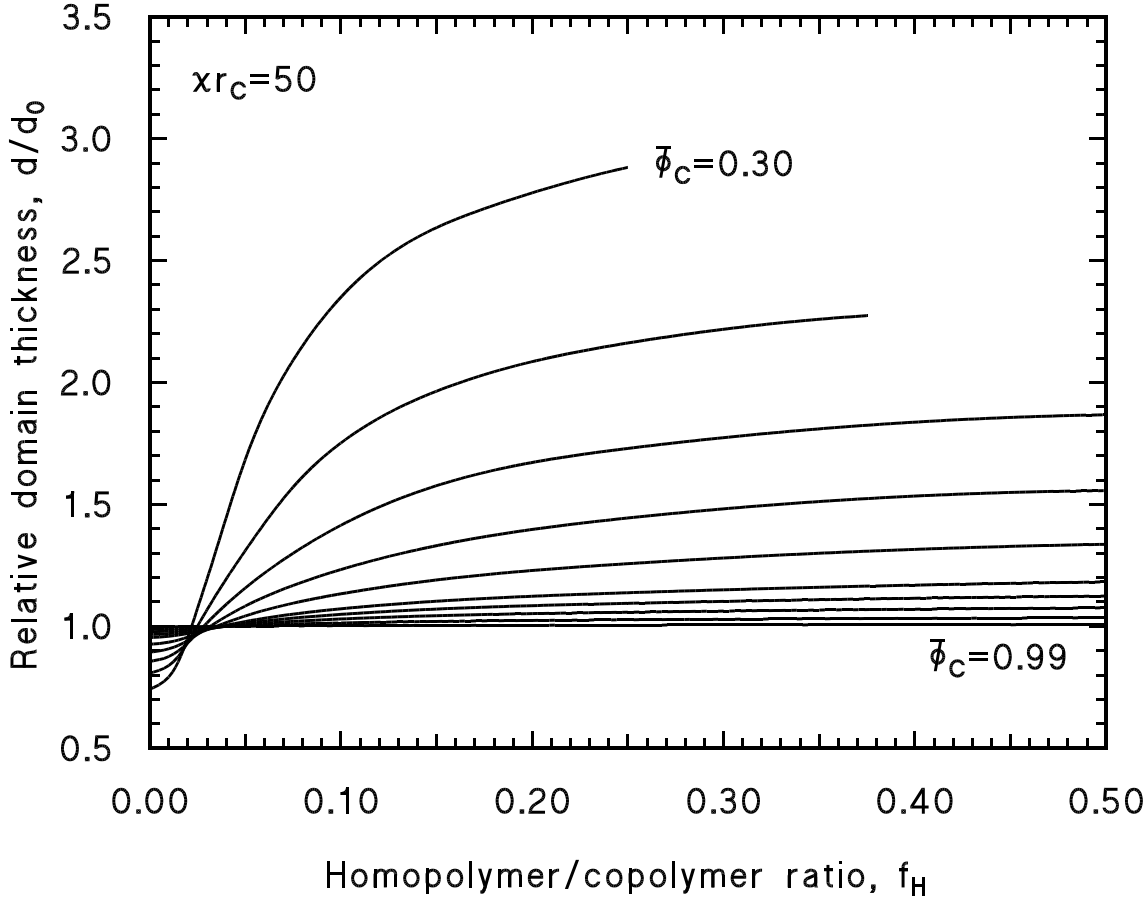

Figure 3.9: Domain thickness as a function of f_H for $\chi r_C = 50$. d_0 represents the domain thickness for the neat copolymer system wherein $\chi r_C = 50$. $\overline{\phi}_C = 0.3$, 0.4, 0.5, 0.6, 0.7, 0.8, 0.85, 0.9, 0.95, and 0.99 are shown.

the homopolymer to the role of a simple solvent molecule.

Intuitively, as outlined in Section 3.1, this limit may be understood as a $Z_H \to 1$ limit for large Z_C resulting in f_H being negligibly small. In this limit we are considering a blend of copolymer with simply monomers of species A – the selective solvent case. [10]

Analytically, this result can also be obtained by considering the diffusion equation, Eq. 2.61. When $f_H \to 0$, τ dominates the evolution of $q_H(\boldsymbol{r}, \tau)$ and the spacial component, $\beta\nabla^2$ may be neglected. Eq. 2.61 thus reduces to

$$-\omega_H(\boldsymbol{r}) q_H(\boldsymbol{r}, \tau) \;=\; \frac{1}{f_H}\frac{\partial}{\partial \tau} q_H(\boldsymbol{r}, \tau). \tag{3.8}$$

Solving for $q_H(\boldsymbol{r}, \tau)$ subject to the restriction of Eq. 2.48 gives

$$q_H(\boldsymbol{r}, \tau) \;=\; e^{-f_H \omega_H(\boldsymbol{r})\tau}. \tag{3.9}$$

Substituting this result into the NSCF formalism recovers the formalism for the selective solvent as found in Ref. [10].

In a typical low-f_H system such as that shown in Figure 3.10, the homopolymer density distribution $\phi_H(x)$ was found to be nearly homogeneous, as would be the case in a comparable copolymer-solvent blend. [10] The explanation for why homopolymer would be found in the B subdomain despite the repulsive interaction between the homopolymer/solvent and the B block of the copolymer would seem to be rooted in the entropy considerations. Explicitly, for the $f_H = 0.0008$ case, the homopolymer is over three orders of magnitude smaller than the copolymer.

From Eq. 2.61, polymer molecules may be regarded as random walks, perturbed by a repulsive interaction which biases them so that the blocks end up preferentially separated. The incompressibility condition demands that there be no "empty space", however. In the low-f_H scenario, the homopolymer molecules are several orders of magnitude smaller than the copolymer. Though the copolymer A block and the homopolymer are both

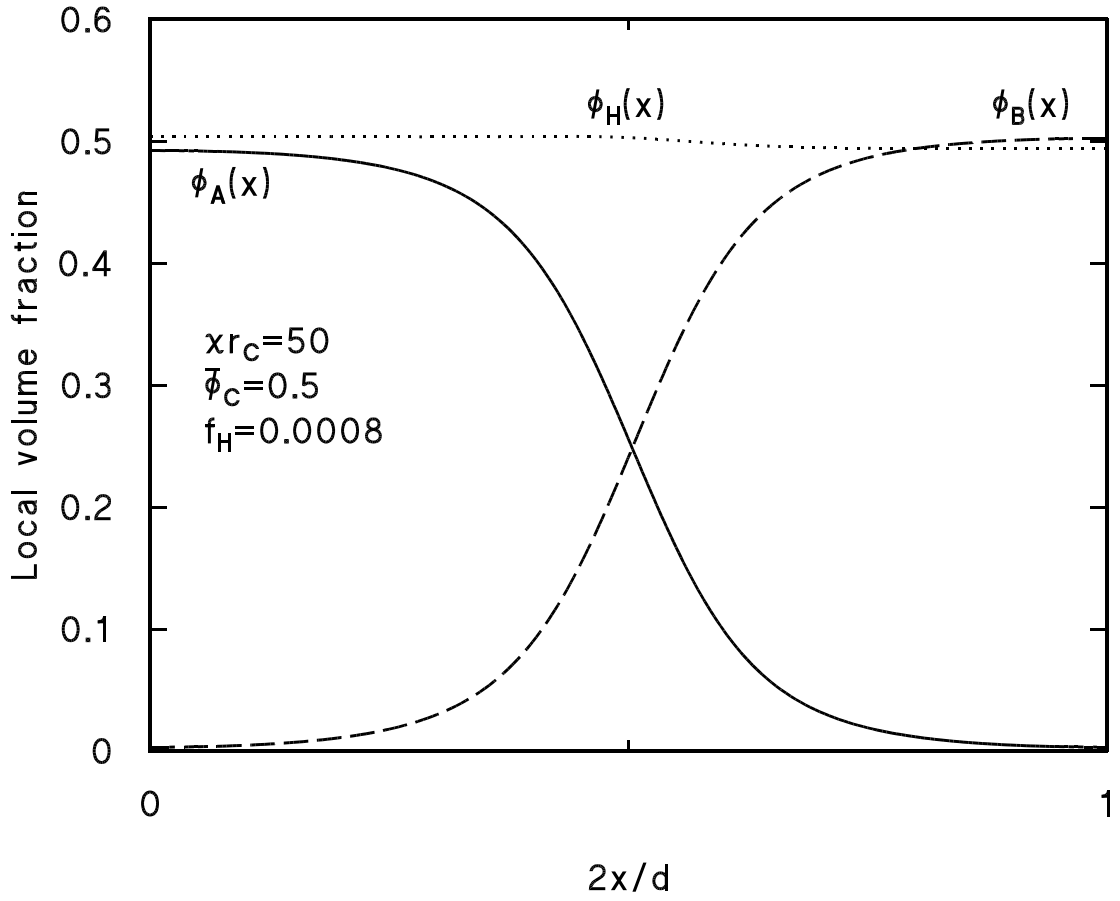

Figure 3.10: Density profile for a typical copolymer-homopolymer blend for very small f_H. In the investigation of neutral solvents, inhomogeneities in the solvent distribution were found to be larger when $\overline{\phi}_C \approx 0.5$ and χr_C was large. In consideration of this limit, the most-likely system to exhibit inhomogeneities from those investigated would be $\chi r_C = 50$, $\overline{\phi}_C = 0.5$. Despite this optimal selection, the $\chi r_C = 50$, $\overline{\phi}_C = 0.5$, $f_H = 0.0008$ system illustrated here exhibited less than a 1% variance in the local homopolymer volume fraction throughout the entire cell. All other systems with $f_H = 0.0008$ had equal or better homogeneity in their homopolymer distributions. This indicates that, in the "good solvent" limit of small f_H, there is a strong analogy with the dilution approximation in copolymer-neutral solvent blends.

repulsed by the B subdomain, the distribution of the homopolymer is controlled by entropy. With insufficient repulsion ($\chi r_H \ll 0.5$), the homopolymer acts as a good solvent and uniformly distributes throughout the system. Though the homopolymer perturbs the B block's potential, it does so homogeneously, so the B block's random walk is not biased by the presence of the uniformly-distributed homopolymer. However, the presence of homopolymer reduces the A and B blocks' monomer concentrations via incompressibility condition, Eq. 2.27. Such a reduction is entirely analogous to the dilution approximation in neutral solvents. [2, 9, 18]

So, the presence of homopolymer will dilute the repulsion between the A and B blocks of the copolymer. With a weaker effective χ, the copolymer does not extend itself so much to minimise contact between species A and B. Since the extension of the copolymer is the primary contributor to determining the domain thickness, the presence of a low-f_H homopolymer leads to a lower value of d than would be obtained in an unscreened system of neat copolymers.

The idealised limit of this effect occurs when the homopolymer/solvent's density distribution is perfectly homogeneous throughout the system. Based on the observation that the homopolymer becomes more homogeneously-distributed as f_H decreases, we hypothesised that the dilution approximation was a valid analogue for the $f_H \to 0$ limit for the system, where one would have an ideally good solvent (since $\chi r_H \to 0$). The NSCF equations were solved for systems representing the dilution approximation limit for all values of χr_C and $\overline{\phi}_C$ in Table 3.1. These systems, included in the Figures 3.5 through 3.9, did indeed fall in line as valid extrapolations of the d vs. f_H curves to the $f_H \to 0$ limit.

Thus, based on trends in the domain thickness and distribution of homopolymer in the low-f_H systems, the dilution approximation appears to be a valid representation of the $f_H \to 0$ limit.

Away from the low-f_H limit, the behaviour is somewhat different. As f_H increases for any fixed values of χr_C and $\overline{\phi}_C$, the domain thickness first increases in an approximately-linear fashion. At some intermediate value of f_H, it passes d_0, the thickness for a corresponding neat system of the same χr_C value. (This transition value for f_H, the so-called "threshold value", will be discussed in more detail in Section 3.3.) As f_H further increases, the domain thickness continues to increase, though less rapidly. For f_H on the order of the size of the copolymer blocks (i.e. $f_H = 0.5$), we see that in most cases the d vs. f_H dependence has begun to plateau.

One must ask why there is such a plateauing effect as f_H grows large. In the small f_H limit, the addition of homopolymer tends to dilute the system, distributing homogeneously, effectively screening the normally repulsive interaction quantified by the χr_C segregation parameter. For larger values of f_H, the situation is reversed; the addition of homopolymer *increases* the domain thickness. And, more interestingly, beyond $f_H \simeq 0.5$, the specific value of f_H no longer has a strong role to play.

To illuminate the mechanism involved in the high-f_H behaviour, one may again turn to the density profiles. Figure 3.11 illustrates what is happening inside the unit cell in a case typical of the high-f_H range. It is a very different picture than the one represented in Figure 3.10. The most distinguishing feature is that the homopolymer, represented by $\phi_H(x)$, has been nearly-completely expelled from the B subdomain. That is, to the right of the interphase where the B subdomain lies, $\phi_H(x)$ is essentially zero. In fact, the homopolymer has so strongly segregated from the B species that it has localised in the middle of the A subdomain (i.e. the left of the figure).

To understand this, we again think of the polymers in terms of a perturbed random walk, except now, in the large-f_H limit, the extended nature of the homopolymer also comes into play. The homopolymer's random walk is biased by the repulsive interaction with species B. The longer the homopolymer, the greater the number of steps in this

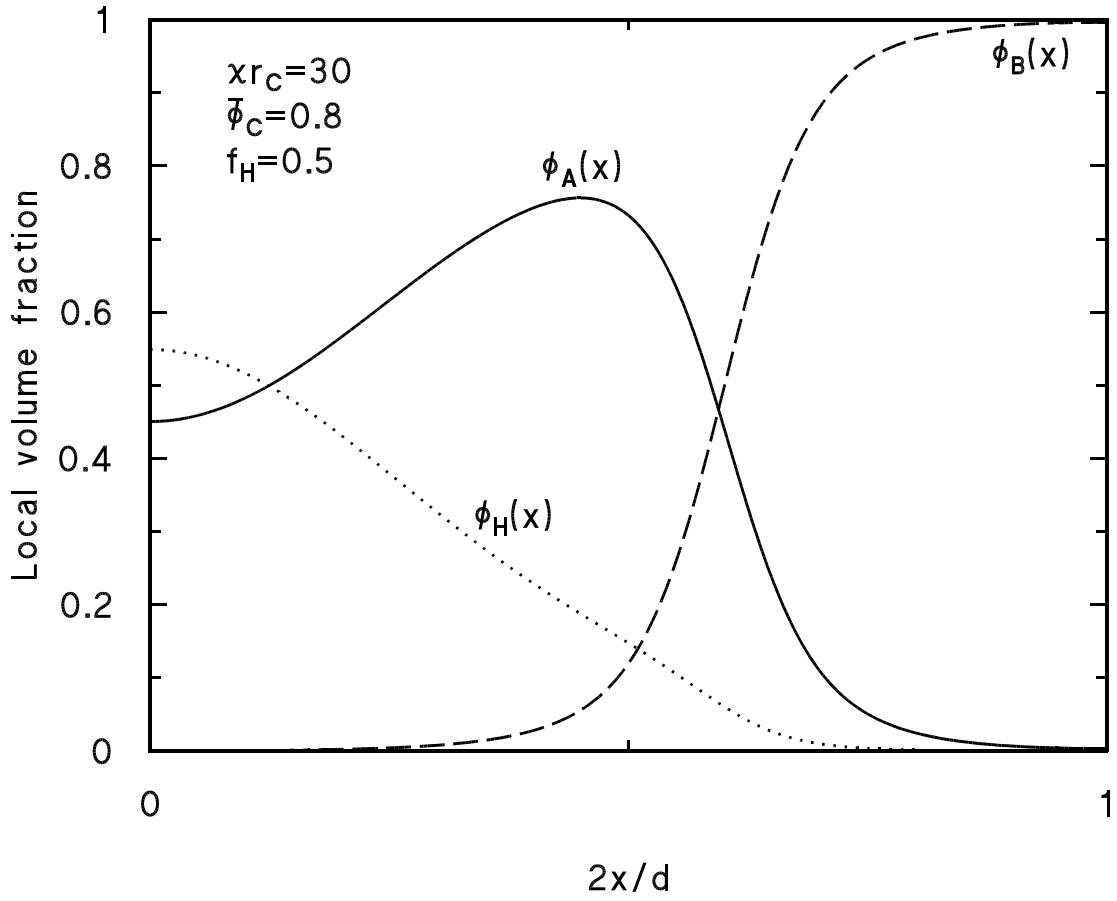

Figure 3.11: Density profile for a typical copolymer-homopolymer blend in the high-f_H limit. In this example, we have $\chi r_C = 30$, $\overline{\phi}_C = 0.8$, and $f_H = 0.5$. The system considered here is believed *not* to be one in which macrophase separation would occur. (See Section 4.2 for more details on macrophase separation.)

random walk within a biased field, and so the greater the probability that a monomer in the homopolymer (particularly in the "tail end" of the walk) will end up farther away from the B subdomain and the interphase. With the homopolymer out of the crucial interphase region, there is nothing to screen the copolymer's A block from its B block, and nowhere for the homopolymer to go except to enlarge the A subdomain to make room for itself there. This creates three zones of dominance:

1. the centre of the A subdomain which is dominated by homopolymer,

2. the A block of the copolymer wedged between the homopolymer and the interphase, facing an entropic deficit if it extends into the homopolymer-dominated region to its left and an energy deficit if it interacts with the immiscible B block to its right; and,

3. the B block of the copolymer, repelled primarily by the A block at the edge of its subdomain.

As the interphase interaction is primarily one between the A block and B block, one would expect its behaviour to be substantially similar to the neat copolymer case. What remains in the A subdomain is an entropic struggle between the A block of the copolymer and the like-species monomers in the homopolymer. This influence appears to be weak in comparison to the repulsive interaction. Essentially, then, once the homopolymer is out-of-play in the interactions of the interphase, the unit cell is largely unaffected by further changes to f_H.

The entropic contribution does continue to have some influence, of course. Increasing the value of f_H increases the length of the homopolymer. The longer the homopolymer, the farther it will end up away from subdomain B due to the biased random walk represented by Eq. 2.61. The more "tightly curled up" the homopolymer ends in the

centre of subdomain A, and the more it expels block A of the copolymer. When the entropic deficit of localising the homopolymer becomes too great, it ultimately leads to "macrophase separation", [3] wherein the homopolymer isolates itself completely from the copolymer within the system instead of finding itself sandwiched in between each consecutive layer of the unit cell. The phenomenon of macrophase separation is considered in more detail in Section 4.2.

The plateauing of domain thickness is indeed very persistent once f_H is sufficiently large. For one test case ($\chi r_C = 15$, $\overline{\phi}_C = 0.9$) the value of f_H was taken as high as 10 and still the domain thickness increased by only 4% over its value at $f_H = 0.5$. Admittedly, $f_H = 10$ is a fairly unrealistic system; it is a very likely candidate for macrophase separation. However, the projection of theory into this range does demonstrate how the driving force that changes the domain thickness in binary blends is the intrusion of homopolymer A into the interphase and immiscible species B's subdomain.

3.3 Domain Thickness vs. Copolymer Volume Fraction

Section 3.2 outlined the variance of domain thickness with copolymer size. While this relation is of key interest in studying the behaviour of copolymer-homopolymer blends, it is not a quality that can be varied dynamically within a given system. That is, copolymers and homopolymers are synthesised to be a particular size, prior to the experimental investigation of the blends and their characteristics. At best, a small, discrete selection of unique homopolymer sizes are synthesised which are then blended with a common copolymer. [25, 26] Consequently, behaviours may be investigated at only a few f_H values in a single experimental investigation. It is beyond the realm of experiment to investigate the variation of characteristics as a result of the *continuous* variation of f_H.

By contrast, continuous variations with $\overline{\phi}_C$ are more readily accomplished. In experiment, one need simply introduce the homopolymer into the blend in discrete steps as small as desired. Of course, special care may still be required to ensure that the system attains a globally stable equilibrium.

As presented in the previous section, the chief characteristics of the dependence of the domain thickness on $\overline{\phi}_C$ are that:

1. for small f_H, the homopolymer acts as a good solvent, distributing homogeneously in analogy to the dilution approximation for neutral solvents, and the presence of homopolymer reduces the interaction between the A and B blocks of the copolymer and thus reduces the domain size,

2. for larger f_H (approaching 0.5), the addition of homopolymer (and corresponding decrease in $\overline{\phi}_C$) increases the domain thickness; and,

3. at some intermediate f_H, the addition of homopolymer has a minimal effect on the domain thickness. For the weak-segregation case investigated in Ref. [3], this

"threshold" f_H was found to be approximately 1/5.

The first case – that of $f_H \to 0$ – is the easiest to consider. As stated in the previous section, the good solvent analogy with the dilution approximation grows increasingly applicable as f_H decreases. For all practical purposes then, we already know all we need to know about this limit from the neat copolymer studies [1] and Eq. 3.3. Namely, from the derivation of Eq. 3.3, we have

$$d/d_0 \quad \propto \quad \overline{\phi}_C{}^p, \tag{3.10}$$

where p is weakly dependent on $\chi_{eff} r_C$.

Figure 3.12(a) presents the scaling relation between relative domain thickness, d/d_0, and copolymer volume fraction $\overline{\phi}_C$ in the $f_H \to 0$ limit for select values of χr_C. In Figure 3.12(b) we see that these results may be plotted on a single graph by instead considering the dependence of d/d_0 on $\overline{\phi}_C \chi r_C$.

As seen in Figure 3.12(a), the scaling relation of Eq. 3.10 is a relatively good one. In the lowest χr_C considered, $\chi r_C = 15$, the d vs. $\overline{\phi}_C$ dependence goes roughly as Eq. 3.10 with p varying from 0.3 at $\overline{\phi}_C = 1$ to 0.5 at the lower cut-off where $\chi_{eff} r_C = 10.5$. In the high-end $\chi r_C = 50$ case, the scaling relation is again obeyed with p varying from 0.2 at $\overline{\phi}_C = 1$ to 0.3 for the lower considered-values of $\overline{\phi}_C$.

Next, we consider the domain thickness vs. $\overline{\phi}_C$ relation in the high-f_H limit, as plotted in Figure 3.13. There is a clear inverse dependence on $\overline{\phi}_C$ evident. Again, it is a scaling relation of the form given in Eq. 3.10 even in this high-f_H limit. However, p, here, for small additions of homopolymer (i.e. where $\overline{\phi}_C \to 1$), starts out at $-\frac{2}{3}$. It quickly shifts to a simple inverse relation, however, with $p = -1$ as more homopolymer is added.

As suggested in Section 3.2, when f_H is large the localisation of the homopolymer in the middle of the A subdomain – away from the interactions of the interphase – effectively splits the system into a zone of homopolymer and a zone of segregated neat copolymer.

(a)

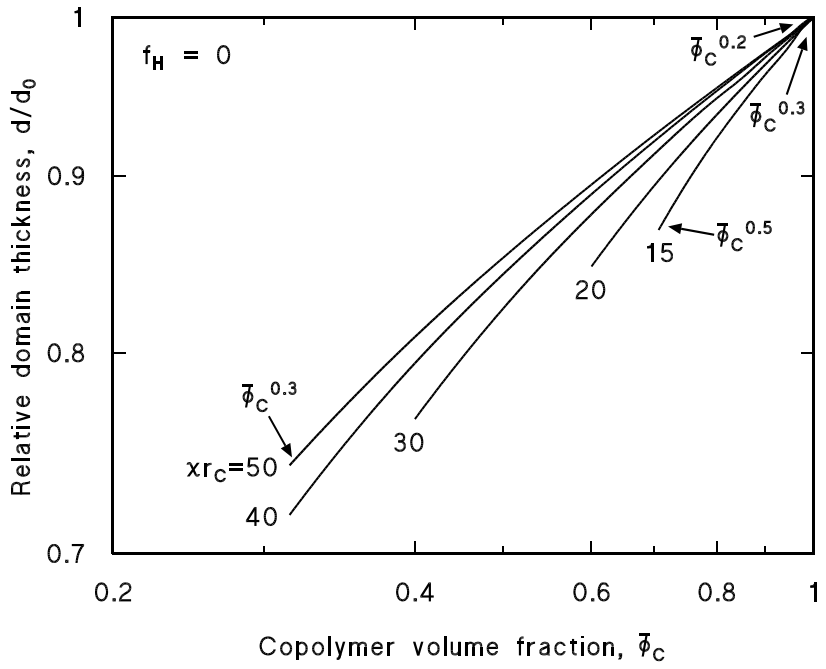

(b)

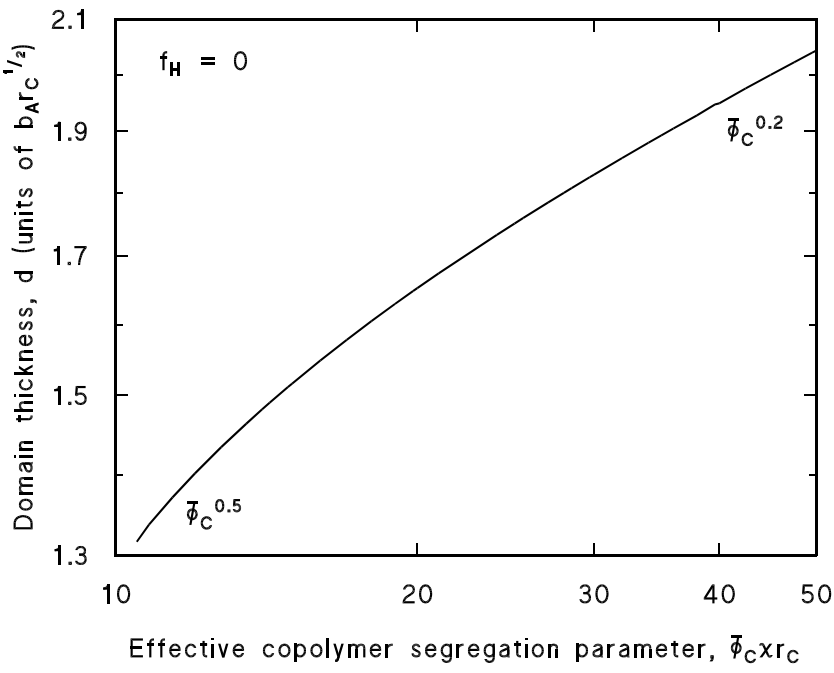

Figure 3.12: Scaling of domain thickness with copolymer volume fraction, $\overline{\phi}_C$, in the limit of $f_H \to 0$. (a) Relative domain thickness has been plotted on a log-log scale against $\overline{\phi}_C$ for each of the investigated values of χr_C tabulated in Table 3.1. (b) Here the relative domain thicknesses have been collected into a single plot as a function of $\overline{\phi}_C \chi r_C$, illustrating the analogy between a good solvent and the dilution approximation in this context.

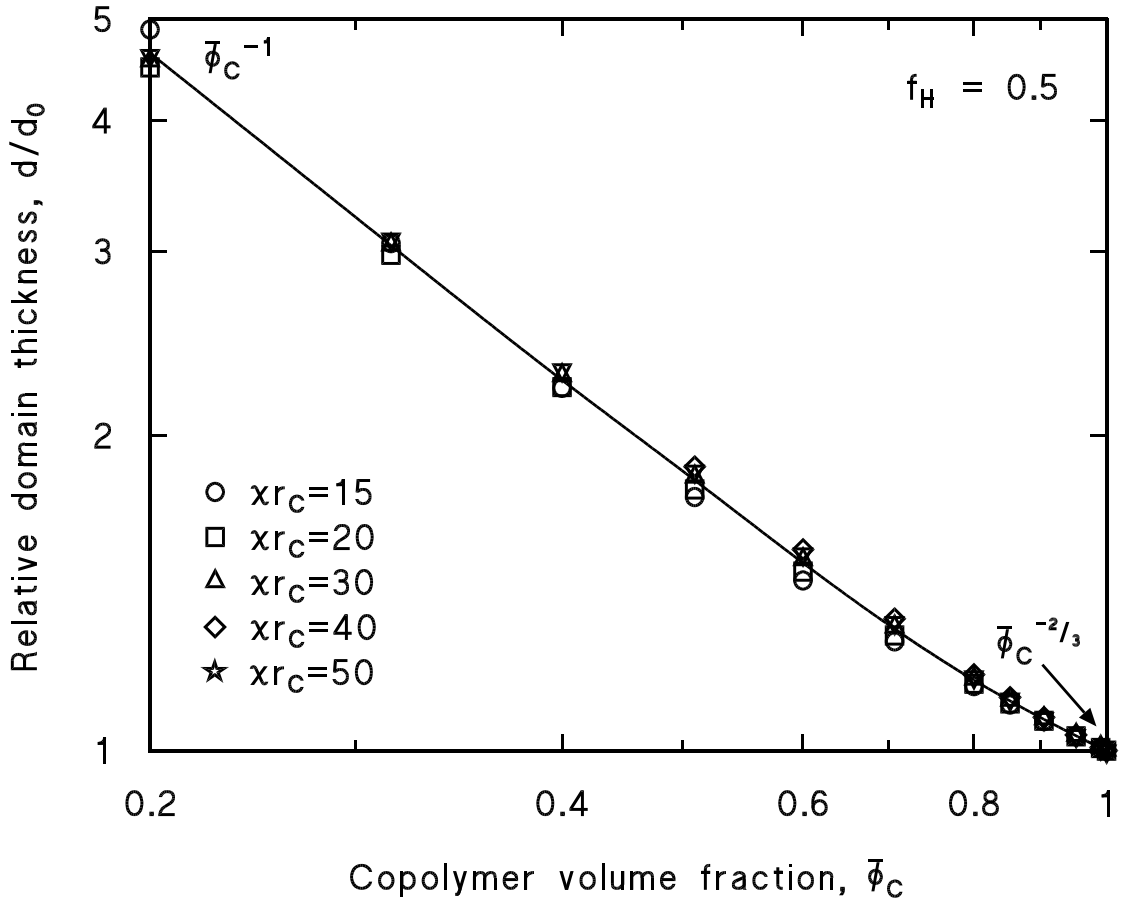

Figure 3.13: Scaling of domain thickness with copolymer volume fraction, $\overline{\phi}_C$, in high-f_H limit.

The impact of the addition of homopolymer on domain thickness should become a simple matter of geometry. As such, the inverse relation between d/d_0 and $\overline{\phi}_C$ is a simple one to justify physically. Consider a unit cell similar to that represented in Figure 3.11, without significant intermixing between the homopolymer and the B block of the copolymer. The thickness of subdomain B would remain the same as $d_{B,0}$, the B subdomain thickness for the neat case. Block B represents a volume fraction of $\overline{\phi}_B$ of the system volume. Hence, the domain thickness d would be given by $d_{B,0}/\overline{\phi}_B$. Using the geometric relations $d_{B,0} = f_B d_0$ and $\overline{\phi}_B = f_B \overline{\phi}_C$, we obtain $d = d_0/\overline{\phi}_C$ as hoped.

Conversely, then, the $\overline{\phi}_C{}^{-\frac{2}{3}}$ behaviour as $\overline{\phi}_C \to 1$ represents a situation where a greater degree of intermixing occurs between the homopolymer and subdomain B – enough to lessen the effect on domain thickness, but not so homogeneously intermixed that it causes a reduction in domain thickness as it would due to the screening effect in the dilution limit.

And so, with the two extremal cases considered it remains only to examine the "threshold" value of f_H where domain thickness remains unchanged by the introduction of homopolymer. Based on the extremal cases described above, this threshold f_H would represent a balance between the thickness-reducing effects of dilution and the thickness-enhancing effects of homopolymer localisation in the A subdomain.

From Figures 3.5 through 3.9, it seems that for a fixed χr_C the threshold varies only weakly with $\overline{\phi}_C$, if at all. By taking each curve in these figures and using a spline interpolation, we are able to determine the value of f_H at which $d = d_0$. The results of this intercept calculation for each value of χr_C are shown in Figure 3.14.

We find that this threshold $f_{H,thresh}$ obeys a simple relation. For a given $\overline{\phi}_C$, the threshold $f_{H,thresh}$ has an inverse dependence on χr_C; and so, $\chi r_C f_{H,thresh}$ is independent of χr_C leaving only a $\overline{\phi}_C$ dependence. Recall that f_H is the ratio of the dimensionless homopolymer and copolymer volumes, respectively termed r_H and r_C. Thus,

(a)

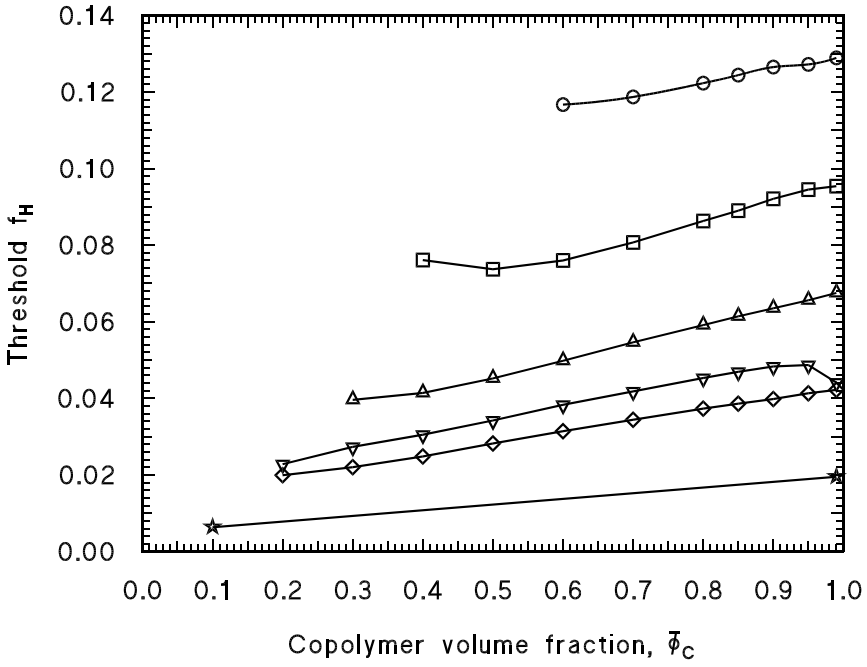

(b)

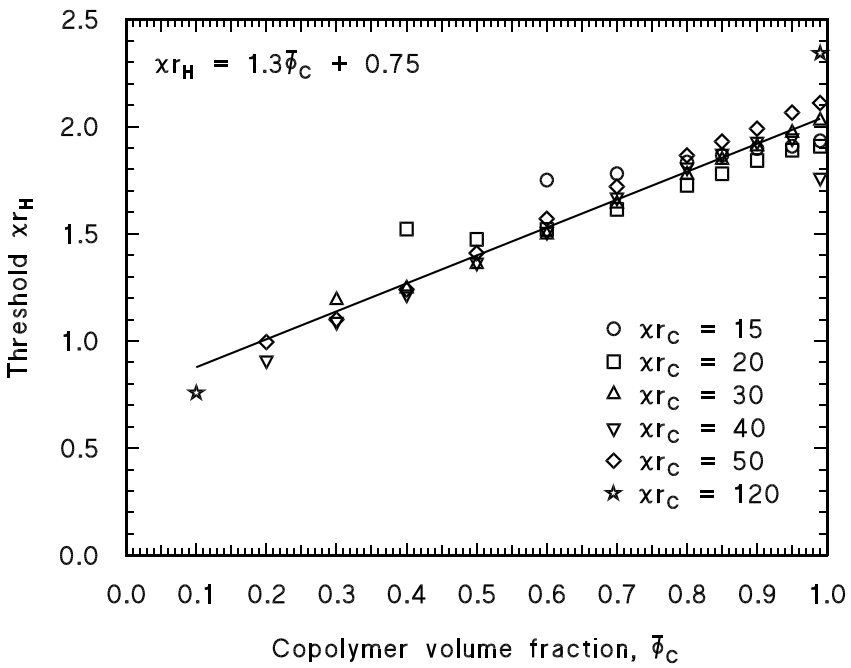

Figure 3.14: Threshold value of f_H below which domain thickness increases with $\overline{\phi}_C$ and above which it decreases with $\overline{\phi}_C$. (a) The threshold value of f_H, where d was found equal to d_0, is plotted against $\overline{\phi}_C$ for each χr_C value. These values were obtained by spline interpolation of Figures 3.5 through 3.9 and additional equivalent data for $\chi r_C = 120$. (b) The same threshold values are multiplied by χr_C and again plotted against $\overline{\phi}_C$. In this representation, we find the threshold is given by $\chi r_{H,thresh} = 1.3\overline{\phi}_C + 0.75$ where, by definition, $f_H = (\chi r_H)/(\chi r_C)$.

$\chi r_{CH,thresh} = \chi r_{H,thresh}$. What we are left with from Figure 3.14 is a single plot of $\chi r_{H,thresh}$ vs. $\overline{\phi}_C$, giving the $d = d_0$ threshold as

$$\chi r_{H,thresh} = 1.3\overline{\phi}_C + 0.75. \tag{3.11}$$

What Eq. 3.11 says is that the balance required to obtain $d = d_0$ is governed by two effective parameters: the product of the Flory interaction parameter and the size of the homopolymer, χr_H, and the copolymer volume fraction of the blend, $\overline{\phi}_C$. With the results we have found to date, the dependence on these three parameters is not surprising. The χ and r_H parameters both influence the "biased random walk" of the homopolymer in Eq. 2.61. This biasing of the homopolymer must be just right – too great and too much homopolymer is expelled from the interphase resulting in an increase in domain thickness, not enough and the homopolymer reduces the thickness by diluting the interphase and thus the segregation of the copolymer blocks. As for the $\overline{\phi}_C$ dependence, we do find even from the high-f_H result that there is a weaker variation in behaviour due to $\overline{\phi}_C$.

How does this result compare to the $f_H \simeq 1/5$ result obtained from the Many-Wave Approximation? Initially, one might speculate "not well". However, to look at the weak-segregation limit of Eq. 3.11 we consider $\overline{\phi}_C \to 1$ and $\chi r_C = 10.5$, representing the extreme of weak segregation. Re-expressing Eq. 3.11 as

$$f_{H,thresh} = \frac{1}{\chi r_C}(1.3\overline{\phi}_C + 0.75), \tag{3.12}$$

we see that these values would yield a $f_{H,thresh}$ of 0.19 – very much in agreement with the MWA result.

This may suggest that the MWA combined with the fourth-order energy approximation is still restricted to the weak-segregation limit and that the dependencies on $\overline{\phi}_C$ and χr_C are due to higher order effects, or perhaps it simply suggests that the MWA investigation did not probe a wide enough range of $\overline{\phi}_C$ and χr_C values to expose these dependencies.

When referring back to Figures 3.5 through 3.9, one might be sceptical about the strength of the threshold's dependence on $\overline{\phi}_C$ as implied by Eq. 3.11. Certainly, in these figures the lines seem more tightly "pinched" at a specific f_H, particularly in Figure 3.5, than Eq. 3.11 would suggest. The explanation for this is simple: the f_H at which the tightest overlap of the various d/d_0 vs. f_H lines occurs does *not* correspond to $d/d_0 = 1$, but rather a d/d_0 which is marginally less than 1. As the lines in Figure 3.5 ascend across the $d/d_0 = 1$ horizontal, they have already "fanned out" from the pinch, resulting in a spread of intercepts such as clearly seen in Eq. 3.11.

It is interesting that the closest crossing of the d/d_0 vs. f_H curves of Figures 3.5 through 3.9 should occur at a d marginally small than d_0. By definition, this closest crossing is where the domain thickness is least influenced by variations in $\overline{\phi}_C$. If it were the case that d/d_0 were independent of $\overline{\phi}_C$ altogether, then d/d_0 should be 1 since it is so at $\overline{\phi}_C = 1$. However, its marginal offset of d to slightly less than d_0 implies that the interphase is slightly diluted before d becomes independent of further additions of homopolymer. Initially, perhaps the first fraction of homopolymer introduced to the system does distribute so as to screen the system marginally. From *there*, additional homopolymer of this special f_H value has no further effect on the domain thickness.

The notion that the initial fraction of homopolymer introduced should have a different effect than the subsequent addition of homopolymer has already been seen in Figure 3.13. There, the first homopolymer also appeared to relieve the interphase's A-B interaction marginally, retarding the increase of domain thickness from what it would be if the homopolymer were fully segregated as the high-f_H trend tells us to expect. Here, we seem to be seeing a similar effect.

Table 3.2 enumerates the nearest-crossing of the d/d_0 vs. f_H lines in Figures 3.5 through 3.9. The relation between this nearest-crossing value of f_H and χr_C is not as

χr_C	f_H *at crossing*	d/d_0 *at crossing*
15	0.117	0.999
20	0.075	0.993
30	0.045	0.990
40	0.029	0.970
50	0.023	0.960

Table 3.2: Values of f_H at which domain thickness exhibited the least dependence on $\overline{\phi}_C$.

simple as in Eq. 3.11. The best fit to the results in Table 3.2 was the scaling relation

$$f_{H,cross} \;=\; 4.50(\chi r_C)^{-1.36}. \tag{3.13}$$

For comparison with the MWA, in the $\chi r_C = 10.5$ MST limit we note that $f_{H,cross}$ would be approximately 0.18, which is again in good agreement with the simpler MWA prediction of a threshold of $f_H \simeq 1/5$. The agreement between $f_{H,cross}$ and $f_{H,thresh}$ would seem to wane, however, as χr_C increases. This can be attributed to the fact that the crossing point as shown in Table 3.2 occurs further and further away from the $d = d_0$ horizontal as χr_C increases. Physically, it would seem then that the screening influence due to the initial introduction of small amounts of homopolymer is more profound as χr_C increases.

Ultimately, then, NSCF appears to reveal more complex dependencies around the threshold value of f_H where $d \simeq d_0$. However, it is reassuring that the more basic results of the earlier MWA threshold investigation can be recovered in the MST limit.

3.4 Subdomain Thickness

In Ref. [3], Banaszak and Whitmore considered the individual variations of the thicknesses of both subdomains, d_A and d_B, in addition to the total domain thickness, d. There, the subdomain boundary was defined as the offset within the cell, x_{bound}, such that $\phi_A(x_{bound})$ was an inflection point. [28] We use an analogous criterion in the present investigation. In the case of more than one inflection point, e.g. as seen in Figure 3.11, we use the inflection point closest to the centre of the B subdomain.

The physical significance of this inflection point is that the local volume fraction $\phi_A(x)$ has reached its steepest descent, with the B species beginning to dominate. This would mark a meaningful termination of the A subdomain, as $\phi_A(x)$ to the right of this boundary will have a positive curvature – a decay-like shape – signifying the decaying penetration of species A into subdomain B, as may happen in weak segregation. As documented in Chapter 5 we found that for $\epsilon_\kappa = 1$ this point of inflection also coincides with the most-probable location of the copolymer joints. Thus, this should serve as a satisfying definition of the A-B subdomain boundary.

With this definition, we are now clear to consider trends in subdomain thickness. As mentioned above, Ref. [3] chose to focus on d_A and d_B. These results were calculated in the NSCF formalism in panels (b) and (c) of Figure 3.1. Both Ref. [3] and our present Figure 3.1 fail to exhibit intuitive trends, particularly in d_B. This is likely due to the complex interplay of effects on d_A and d_B including:

1. As is well-known d_0 has a scaling dependence on χr_C. [1, 2, 9, 10]

2. As seen in Sections 3.2 and 3.3, d/d_0 has a dependence on both f_H and $\overline{\phi}_C$, increasing or decreasing with $\overline{\phi}_C$ according to the choice of f_H.

3. The relative position of the subdomain boundary within the unit cell, given by

d_A/d, has a yet-unspecified dependence on system parameters.

Since d_A is a result of these three factors and d_B is given by $d_B = d - d_A$, it is easy to understand why the subdomains' behaviours may be more complex.

Furthermore, items 2 and 3 above seem intimately intertwined. We have observed that whether d/d_0 increases or decreases with $\overline{\phi}_C$ depends on f_H. The proposed mechanism for this dependence is the degree to which a specific choice of f_H allows the homopolymer to penetrate the B subdomain (or, conversely, the degree to which it results in the homopolymer localising in the middle of the A subdomain). When homopolymer is localised in the A subdomain as in Figure 3.11, it will tend to shift the relative boundary d_A/d to the right, enlarging d_A. When the homopolymer penetrates the A and B subdomains more equally, as in Figure 3.10, there is no such bias and so the d_A/d boundary remains in largely the same location as it would be in the neat copolymer case.

From this perspective it seems logical to consider how the relative boundary position, d_A/d, varies alone with system parameters as this dependence is likely to be simpler than d_A's dependence. With a clear understanding of this relation, we can combine our prior understanding of d_0 and d/d_0's dependence on system parameters, to determine the behaviour of d_A and d_B.

This investigation was undertaken for 683 successfully-converged NSCF calculations which yielded microphase-separated results, including all the converged, inhomogeneous results from those systems tabulated in Table 3.1. It was found that, like the f_H thresholds discussed in Section 3.3, d_A/d effectively depended on only two parameters: χr_H and $\overline{\phi}_C$. Figure 3.15 plots the results of this investigation.

The results in Figure 3.15 follow a very systematic progression. At $\chi r_H = 0$, we have $f_H \to 0$ which is the now-familiar good solvent limit. Since we are considering only systems where $f_A = f_B$ and $\epsilon_\kappa = 1$, a neat system with such parameters is perfectly

(a)

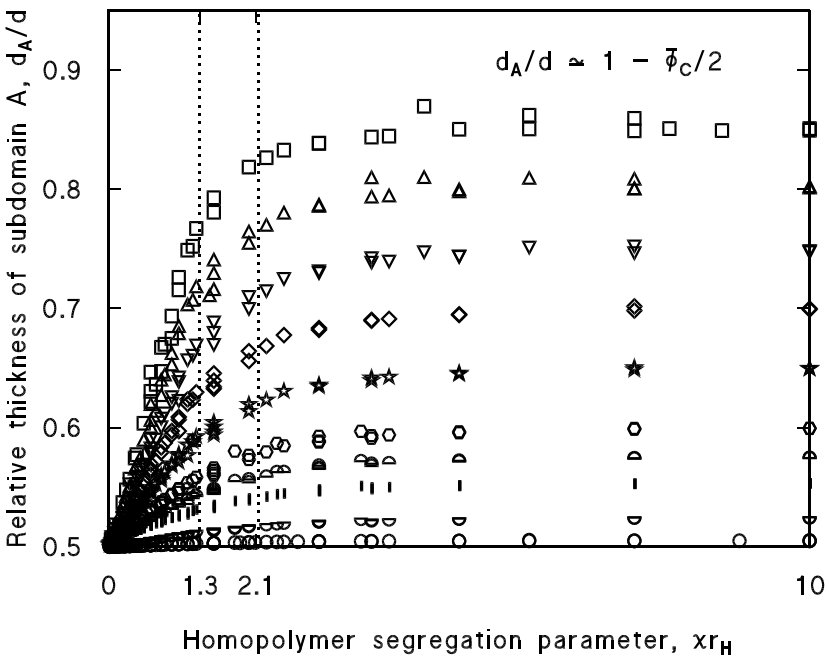

(b)

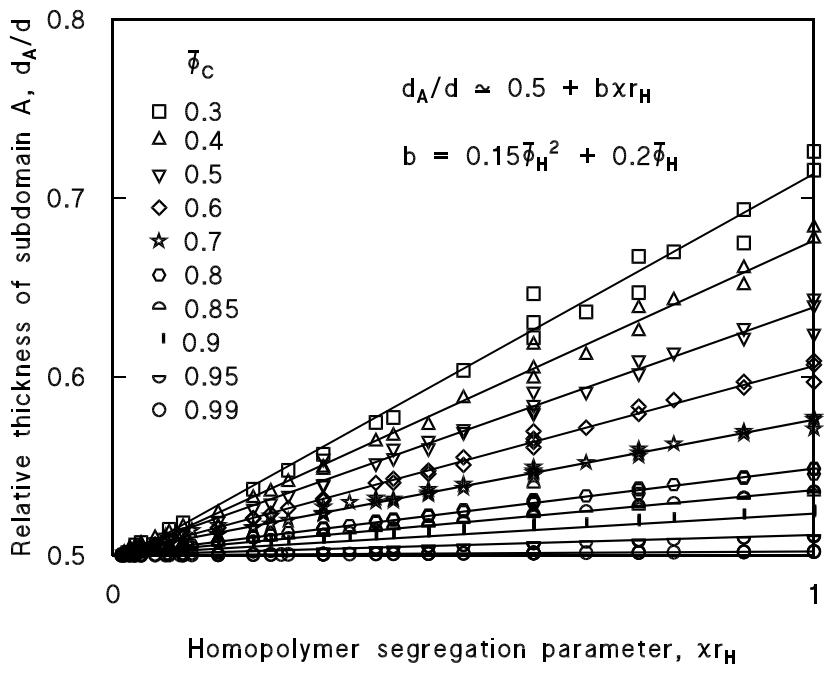

Figure 3.15: Relative thickness of subdomain A as a function of system parameters. (a) 683 data points have been plotted including all converged, inhomogeneous solutions for systems enumerated in Table 3.1. For comparison, the $d = d_0$ threshold range of χr_H given by Eq. 3.11 has been marked, with the left-hand dashed vertical line at $\chi r_H = 1.3$ corresponding to the threshold in the $\overline{\phi}_C \to 0$ limit and the right-hand line at $\chi r_H = 2.1$ indicating the $\overline{\phi}_C \to 1$ threshold limit. (b) shows a magnification of the results below $\chi r_H = 1$, where the d_A/d dependence on χr_H is well-represented by a linear fit.

symmetric and so it should follow that $d_A = d_B$ giving $d_A/d = 0.5$. For a good solvent, homopolymer is distributed homogeneously in the system, adding to both subdomains in equal measure. Thus, in the $f_H \to 0$ limit, we should expect that $d_A/d = 0.5$ irrespective of the choice of $\overline{\phi}_C$.

Moving away from $f_H \to 0$ and considering small values of χr_H (e.g. less than 1), d_A/d exhibits a nearly-linear dependence on χr_H, and so obeys the relation

$$d_A/d \;=\; 0.5 + b\chi r_H \quad \text{if } \chi r_H \lesssim 1, \tag{3.14}$$

where b is a constant of proportionality that increases monotonically with $\overline{\phi}_C$.

In the large χr_H limit, d_A/d plateaus to

$$d_A/d \;\simeq\; 1 - \overline{\phi}_C/2 \quad \text{if } \chi r_H \gtrsim 2. \tag{3.15}$$

This later result is exactly what one would expect for a system where the homopolymer had been completely expelled from the B subdomain. Given that block B accounts for $\overline{\phi}_B$ of the total volume of the cell, if all of block B were concentrated into a discrete, exclusive volume within the cell, then that volume would have width $d_B = \overline{\phi}_B d$. The complementary volume d_A is then $1 - \overline{\phi}_B d$, but $\overline{\phi}_B$ is by definition simply $\overline{\phi}_C f_B$. In our investigation, $f_B = \frac{1}{2}$ leading precisely to Eq. 3.15.

Interestingly, the intermediate values of χr_H wherein the transition from Eq. 3.14 to 3.15 occurs are the same values at which the $d = d_0$ threshold can be found. It is this transitionary state that likely causes the balance necessary to achieve the non-trivial $d = d_0$ condition for blends. As this transition occurs very roughly in the $1 \lesssim \chi r_H \lesssim 2$ range independent of $\overline{\phi}_C$, the constant of proportionality, b, in Eq. 3.14 would appear simply to be the one that brings d_A/d vs. χr_H sufficiently close to the asymptotic limit of Eq. 3.15 by the time χr_H reaches the transition range. (Aside from its monotonic increase with $\overline{\phi}_H$, the equation for b given in Figure 3.15 is not quantitatively significant as it represents a fit to the data with an artificial cut-off of $\chi r_H \leq 1$.)

In summary, then, we find that Figure 3.15 illustrates precisely the shift hypothesised in Section 3.2, with homopolymer starting out homogeneously distributed in small f_H limits and ending up localised in the middle of the A subdomain in the high f_H limit. This figure also provides a clear systematic way to understand the dependence of d_A on system parameters.

Chapter 4

Phase Behaviour

4.1 Microphase Separation Transition

The microphase separation transition (MST) defines a bound on system parameters outside of which no ordered structures such as lamellae, cylinders, spheres, etc. are observed. The absence of these structures physically is due to them not being energetically favourable. In the numerical results, this will happen when the NSCF equations in an ordered symmetry produces solutions with positive relative free energy. A positive Δf would indicate that the ordering is a higher energy state than the disordered homogeneous state of the system. If the disordered state has the lowest free energy, then it will be the stable equilibrium state of the system.

When a variation of a system parameter causes the relative free energy of an ordered solution of the NSCF equations to go positive, then we have a "first-order transition". A first-order transition is so-called because the first-order derivative of the free energy at the transition is non-zero when evaluated with respect to the system parameter being varied.

In neat copolymer systems, a first-order transition happens whenever we make the transition from order to disorder by lowering χr_C when $f_A \neq f_B$. [1]

Another way to achieve the transition to a disordered phase is if the free energy goes smoothly to zero. This would be the case if altering a system parameter resulted in the amplitude of the variations in $\phi_A(\boldsymbol{r})$ and $\phi_B(\boldsymbol{r})$ decaying smoothly to zero. In this

smooth decay to zero, there would be no positive Δf solution of the NSCF equations. Rather, Δf would go smoothly to zero as well. Thus, Δf's first-order derivative with respect to the varied system parameter would be zero. Naturally, then, this is termed a second-order transition.

In neat copolymer systems in the mean field theory, crossing the MST by lowering χr_C when $f_A = f_B$ is a second order transition. [1] That is, lowering χr_C on a symmetric copolymer will cause the density variations $\phi_A(\boldsymbol{r})$ and $\phi_B(\boldsymbol{r})$ to decay smoothly to zero.

In a copolymer-homopolymer blend, the notion of first-order and second-order transitions is the same, only now $\phi_H(\boldsymbol{r})$ must also be considered in the decay to homogeneity.

For the present data set as summarised in Table 3.1, we have three ways to cross the MST boundary: by varying χr_C, by varying f_H, and by varying $\overline{\phi}_C$. We know from neat copolymer investigations that decreasing χr_C in a symmetric copolymer induces a smooth second-order transition to homogeneity. The parameter f_H is not one that can be varied dynamically. This leaves only $\overline{\phi}_C$ of remaining interest in considering the MST in copolymer-homopolymer blends.

For each chosen combination of χr_C and f_H in our data set, we have considered Δf vs. $\overline{\phi}_C$. The intent is to extrapolate this curve to locate the value of $\overline{\phi}_C$ such that $\Delta f_{\chi r_C, f_H}(\overline{\phi}_C) = 0$.

Using the 0.1 steps in $\overline{\phi}_C$ from the original data set is far too crude a step to obtain a reliable extrapolation. However, by using the crude extrapolation from this method (where a third-order polynomial is fitted to the lower four or five values of $\overline{\phi}_C$ that yielded non-trivial Δf's) we can find a coarse value for $\overline{\phi}_C$ at the MST which can then be used to guide further NSCF calculations, now using 0.01 steps in $\overline{\phi}_C$ to approach the MST boundary. Repeating the extrapolation method for the last few 0.01-stepped values of $\overline{\phi}_C$ before the MST, we obtained a satisfactory extrapolation of $\overline{\phi}_C$ at MST.

The first and most striking feature of these results was that, to numerical precision,

all approaches to MST appeared to be second-order. The first, coarse 0.1-stepped initial plot of Δf vs. $\overline{\phi}_C$ sometimes gave a curve of positive curvature which, when extrapolated, had a very significant slope as it crossed $\Delta f = 0$. One might have easily concluded the transitions were first order. However, the finer 0.01-stepped result revealed that Δf quickly reversed curvature to meet $\Delta f = 0$ smoothly – within expected numerical error – as MST was approached.

This observation is reinforced by the fact that at no time in any NSCF calculation was a lamellar solution obtained that had positive free energy. Such an occurrence would have been indicative of a first-order transition. However, in the nearly 1500 data sets investigated – both for those tabulated in Table 3.1 and as supplemental explorations – this was never observed.

Consquently, it can be stated that for all systems investigated, the $\overline{\phi}_C$-induced MST is a second-order transition. The specific results for MST are tabulated in Figure 4.1.

In potential opposition to this result, the work of Fredrickson and Leibler suggests that the MST transition in a blend of copolymer and *neutral* solvent may be very weakly first-order for the $f_A = f_B = \frac{1}{2}$ case. [29] To the extent that our homopolymer is a good solvent, one may expect a comparable result here. However, the contribution which makes the transition first-order is of order $1/r_C$, meaning that it would disappear as $f_H \to 0$. Away from $f_H \to 0$, we are no longer considering a good solvent, and so Fredrickson and Leibler's formalism would not apply. Specifically, their formalism uses a finite truncation of free energy and so its validity would be called into question for high-f_H profiles such as Figure 3.11. Our numerical results indicate that such profiles are not well-represented by a many-wave approximation even as MST is approached. Nonetheless, it is not possible to rule out a weak first-order transition strictly from our numerical results.

Returning to Figure 4.1, the $\chi r_C = 50$ boundary could not be calculated as it was not possible to coarse-step near enough to the MST to get a meaningful extrapolation. When

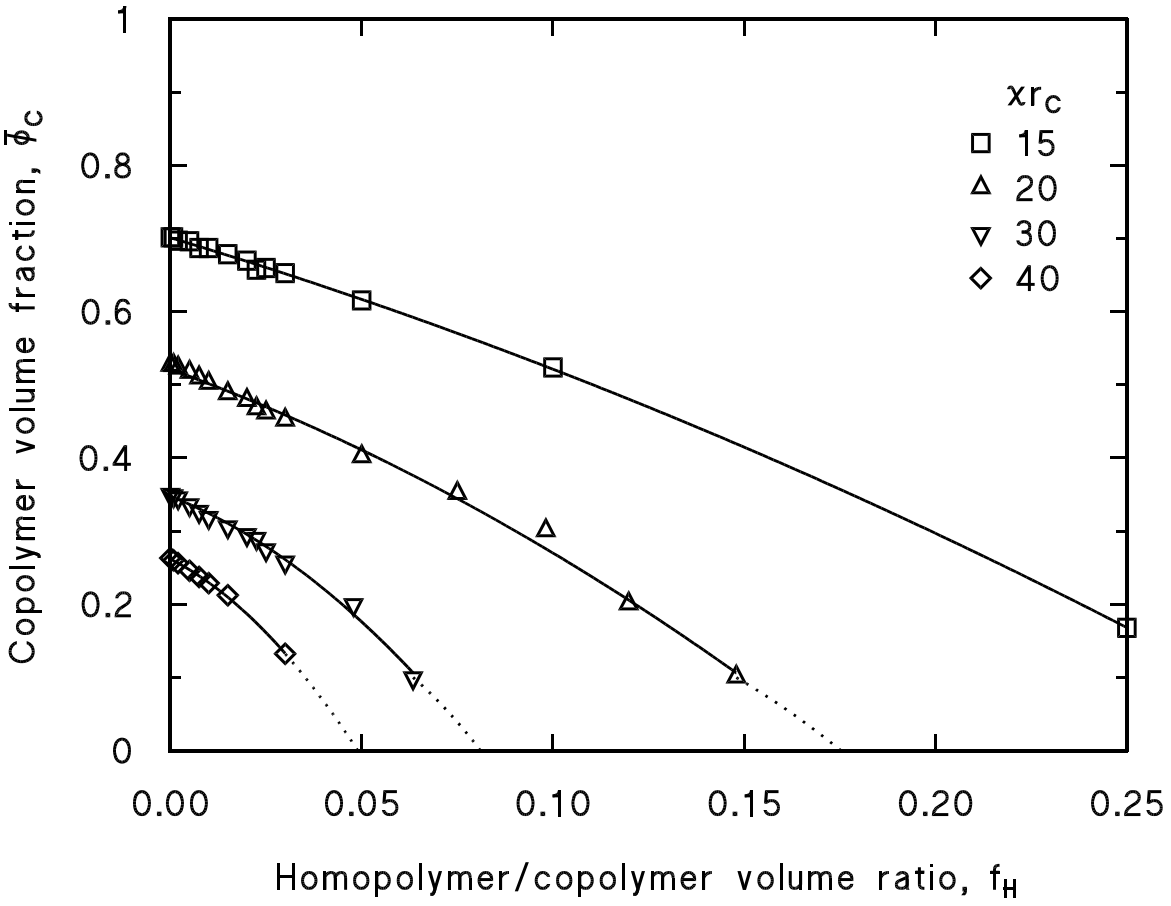

Figure 4.1: Microphase separation transition boundaries for various χr_C. The dashed lines indicate extrapolated boundaries. The χr_C=50 boundary could not be calculated as it was not possible to get the NSCF calculations to converge for $\overline{\phi}_C < 0.2$.

$\overline{\phi}_C$ descended below 0.2 for χr_C, many times the density profiles were *extremely* strongly segregated as a result of an overwhelming tendency for the homopolymer to localise in the middle of the A subdomain. The B subdomain was thus quite minute with $d_B < 0.1d$ as expected by Eq. 3.15. The small width and step-like behaviour of $\phi_B(\boldsymbol{r})$ could not be suitably resolved by the numerical methods employed.

However, with the $15 \leq \chi r_C \leq 40$ boundaries, we do see a clear trend. Increasing χr_C naturally tends the system to stronger segregation, and so, if hoping to reach the MST by the addition of homopolymer to the blend, one must add more homopolymer to compensate as χr_C increases, or else use smaller homopolymer molecules to increase its effectiveness as a good solvent wherein it will dilute the copolymer and thus reduce its effective interaction, χr_C.

The $f_H \to 0$ intercept of the MST boundary falls in line with the results of the previous copolymer-solvent blend investigations. [9, 10] To the extent that $f_H \to 0$ represents a good solvent, the $f_H \to 0$ MST results are also analogous to the dilution approximation. By extension, it would seem that the perturbations in the MST found in Ref. [9] were a consequence of the finite size of the solvent molecule (i.e. f_H was small but non-zero). Ref. [9] indicated that the perturbation of the MST was more prevalent as the size of the copolymer decreased. This is consistent with the present result, as even for $r_H \ll r_C$, as the copolymer decreases in size, the approximation that $f_H = r_H/r_C \simeq 0$ becomes less accurate. So, to map real solvents into the copolymer-homopolymer formalism, one should select a small but non-zero f_H to represent the true ratio of the solvent and copolymer molecule sizes.

4.2 Macrophase Separation

Macrophase separation can occur when it is more energetically favourable that a copolymer-homopolymer blend exist as two distinct systems rather than as a single blend. The most simplistic example of macrophase separation is where it is more energetically favourable that the homopolymer and copolymer remain entirely unmixed. Macrophase separation can occur when it is energetically favourable for a system to evolve into a separated state.

How might a system evolve into a separated system? Consider a system of volume V containing a copolymer-homopolymer blend with a copolymer volume fraction of $\overline{\phi}_C$. Cut this volume artificially into two sub-volumes, V_1 and V_2. V_1 and V_2 will have indistinguishable content. However, consider if some small volume of copolymer molecules, say Δv, were to migrate from V_1 to V_2. Homopolymer would also have to pass from V_2 to V_1 to conserve volume. The new volume fraction of copolymer in volumes V_1 and V_2 respectively would be

$$\overline{\phi}_{C,1} = \overline{\phi}_C - \Delta v/V_1, \tag{4.1}$$

and

$$\overline{\phi}_{C,2} = \overline{\phi}_C + \Delta v/V_2. \tag{4.2}$$

This new state will be stable relative to the original state if

$$V f(\overline{\phi}_C) > V_1 f(\overline{\phi}_{C,1}) + V_2 f(\overline{\phi}_{C,2}). \tag{4.3}$$

Here, f represents the free energy density of a system of the specified copolymer volume fraction with constant, implicit values of χr_C, ϵ_κ, and f_H. The left-hand side of Eq. 4.3 represents the total free energy of the combined system before the migration, and the right-hand side represents the sum of the free energy contributions from the volumes

V_1 and V_2 respectively after the migration. If the new state is of lower free energy for infinitesimally small Δv, then we have an avenue wherein the system macrophase separates.

By induction, for finite Δv we can have an avenue for macrophase separation if Eq. 4.3 holds true for all $\overline{\phi}_C$ such that $\overline{\phi}_{C,1} < \overline{\phi}_C < \overline{\phi}_{C,2}$. This does leave ambiguity in that V_1 and V_2 are unknown. However, with some algebra it is possible to obtain a practical numerical test for macrophase separation. One begins by noting that, by definition, $V_1 = V - V_2$. Substituting this into Eq. 4.3 and collecting V terms to the left and V_2 terms to the right, we have

$$V[f(\overline{\phi}_C) - f(\overline{\phi}_{C,1})] \;>\; V_2[f(\overline{\phi}_{C,2}) - f(\overline{\phi}_{C,1})]. \tag{4.4}$$

Further, Eqs. 4.1 and 4.2 may be rearranged to give

$$V_1 \;=\; \frac{\Delta v}{\overline{\phi}_C - \overline{\phi}_{C,1}}, \tag{4.5}$$

and

$$V_2 \;=\; \frac{\Delta v}{\overline{\phi}_{C,2} - \overline{\phi}_C}. \tag{4.6}$$

By multiplying both sides of Eq. 4.4 by V/V_1 and substituting the above expressions for V_1 and V_2, we ultimately obtain

$$\frac{f(\overline{\phi}_C) - f(\overline{\phi}_{C,1})}{\overline{\phi}_C - \overline{\phi}_{C,1}} \;>\; \frac{f(\overline{\phi}_{C,2}) - f(\overline{\phi}_{C,1})}{\overline{\phi}_{C,2} - \overline{\phi}_{C,1}}. \tag{4.7}$$

Both the left-hand and right-hand sides of this inequality are slopes of chords on f vs. $\overline{\phi}_C$. The left-hand side represents a chord from $\overline{\phi}_{C,1}$ to $\overline{\phi}_C$ and the right-hand side represents a chord from $\overline{\phi}_{C,1}$ to $\overline{\phi}_{C,2}$. This inequality requires that slope of the line joining $f(\overline{\phi}_{C,1})$ and $f(\overline{\phi}_{C,2})$ on the f vs. $\overline{\phi}_C$ graph be less than the slope of a line joining $f(\overline{\phi}_{C,1})$ to any intermediate point between $\overline{\phi}_{C,1}$ and $\overline{\phi}_{C,2}$. Such a condition is satisfied when $f(\overline{\phi}_C)$ for all intermediate points lie above the chord between $\overline{\phi}_{C,1}$ and $\overline{\phi}_{C,2}$.

Thus, macrophase separation can proceed to the most extreme values of $\overline{\phi}_{C,1}$ and $\overline{\phi}_{C,2}$ which satisfy this condition. These extreme values are obtained by finding the tangent to the curve f vs. $\overline{\phi}_C$ which touches at $\overline{\phi}_{C,1}$ and $\overline{\phi}_{C,2}$ where $\overline{\phi}_{C,1} < \overline{\phi}_C < \overline{\phi}_{C,2}$. This defines the *binodal* and is the binary blend equivalent of the condition stated in Ref. [19] for ternary blends.

The bottom line of this derivation is that it is not possible to determine whether macrophase separation will occur by doing a single NSCF calculation for the target system's parameters. Instead, we must know what the f vs. $\overline{\phi}_C$ dependence is around the target system.

The free energy density, f, may be regarded to have three components. In Section 2.3 we resolved the free energy into a homogeneous component, f_{hom} and a relative component Δf. The homogeneous component may be further resolved into a free energy of mixing, f_{mixing} and a demixed component $f_{demixed}$. The demixed component is the free energy of a system which has had the homopolymer completely separated from the copolymer. As such, it may be regarded as two homogeneous systems – one of volume $\Omega' = \overline{\phi}_C\Omega$ and $\overline{\phi}_C{}' = 1$ and the other with volume $\Omega' = \overline{\phi}_H\Omega$ and $\overline{\phi}_C{}' = 0$. The free energy of mixing, then, would be given by the difference between f_{hom} for the blend, and f'_{hom} for the two separated systems. Explicitly, using Eq. 2.55 this comes out to be

$$\begin{aligned} f_{mixing} &= f_{hom}(\Omega, \overline{\phi}_C) - f_{hom}(\overline{\phi}_C\Omega, 1) - f_{hom}(\overline{\phi}_H\Omega, 0), \\ &= \frac{k_BT}{r_C}\Big\{\overline{\phi}_C \ln \overline{\phi}_C + \frac{\overline{\phi}_H}{f_H} \ln \overline{\phi}_H + \sum_{\kappa\kappa'} \chi_{\kappa\kappa'} r_C \bar{\phi}_\kappa \bar{\phi}_{\kappa'}\Big\}, \end{aligned} \tag{4.8}$$

where various relations such as Eqs. 2.58 and 2.67 have been used to simplify the expression. And so, for a given set of $\chi_{\kappa\kappa'}r_C$'s and f_κ's, we have an analytic expression for f_{mixing} vs. $\overline{\phi}_C$.

It is the sum of f_{mixing} and Δf that we must consider in evaluating Eq. 4.7. Unfortunately, each NSCF calculation obtains the energy of microphase separation, Δf, for only

a single value of $\overline{\phi}_C$ (in combination with specific choices for the other system parameters). To do a sufficiently detailed Δf vs. $\overline{\phi}_C$ plot, one needs in the neighbourhood of 100 points. As this would need to be done for each selected value of χr_C and f_H tabulated in Table 3.1, we would ultimately have to consider 7500 NSCF calculations – likely more if the $0.1 < f_H < 0.5$ range requires further detailing – which is a prohibitively large number for this investigation.

For the current results, however, it is possible to get something of a qualitative glimpse of the macrophase separation behaviour, leaving the more intense quantitative study for later investigation should it be warranted. The results in Table 4.1 were obtained by generating a 3^{rd}-order polynomial fit to each of the 75 candidate Δf vs. $\overline{\phi}_C$ curves. The 3^{rd}-order fit proved largely sufficient for the coarse-stepping of $\overline{\phi}_C$ noted in Table 3.1. For each given f_H and χr_C, an approximate f vs. $\overline{\phi}_C$ relation was obtained as

$$f(\overline{\phi}_C) = f_{mixing}(\overline{\phi}_C) + a_3\overline{\phi}_C{}^3 + a_2\overline{\phi}_C{}^2 + a_1\overline{\phi}_C + a_0, \tag{4.9}$$

where a_i represent the coefficients of the polynomial fit to $\Delta f(\overline{\phi}_C)$. (N.B. this fit differs from that used in Section 4.1 as it is over the full range of $\overline{\phi}_C$, and so the coefficients here are not suitable for resolving a precise MST.) A small iterative program was then developed which stepped through all values of $\overline{\phi}_{C,1}$ and $\overline{\phi}_{C,2}$ (in steps of $\Delta\overline{\phi}_C = 0.001$) in an attempt to find the most extremal values which satisfied Eq. 4.7. In many cases, no binodal was found. Those that were found are summarised in Table 4.1.

Though precision finer than 0.1 is likely not quantitatively meaningful, some features were still apparent:

1. Macrophase separation is more common as f_H increases.

2. As χr_C increases, the minimum value of f_H at which macrophase separation occurs, decreases.

	$\chi r_C = 15$		$\chi r_C = 20$		$\chi r_C = 30$		$\chi r_C = 40$		$\chi r_C = 50$	
f_H	$\overline{\phi}_{C,1}$	$\overline{\phi}_{C,2}$	$\overline{\phi}_{C,1}$	$\overline{\phi}_{C,2}$	$\overline{\phi}_{C,1}$	$\overline{\phi}_{C,2}$	$\overline{\phi}_{C,1}$	$\overline{\phi}_{C,2}$	$\overline{\phi}_{C,1}$	$\overline{\phi}_{C,2}$
0.075							0.077	0.329	0.059	0.384
0.100					0.103	0.321	0.060	0.428	0.029	0.521
0.250	0.204	0.334	0.124	0.469	0.110	0.538	0.111	0.571	0.059	0.659
0.500	0.180	0.553	0.171	0.597	0.174	0.645	0.179	0.675	*	*

Table 4.1: Binodals of macrophase separation. No binodals were found for $f_H \leq 0.05$. A binodal is believed to exist for $\chi r_C = 50$, $f_H = 0.5$, however the polynomial fit was believed inadequate for interpolation. Due to the lack of sufficient data points, there may be considerable uncertainty in these boundaries.

3. For a given f_H, the width of the binodal, $\overline{\phi}_{C,2} - \overline{\phi}_{C,1}$, increases with χr_C.

4. The upper endpoint of the binodal, $\overline{\phi}_{C,2}$, seems more significantly impacted by an increase in χr_C than the lower endpoint.

All four of these phenomena appear consistent with the results of Ref. [30].

It is not surprising that the phenomenon of macrophase separation should occur at larger values of f_H, and more easily as χr_C increases. As described in Section 3.2, as f_H increases, the homopolymer becomes completely expelled from the B subdomain (see Figure 3.11). There is a "strain" on the A copolymer as it is forced to curl up closer to the interphase as a result of the homopolymer crowding the centre of the A subdomain. This causes both an entropic deficit and also an increase in the interaction energy. It is not surprising that when this phenomenon becomes sufficiently extreme, macrophase separation will occur.

It is also not surprising that increasing χr_C should decrease the minimum f_H required to induce macrophase separation. The increased values of χr_C would increase the forces that expel the homopolymer from subdomain B. This increases the bias of the random walk in Eq. 2.61 (discussed further in Section 3.2), and so the homopolymer

could reach deeper into the centre of the A subdomain in fewer steps – i.e. with a smaller homopolymer, which means a smaller f_H.

It is interesting to note how the upper endpoint of the binodal appears more impacted by increase in χr_C than the lower endpoint. One might hypothesise that the upper endpoint, representing a smaller fraction of homopolymer in the system, has greater flexibility in the distribution of homopolymer than the system represented by the lower $\overline{\phi}_C$ endpoint which has a higher $\overline{\phi}_H$. The greater flexibility allows for lower homopolymer content to migrate more easily to the middle of the A subdomain.

Of particular note is the fact that Banaszak and Whitmore's MWA predicted that macrophase separation in binary blends can only occur above $\chi r_H \gtrsim 2$. [30] De Gennes derived the result that phase separation will also occur in symmetric homopolymer-homopolymer blends when $\chi r_H \gtrsim 2$. [27] From Section 3.4, we found that this is the same condition under which expulsion of the homopolymer from the B subdomain in a copolymer-homopolymer blend is roughly complete. This cut-off is consistent with the results in Table 4.1 and would appear quite robust.

Overall, it does appear that the migration of homopolymer to the A subdomain is the precursor to macrophase separation, and that it occurs primarily due to the resulting energy and entropy impact of the coiling of the copolymer's A block toward the interphase and the repulsive B subdomain.

4.3 A Note on Other Morphologies

While in neat copolymer systems, $f_A = f_B$ guarantees that the microphase will exhibit a lamellar morphology, [1, 7, 8] such an assumption cannot be counted upon in the present case of copolymer-homopolymer blends. In fact, it has been verified experimentally that even for copolymers wherein $f_A \simeq f_B$, the cylindrical morphology is possible. [26]

The numerical methodology of this investigation does not have the stamina to resolve the full 3-D form of the NSCF equations given in the conclusion of Section 2.2 with the requisite degree of precision. Previous investigations employed the "unit-cell approximation" (UCA) to probe cylindrical and spherical morphologies. [1, 20] In this approximation, instead of the hexagonal unit cell that accomplishes close-packing in the cylindrical morphology, a cylindrical cell is considered. Like the proper Wigner-Seitz cell, this UCA cell will have mirrored boundary conditions (e.g. $\phi_A(R+r) = \phi_A(R-r)$). By enforcing a higher symmetry, only the radial variation in the NSCF equations need be considered, which effectively reduces the exercise to a 1-D problem.

A similar replacement of the body-centred-cubic cell for the spherical morphology with a mirror-bounded spherical cell is used to reduce the spherical morphology to 1-D.

The equilibrium morphology is determined by solving the NSCF equations in these three different symmetries and comparing the resulting free energy density. The lowest free energy density is considered the equilibrium morphology.

While the mirrored boundary conditions are expected, the deformation of the unit cell from hexagon to cylinder or *bcc* to sphere is known to cause some discrepancy in the results. [31] However, the UCA is still a good first approximation which can help to distinguish the equilibrium morphologies.

In our present data set, there is cause to believe morphologies other than lamellae may result. In the more strongly segregated systems where both χr_C and f_H are high,

the ratio of the B subdomain to the whole domain thickness is effectively $\overline{\phi}_C f_B$. (See, for example, Figure 3.11.) In neat copolymer systems, when there is high asymmetry between the thickness of subdomain A and thickness of subdomain B, cylinders and spheres are likely morphologies.

We thus looked at two representative "strong segregation" cases within our current data set and used the UCA to solve the NSCF equations in the cylindrical symmetry. In the system $\chi r_C = 40$, $\overline{\phi}_C = 0.3$, $f_H = 0.5$, the lamellar solution was still stable with respect to the cylindrical solution.

In the system $\chi r_C = 50$, $\overline{\phi}_C = 0.3$, $f_H = 0.25$, the cylindrical solution *was* energetically preferable to the lamellar solution.

While this is hardly a definitive study, the two systems in question were among the more extremely segregated from those in the investigated data set. Yet, in the $\chi r_C = 40$ case lamellae maintained their dominance over cylinders, and only in the extremes of high-f_H in the $\chi r_C = 50$ case did cylinders begin to appear.

This should alleviate some concern about the applicability of the range of parameters chosen for this investigation of lamellar behaviour, though one must remember that this result is specific to the $f_A = f_B = \frac{1}{2}$, $\epsilon_A = \epsilon_B = 1$ case considered here. The persistence of the lamellar phase will not be so robust in systems which do not have this special symmetry. [13]

Chapter 5

Homopolymer Localisation at the Copolymer Interphase

5.1 Fluorescence Decay Experiments

Experimentalists such as Winnik et al [32, 33, 34] have utilised fluorescence decay as a method of probing the details of structure within lamellar unit cells. The process involves the grafting of fluorescent dye molecules onto the copolymer and homopolymer chains. There are two species of tags: a donor and an acceptor. When an excited donor tag comes within proximity of an acceptor molecule, an energy transfer occurs between the donor and acceptor, causing a fluorescent emission – analogous to an electric spark. The rate depends on separation as r^{-6} and so decreases very rapidly with donor-acceptor separation, becoming virtually non-existent at ranges more than a couple nanometres.

Utilising this tool, Winnik et al conducted experiments which probed the amount of homopolymer localisation at the copolymer interphase. [32] They tagged the copolymer joints with an acceptor molecule and tagged each homopolymer randomly along its entire length with donor molecules. By observing the integrated intensity of fluorescent emissions, they intended to determine the degree to which homopolymer localised at the interphase.

Since the energy transfer is such a short-range effect, high values for this integrated intensity (referred to as the "quantum efficiency") will indicate close proximity between the copolymer joints and the homopolymer. Not surprisingly, the copolymer joints are expected to reside primarily at the interphase. And so, fluorescence decay experiments

provide a method to measure homopolymer localisation at the interphase.

Preliminary experiments showed a significant non-linear increase in quantum efficiency as $\overline{\phi}_C \rightarrow 1$. [32] The inference initially drawn was that the first quantity of homopolymer introduced to the system localised very preferentially at the interphase. This proposition is similar to the inferences drawn in Section 3.3, but to a much greater extreme. Unfortunately, it was later found that these results contained a significant systematic error, in that the polystyrene in the copolymer was contributing to the energy transfer, causing spurious emissions from the donors. When this source of error was identified, the experiments were repeated. At the time of this writing, preliminary results yielded quantum efficiencies much more in line with expected homopolymer distributions where there was little, if any, localisation at the interphase.

Nonetheless, these experiments do raise some interesting questions, and are the driving force behind the investigation covered in this chapter. In particular, one wishes to have an idealised theoretical model on which to base experimental expectations. If the model is successful in predicting experiment, then it will breed confidence in the model's usefulness as a tool in probing details of configuration within the unit cell.

The formalism for fluorescence decay requires continuous distributions of homopolymer and copolymer [33] as would be obtained from the NSCF calculations. So, if a continuous function can be obtained from the NSCF calculations for local joint concentration, we will have all of the aspects of the model necessary to predict the quantum efficiency for a given experimental system.

Recall from the NSCF derivation in Chapter 2 that, given a monomer of species κ in a polymer chain at location $\boldsymbol{r}$, the probability of finding a monomer τ steps further down the chain at $\boldsymbol{r}'$ will be given by the propagator $Q_\kappa(\boldsymbol{r}', \tau|\boldsymbol{r})$. In the NSCF equation for $\phi_\kappa(\boldsymbol{r})$, Eq. 2.63, we have then that the probability of finding monomer τ in chain κ

at $\boldsymbol{r}$ to be

$$P_\kappa(\boldsymbol{r},\tau) \quad \propto \quad q_\kappa(\boldsymbol{r},\tau)q'_\kappa(\boldsymbol{r},1-\tau), \tag{5.1}$$

where τ is now rescaled to be between 0 and 1 representing both extremes of the chain and q_κ and q'_κ are the solutions to the diffusion equation, Eq. 2.61, subject to the initial conditions given by Eqs. 2.48 and 2.62. The probability, then, of finding an A-B block joint at $\boldsymbol{r}$ is simply $J(\boldsymbol{r}) \equiv P_\kappa(\boldsymbol{r},1)$. Using Eq. 2.62 we find, then, that [28]

$$J(\boldsymbol{r}) \quad \propto \quad q_A(\boldsymbol{r},1)q_B(\boldsymbol{r},1), \tag{5.2}$$

regardless of whether we evaluate Eq. 5.1 using $\kappa = A$ or $\kappa = B$. This is reassuring as the probability of a joint being at $\boldsymbol{r}$ should be independent of whether we approached it from the A block or the B block.

Integrating Eq. 5.2 over $\boldsymbol{r}$, it is trivial to see that the constant of proportionality should be $1/Q_C$, where Q_C is given by Eq. 2.12. Thus we have an expression for the probability of finding a joint at some position $\boldsymbol{r}$ within a system. Multiplying this by the concentration of joints in the system (which is one per copolymer volume, or equivalently ρ_{ref}/r_C) gives the local concentration of joints in the system, which is the concentration required by the fluorescence decay formalism.

A more rigourous derivation of $J(\boldsymbol{r})$ from first-principles is also possible by calculating $< J(\boldsymbol{r}) >$. This would be done in the same manner as $< \hat{\rho}_\kappa(\boldsymbol{r}) >$ in Eq. 2.28. One would consider an integral over all possible configurations of the system and then introduce a delta-functional to restrict consideration to only those configurations where a joint passes through $\boldsymbol{r}$. After much tedious derivation analogous to the procedure in Chapter 2, one would eventually arrive at the same conclusion as the more intuitive approach above.

For the homopolymer distribution, it is much more straight-forward. We already have the volume fraction $\phi_H(\boldsymbol{r})$. The concentration is thus just the average monomer concentration for homopolymer, ρ_{0H}, multiplied by the local homopolymer volume fraction,

$\phi_H(\boldsymbol{r})$. (There may be need of an additional pre-factor of $1/n$ if there is only one donor tag per n homopolymer monomers, since it is actually donor concentration we need.)

In principle, this is all we need to calculate the precise fluorescence intensity decay curve which is integrated to get the quantum efficiency. [33] Practically speaking, though, this is a very difficult calculation to perform using numerical data for concentrations, as many nested integrals and exponentiations abound. The risk for amplification of numerical error is great.

Without reproducing the fluorescence decay formalism of Yekta et al in Ref. [33] here in its full detail, at the core of the problem is the Klafter-Blumen equation

$$\varphi(z_0,t) \;=\; \exp\Big\{-\int_V\{1-\exp[-tw(r)]\}C_A(z_0+z)\mathrm{d}V\Big\}. \tag{5.3}$$

Eq. 5.3 defines the survival probability as a function of time, t, of an excited donor located at z_0 in a system with an acceptor concentration of $C_A(z)$. V represents the system volume, with an integral over all three spacial co-ordinates, x, y, and z. Due to the lamellar symmetry of the system, concentration is expressed as a function only of the z co-ordinate (equivalent to our x co-ordinate). The function $w(r)$ contains the variation of rate with distance and is proportional to r^{-6} where $r^2 = x^2 + y^2 + z^2$.

If one makes the supposition that $C_A(z)$ is slowly varying on the scale at which there is significant energy transfer (i.e. a nanometre or two), then one could say $C_A(z_0 + z) \simeq C_A(z_0)$ over the effective range of r, and thus take $C_A(z_0)$ outside the integral. (N.B. a more robust approximation might be to consider the average $C_A(z)$ over a sphere of radius R_{max} centred on the point z_0. In such case, substitute this new sphere-averaged $\bar{C}_A(z)$ in the expressions that follow.)

If one assumes the above approximation, one can follow the Yekta et al formalism through its machinations and ultimately obtain an intensity decay curve which gives a

quantum efficiency, Φ_{ET}, of

$$\begin{aligned}\Phi_{ET} &= 1 - \frac{\int I_D(t)\mathrm{d}t}{\int I_D^0(t)\mathrm{d}t} \\ &= \sqrt{\pi}\int \mathrm{d}z\ \frac{C_D(z)}{\bar{C}_D} N_A(z)\ \exp[N_A(z)^2]\ \mathrm{erfc}\ N_A(z), \end{aligned} \tag{5.4}$$

where

$$N_A(z) = \frac{2}{3}\pi^{\frac{3}{2}} R_0^3 C_A(z), \tag{5.5}$$

and $C_D(z)$ is the concentration of donors at z, with a system-wide average concentration of $\bar{C}_D$. Here, the new parameter R_0 is the "Förster radius" – a characteristic scale parameter found in the definition of $w(r)$ which gives the fluorescence its effective ~ 2 nm cut-off.

What is interesting is if we further assume that $C_A(z)$ is much less than $1/R_0^3$ – that is, if the concentration of acceptors within the effective radius of a donor is small – then we will have $N_A(z) \ll 1$. This is a reasonable assumption given that $C_A(z)$ represents the number density of copolymer joints in our system, and a typical copolymer volume is several hundred cubic nanometres. With this condition, we have that $\exp[N_A(z)^2]\mathrm{erfc}\ N_A(z) \simeq 1$, and Eq. 5.4 reduces to the very convenient form

$$\Phi_{ET} = \frac{2}{3}\pi^2 R_0^3 \int \mathrm{d}z\ \frac{C_D(z)}{\bar{C}_D} C_A(z). \tag{5.6}$$

We have been left with an integral over the product of donor and acceptor concentrations, a very simple quantity to calculate.

As a footnote, the approximation applied to Eq. 5.3 is reminiscent of the "Perrin approximation" used in fluorescence decay. [35] In this approximation, one presumes that if an acceptor is within a certain cut-off radius (the "Perrin radius") of a donor, energy transfer will occur eventually. If it is outside the Perrin radius, energy transfer will not occur. Thus, if $C_A(\boldsymbol{r})$ represents the probability of an acceptor being at $\boldsymbol{r}$, then

$\frac{4}{3}\pi R_{max}^3 \bar{C}_A(\boldsymbol{r}_0)$ represents the probability that an acceptor will be within a sphere of R_{max} centred at $\boldsymbol{r}_0$. (This probability may be greater than 1 as a single donor can "quench" multiple acceptors.) Here R_{max} is the Perrin radius and $\bar{C}_A(\boldsymbol{r}_0)$ is the average acceptor concentration within that sphere centred on r_0. Weighing this over the distribution of all possible donors, $C_D(z)/\bar{C}_D$, gives a total energy transfer of

$$\Phi_{Perrin} = \frac{4}{3}\pi R_{max}^3 \int \mathrm{d}z \, \frac{C_D(z)}{\bar{C}_D} \bar{C}_A(z). \tag{5.7}$$

It is encouraging that from this completely distinct and intuitive approach, we get exactly the same result as Eq. 5.6.

As an interesting side note, if we equate Eq. 5.6 and 5.7, we find a relation between the Perrin radius and the Förster radius, namely $R_{max} = (\pi/2)^{\frac{1}{3}} R_0$.

Eqs. 5.6 and 5.7 indicate that fluorescence decay experiments would be ideal for measuring the overlap of two tagged monomer types within a system. With homopolymer tagged as donor and the copolymer joints tagged as acceptor, we can thus get a very good idea of the quantity of homopolymer at the interphase.

5.2 Predictions of Theory

From the analysis in Section 5.1, the appropriate theoretical measure in the study of homopolymer localisation would be

$$L \equiv \frac{1}{\overline{\phi}_H} \int \mathrm{d}x \; \phi_H(x) J(x). \tag{5.8}$$

The normalisation constants have been chosen so that $L = 1$ represents a homogeneous distribution of homopolymer. When homopolymer localises at the interphase, there will be greater overlap between the homopolymer and joints, resulting in $L > 1$. By contrast, if $L < 1$ the homopolymer would be inhomogeneously shifted away from the interphase. Intuitively, this is clear when considering the ideal strong-segregation case where the copolymer joints are all located at a single offset within the cell. In such case, $J(x) = \delta(x - x_0)$ and L would reflect whether $\phi_H(x_0)$ was less than, equal to, or greater than its homogeneous value, $\overline{\phi}_H$.

To convert Eq. 5.8 into a quantum efficiency, one need only multiply by the prefactor of Eq. 5.6, $\frac{2}{3}\pi^2 R_0^3$, and also $\bar{C}_A \equiv \overline{\phi}_C \rho_{ref}/r_C$.

Figure 5.1 illustrates the results for L for a typical system where $\chi r_C = 30$. Interestingly, homopolymer localisation in the interphase *is* predicted, but primarily for small to intermediate f_H combined with large $\overline{\phi}_C$. The exact bounds on f_H and $\overline{\phi}_C$ are not simple. As $\overline{\phi}_C$ decreases, the upper bound on f_H where $L > 1$ is still detected diminishes. Figure 5.2(a) defines the $\overline{\phi}_C$ vs. f_H boundaries in parameter space delineating the area.

For a given f_H and χr_C, the maximum value of L achieved would seem to be as $\overline{\phi}_C \to 1$. This is consistent with the hypothesis in Section 3.3 that the initial addition of homopolymer to the system would first act to relieve conformational, entropic constraints on the A-b-B copolymer by going to the interphase. Recall that this was hypothesised to explain the reason why domain thickness dipped slightly before becoming independent of

(a)

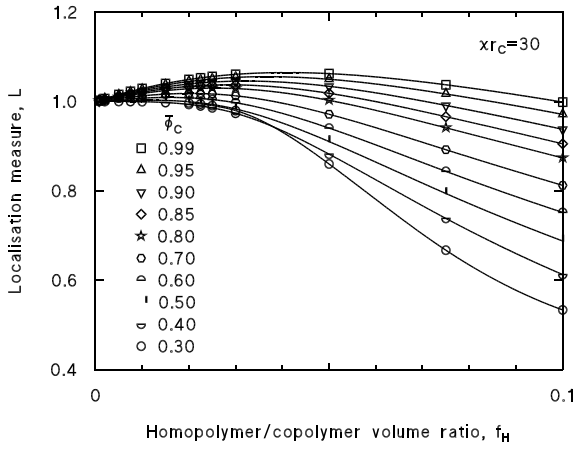

(b)

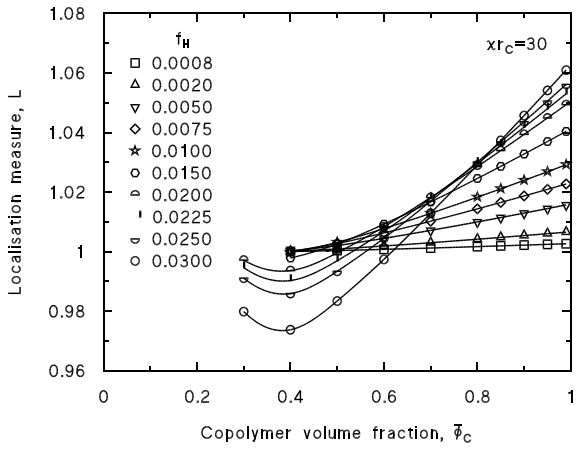

(c)

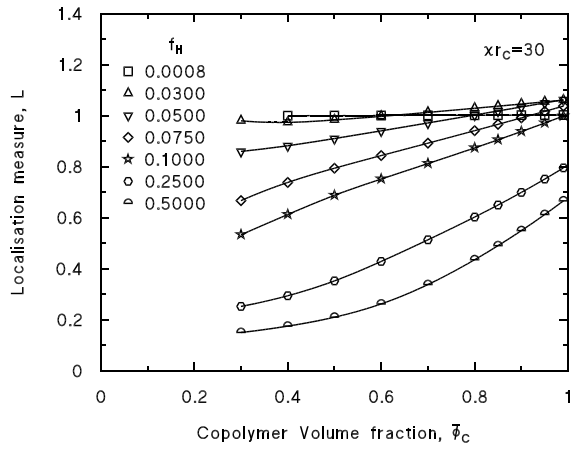

Figure 5.1: Localisation measure as a function of f_H and $\overline{\phi}_C$ for the $\chi r_C = 30$ case. (a) L as a function of f_H for specific $\overline{\phi}_C$'s. (b) L as a function of $\overline{\phi}_C$ for specific f_H's. Only $f_H < 0.03$ is shown here. (c) L as a function of $\overline{\phi}_C$ for remaining f_H's. $f_H < 0.03$ was graphed separately so that features would not be lost due to the large Y-axis scale required for $f_H = 0.5$. $f_H = 0.0008$ and $f_H = 0.03$ appear in both panels for comparison.

(a)

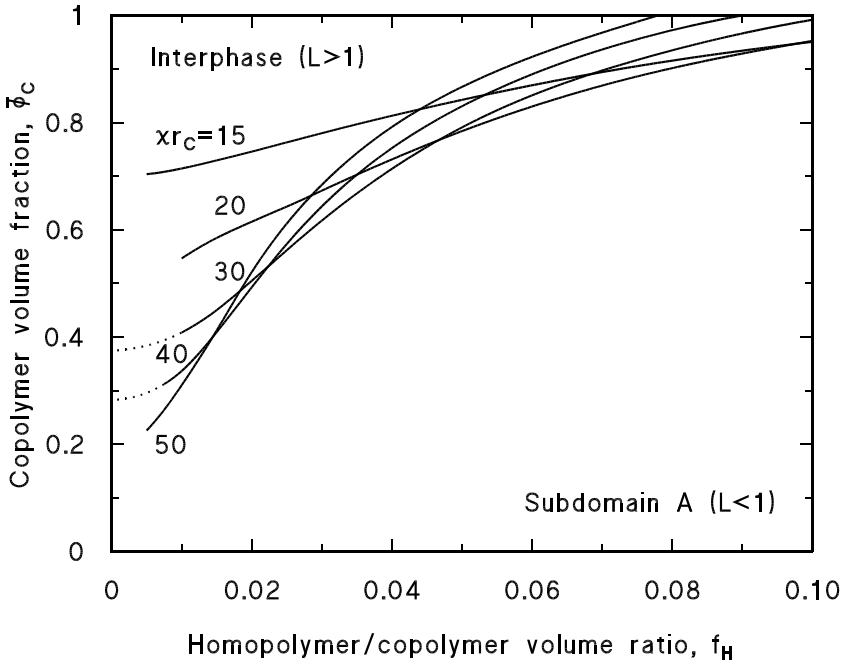

(b)

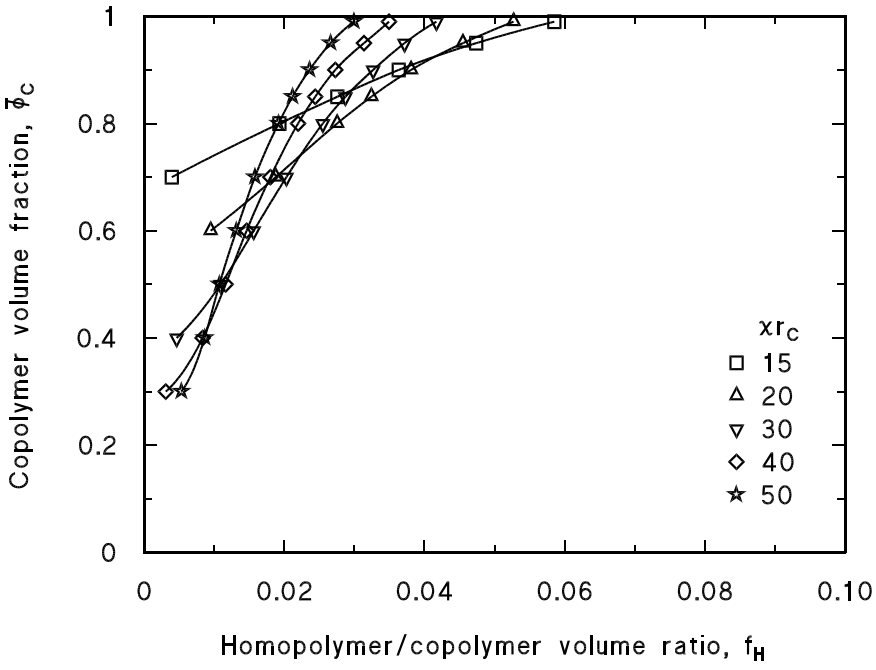

Figure 5.2: Contours in parameter space significant to localisation. (a) Boundaries delineate systems with interphase-localised polymer ($L > 1$) from systems with subdomain-A-localised polymer ($L < 1$). A boundary has been plotted for each investigated value of χr_C. (b) Contours connecting the values of f_H, for a given $\overline{\phi}_C$, that give a maximum in localisation. For comparison, the same scales have been used as in (a).

$\overline{\phi}_C$ at the special $f_{H,cross}$ value. (Refer to the discussion surrounding Eq. 3.13 for further details.)

Interestingly, though $\overline{\phi}_C \to 1$ represents the maximum localisation of homopolymer at the interphase, $f_H \to 0$ does not. As can be seen in Figure 5.1(a), the maximum in L vs. f_H for a given $\overline{\phi}_C$ and χr_C occurs at a small, non-zero f_H. Figure 5.2(b) indicates the f_H at which this maximum occurs as a function of $\overline{\phi}_C$ for our selected χr_C values. The shift of this contour has a similar characteristic as the $L = 1$ boundary in Figure 5.2(a), though the L_{max} contour naturally lies further into the $L > 1$ "Interphase" region of this phase diagram.

The final consideration is the χr_C dependence. Figure 5.3 illustrates how L_{max}, the maximum localisation value for a given $\overline{\phi}_C$, varies with $\overline{\phi}_C$ and χr_C. Paradoxically, the maximum-achievable localisation measure *increases* with χr_C. One could easily expect it to decrease, since a higher χr_C would indicate a higher repulsion between the homopolymer and block B of the copolymer which, in principle should drive the homopolymer away from the interphase and its proximity to block B.

The key to resolving this puzzle is to remember that block A of the copolymer will also experience an increased repulsion due to the increase in χr_C. This results in a narrower interphase and thus a more tightly constrained configuration of copolymer. The addition of homopolymer to the interphase relieves this constriction. Though it results in a greater interaction energy between the homopolymer and block B, the trade-off against entropy due to the relaxation of constraints on the copolymer is a net gain, at least for the smaller values of f_H considered in this investigation.

This trend is also consistent with the d/d_0 vs. χr_C dependence in Table 3.2. As χr_C increases, the $f_{H,cross}$ balance is achieved at decreasing values of the d/d_0 ratio. Since decreasing d/d_0 is achieved by increased dilution by the homopolymer, it would seem to indicate that more homopolymer is collecting at the interphase as χr_C increases.

(a)

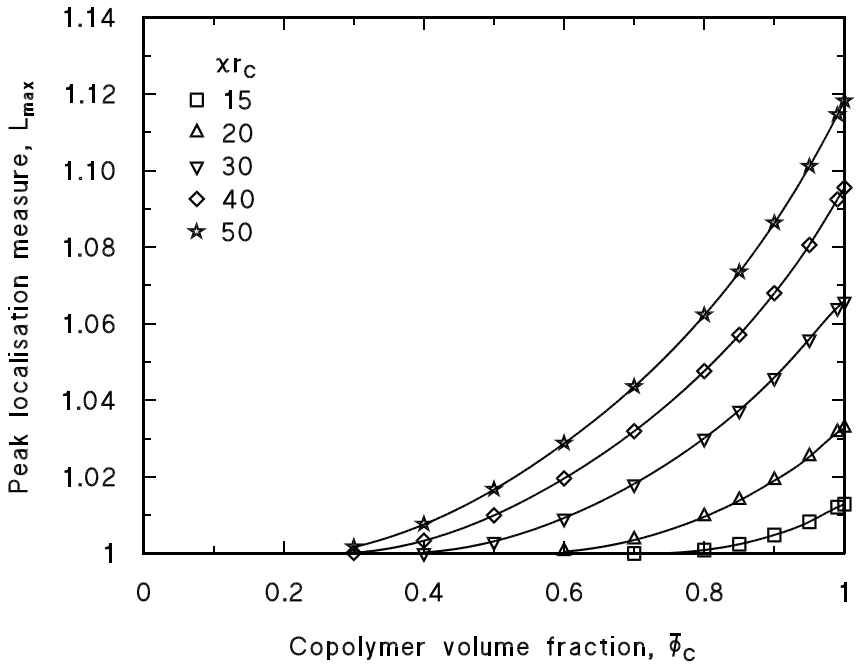

(b)

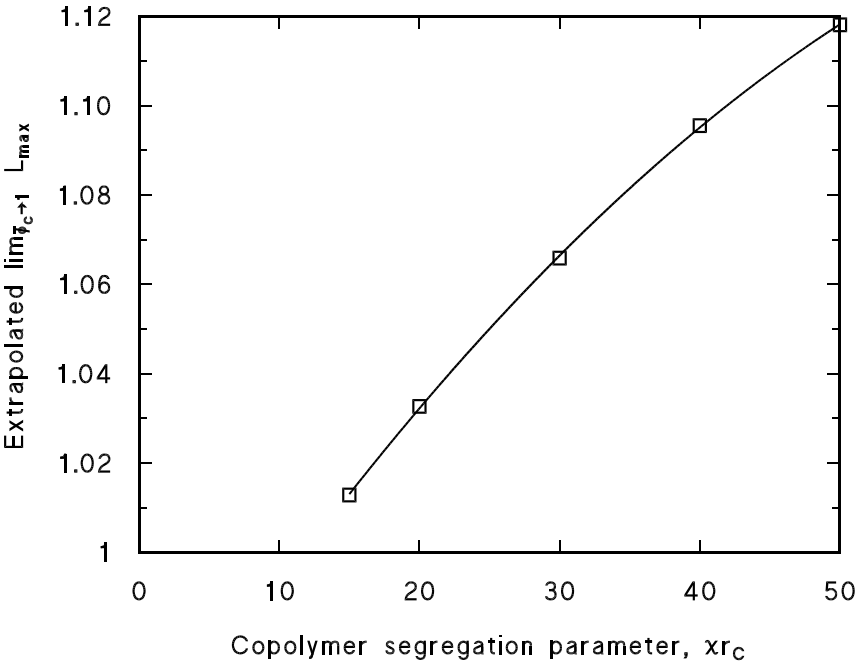

Figure 5.3: (a) Dependence of maximum localisation on $\overline{\phi}_C$ for various values of χr_C. (b) Extrapolating the L_{max} vs. $\overline{\phi}_C$ curves to $\overline{\phi}_C \to 1$, we obtain a maximum L_{max} for each given χr_C.

Ultimately, the localisation effects predicted here are subtle, however, and would likely require careful and directed exploration by experiment in order that they be resolved. It is hoped that the above results may help to guide such studies.

It is important to note, however, that while the above represents an accurate theoretical study of how L varies in the face of changes to system parameters, there is a caveat that should be emphasised. An increase in L does not uniquely guarantee a shift of homopolymer toward the interphase. From Eq. 5.8, one can see that an increase in the dispersion of joints throughout the system (i.e. a less-sharply peaked $J(\boldsymbol{r})$) would also increase L. While this might come down to a matter of semantics, since the homopolymer overlap with the joints *will* increase, it is important when interpreting experimental data to keep in mind that this may be due to the interphase becoming more ill-defined rather than due to the homopolymer migrating toward an unchanging interphase.

Chapter 6

Summary and Conclusions

The preceding chapters illustrate the richness of detail with which the behaviour of copolymer-homopolymer blends can be explored using the numerical self-consistent mean field theory. Even from the theoretical foundations, we were able to obtain the significant result that – to the extent that the mean field approximation is valid – the equilibrium structure of the copolymer-homopolymer blend is entirely determined by eight physical parameters:

- $\overline{\phi}_C$ – the total volume fraction of copolymer in the system.
- f_A – the volume fraction of the A-B copolymer molecule which is of species A.
- f_H – the ratio of the homopolymer's molecular volume to the molecular volume of the copolymer.
- $\chi_{AB}r_C$, $\chi_{AH}r_C$, and $\chi_{BH}r_C$ – the "segregation parameters" for the pair-interactions of each of the three species in the system. These are the product of the appropriate Flory interaction parameter, $\chi_{\kappa\kappa'}$, and the volume of the copolymer molecule, r_C, in units $1/\rho_{ref}$ where ρ_{ref} is the reference volume used in obtaining $\chi_{\kappa\kappa'}$. [5]
- ϵ_A and ϵ_B – the conformational asymmetry parameters, defined as the ratio $\epsilon_\kappa \equiv \rho_{0\kappa}b_\kappa^2/\rho_{0H}b_H^2$ where $\rho_{0\kappa}$ and b_κ are, respectively, the bulk monomer densities and the statistical segment lengths of species κ.

In order to restrict the parameter space investigated to a manageable scope, we considered only systems where $\epsilon_A = \epsilon_B = 1$, $f_A = \frac{1}{2}$, $\chi_{AH} r_C = 0$, and $\chi_{AB} r_C = \chi_{BH} r_C \equiv \chi r_C$, except when reproducing specific experimental results of known parameters different than this restriction.

The ϵ_κ restrictions require that all three monomer species, A, B, and H have the same product $\rho_{0\kappa} b_\kappa^2$, where $\rho_{0\kappa}$ is the monomer density and b_κ is the characteristic statistical segment lengths. If the recasting of $\rho_{0\kappa}$ is performed using Eqs. 3.5 through 3.7 so that $\rho'_{0A} = \rho'_{0B} = \rho'_{0H}$, this ϵ_κ restriction reduces to the requirement that all species have roughly the same effective statistical segment length. In either case, this restriction is not unreasonable given the uncertainty in experiment's ability to discern the distinction in these parameters, even among the more common species investigated. [20]

The $f_A = \frac{1}{2}$ restriction considers systems with blocks A and B of the copolymer being of equivalent size – a compositionally symmetric copolymer. In neat copolymer systems, this restriction optimises the chances of a lamellar structure forming and so was chosen here for our present lamellar study. [1]

Finally, the restriction on $\chi_{\kappa\kappa'}$ specifies that block A of the copolymer be composed of the same species of monomer as the homopolymer molecules in the system. This last restriction, also typical in many experiments, permitted an explicit statement of the field, $\eta(\boldsymbol{r})$, which arises from the assumed incompressibility of the system. This statement, Eq. 2.70, was the equation that completed the closed set of self-consistent equations that determined the mean field of the system.

In Section 3.1 we compared and contrasted the results of the current NSCF result with the previous "Many-Wave Approximation" (MWA). [3] The MWA obtained solutions in the mean field by evaluating a truncated Fourier series representation of the densities and potentials that describe the system, with the free energy contributions of these fields evaluated to the fourth order term. As the MWA considers only a finite number of Fourier

terms, it is best suited to the weak segregation regime where, in neat copolymer systems, density variations have a distinct cosine-like shape. The NSCF approach, by contrast, considers the exact mean field solution, albeit using iterative numerical methods to obtain the result. Eliminating truncation error, the NSCF approach is much more suited to considering systems of intermediate to stronger segregation as expected for $\chi_{\kappa\kappa'} r_C \gtrsim 30$.

In the weak-segregation limit, the NSCF results compared favourably to the previous MWA results, though corrections were present. In particular, the equilibrium domain thicknesses predicted in Figures 3.1 and 3.2 were slightly offset from the MWA result. The MWA result predicted an increase in domain thicknesses when compared to the one-wave approximation. [3] The NSCF result also predicted an offset from the one-wave result, but a more moderate one (by approximately 50%) of the one predicted by the MWA.

Also in contrast to the MWA, the subdomain thicknesses – i.e. the thickness of each A-dominated and B-dominated layer in the system – in the NSCF result did not exhibit a sudden non-linear divergence as the concentration of copolymer went below 80 vol% (that is, for $\overline{\phi}_C < 0.8$). This likely indicates a greater stability in the NSCF calculations for moderate to high concentrations of homopolymer than in the MWA result.

The reason that the MWA would appear to fail under these circumstances is that, in the moderate-to-low-$\overline{\phi}_C$ range, the NSCF results indicated that copolymer often exhibited strong-segregation behaviour, exasperated by localisation of the homopolymer in the middle of the A subdomain, away from the A-B interphase, particularly in realistic ranges of f_H. The presence of homopolymer in the A-B interphase, like the good solvent results, [9, 10] would seem to dilute the A-B interactions and reduce segregation. And so, with homopolymer driven out of the interphase, this effect is absent. Strong-segregation is further encouraged as a response to the compression of the copolymer's A block, forcing it to coil up closer to the interphase and thus creating a greater need for the interphase

to be narrow in order to minimise contact with the B block.

As in the MWA study, it was found that domain thickness increased or decreased with $\overline{\phi}_C$, depending on the value of the homopolymer-to-copolymer volume ratio, f_H. Furthermore, for a special choice of f_H, a balance of competing effects was achieved wherein the domain thickness was found to be largely independent of $\overline{\phi}_C$. That is, for this special $f_{H,thresh}$, $d(\overline{\phi}_C) = d_0$, where $d(\overline{\phi}_C)$ represented the domain thickness of a blend with $\overline{\phi}_C$ copolymer and $\overline{\phi}_H \equiv 1-\overline{\phi}_C$ homopolymer, and d_0 represented the domain thickness of a system consisting only of the copolymer.

Again, there were differences in the details of the NSCF version of this phenomenon, however. The MWA analysis revealed only a $f_{H,thresh}$ value of approximately 1/5. The NSCF result found that the value of f_H wherein $d = d_0$ was given roughly by Eq. 3.11, namely $f_{H,thresh} = (1.3\overline{\phi}_C + 0.75)/\chi r_C$. Encouragingly, this $f_{H,thresh}$ agreed with MWA results in the low homopolymer $\overline{\phi}_C \to 1$ limit near the microphase separation transition (MST) of $\chi r_C \simeq 10.5$, where MWA would seem to be most valid.

Such a significant spread of $f_{H,thresh}$, nearly tripling over the full range of $\overline{\phi}_C$, illuminated a greater complexity in the form of $f_{H,thresh}$ than uncovered in the MWA investigation, wherein the $\overline{\phi}_C$ dependence was not discovered. One intriguing observation from our current investigation, though, was that for each χr_C, all of the d vs. f_H plots in Figures 3.5 through 3.9 *did* cross very close to a common f_H, albeit one where d was slightly less than d_0.

What did this mean? There seemed to be a f_H which we dubbed $f_{H,cross}$ where d seemed effectively independent of $\overline{\phi}_C$. This $f_{H,cross}$ was determined from the data in Table 3.2 to be roughly $4.50(\chi r_C)^{-1.36}$.

If this d were independent of $\overline{\phi}_C$ as $\overline{\phi}_C \to 1$, then it should follow that $d = d_0$. Yet, paradoxically, the stable d seemed to shift further below d_0 as χr_C increased. How should this come about? It was hypothesised that the first addition of homopolymer

preferentially localised in the interphase between the A and B subdomains. This would reduce the contact between copolymer blocks at the interface. Less contact would lead to a reduction in the magnitude of the repulsive interaction and thus would reduce the extension of the molecule. Since the domain thickness relates to the extension of the copolymer molecule, d would be reduced below d_0. After this initial effect, the successive addition of more homopolymer to the system would distribute elsewhere in a manner that balanced entropy considerations in the cell.

This hypothesis was supported by the results of our homopolymer localisation investigation in Chapter 5. The addition of small amounts of homopolymer were seen to have a marginal bias toward first localising at the interphase. This localisation effect decreases monotonically with the addition of homopolymer (i.e. decrease in $\overline{\phi}_C$) for a given f_H and χr_C, but, by contrast, for a specific $\overline{\phi}_C$, the localisation effect was maximised at a finite intermediate value of f_H as seen by the contours in Figure 5.2(b).

As the value of χr_C increases, from Figure 5.2(a) we saw that this localisation persists to lower values of $\overline{\phi}_C$ but at the expense of the upper limit on f_H. This localisation effect has an analogue in copolymer-solvent blends, where a "bump" in the otherwise near-homogeneous distribution of the solvent was reported at the interphase. [2] Though minute, an example of this bump can be seen in Figure 6.1.

Returning to the consideration of the disparate behaviours of d vs. $\overline{\phi}_C$ above and below $f_{H,cross}$, a simple explanation exists for these two extremes. Below $f_{H,cross}$, in the limit of $f_H \to 0$, the homopolymer molecules were very small when compared to the volume of the copolymer molecules. It was thus fair to treat the homopolymer as a good molecular solvent, neglecting the complex effects of extended homopolymers which, for $f_H \to 0$, would be negligible on the scale of the copolymer. Good solvents, being largely dominated by entropy, would permeate the system, including the interphase. The presence of solvent in the interphase and its near-homogeneous penetration into each

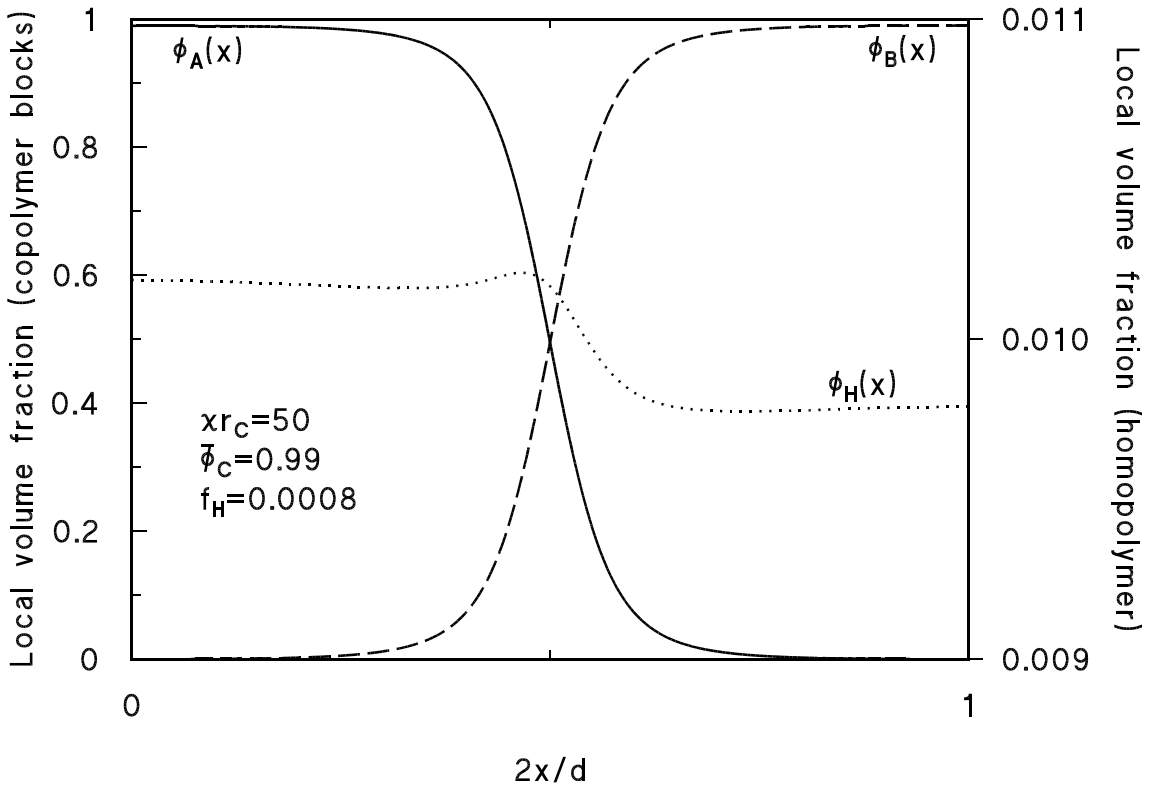

Figure 6.1: The "bump" in local homopolymer volume fraction at the interphase for a typical copolymer-homopolymer blend. Only 1% homopolymer is present, and so $\phi_H(x)$ has been plotted on a separate scale.

of the subdomains would serve to dilute the copolymer and thus reduce the interaction between block A from block B. This effectively reduced the segregation parameter, χr_C. With a weaker repulsion the copolymer molecules would relax their extension, resulting in a reduction in the thickness of the unit cell.

This picture of $f_H \to 0$ homopolymer as a good solvent was reinforced by the approximate scaling behaviour of d vs. $\overline{\phi}_C$ in the $f_H \to 0$ case of Figure 3.1. As good solvents distribute homogeneously in the system in the same manner as a perfectly non-selective solvent, we used this analogy to consider the scaling behaviour of d vs. $\overline{\phi}_H$ in the limit of the dilution approximation. Using a binomial expansion for small $\overline{\phi}_H$, we arrived at the correct slope, namely $d/d_0 \simeq 1 - 0.4\overline{\phi}_H$, for the d vs. $\overline{\phi}_C$ dependence in that limit. By contrast, the MWA predicted a slope of -1 instead of -0.4.

The roughly-homogeneous distribution of the homopolymer in the $f_H \to 0$ limit was confirmed both in the homopolymer localisation study in Chapter 5 and in the determination of relative subdomain sizes as a function of f_H in Section 3.4. In the latter study, it was found in the $f_H \to 0$ limit, the relative size of subdomain A, given by d_A/d, remained roughly equivalent to $f_A = \frac{1}{2}$ as would be expected by a system uniformly diluted by a homogeneously-distributed solvent.

By contrast, in the high-f_H limit, the homopolymer distribution was severely inhomogeneous. By and large, it collected almost exclusively within the middle of the A subdomain. This collection of homopolymer essentially became a separate zone with homopolymer residing in its own exclusive volume. The copolymer was left to segregate with virtually no interaction from the isolated homopolymer, and so ordered with its own fraction of the cell's volume nearly exactly as it would if there were no homopolymer present. Since the neat copolymer case's domain thickness, d_0, would be fixed, and the neat copolymer only accounted for $\overline{\phi}_C$ of the system volume, the complete cell in this

high-f_H scenario should have thickness of $d_0/\overline{\phi}_C$. For a cell of volume V, this would provide a volume $\overline{\phi}_C V$ in which neat copolymer could form a lamellar structure of thickness d_0 and a remaining volume $\overline{\phi}_H V$ and thickness $d_0({\overline{\phi}_C}^{-1} - 1)$ in which the homopolymer could reside.

This model is consistent with the relative subdomain thickness results in the large-f_H limit. In Section 3.4 it was found that for $f_H \gtrsim 2/\chi r_C$, d_A/d approached $1-\overline{\phi}_C f_B$ which is exactly what one would expect when $d_B/d_0 = f_B$ as it would for the neat copolymer case in strong segregation, combined with the definition $d = d_A + d_B$. Once the copolymer and homopolymer had demixed to this extreme, macrophase separation was a possibility, as seen in Section 4.2 and corroborated by Banaszak and Whitmore's MWA, [30] and also seen by de Gennes in homopolymer-homopolymer blends. [27]

Even when some intermixing occurred between the homopolymer and the neighbouring region dominated by compatible block A copolymer, it had very little effect on the domain thickness. This is likely due to the fact that the interpenetration of homopolymer and block A copolymer is merely entropy driven, rather than driven by the Flory interaction potentials which would significantly contribute to the free energy of the system.

The model of this extreme behaviour would seem to indicate that once the homopolymer has sufficiently isolated itself into the A subdomain, further increases to f_H should have no effect on the domain thickness d, since it is now simply a matter of geometry determined by $\overline{\phi}_C$. The results of the NSCF seem consistent with this, showing the d vs. f_H dependence for a given χr_C and $\overline{\phi}_C$ to level off in the limit of large f_H.

That said, even in the large-f_H limit we again saw evidence of the first fraction of homopolymer introduced to a neat system going to the interphase. The above hypothesis describing the relative cell volumes should imply that for fixed χr_C and f_H, d should scale inversely with $\overline{\phi}_C$. However, near $\overline{\phi}_C \to 1$, this dependence is slightly weakened to ${\overline{\phi}_C}^{-2/3}$. As seen in Figure 3.13, the offset to d being slightly less than the ideal value of $d_0/\overline{\phi}_C$ is

never recovered, even in the low $\overline{\phi}_C$ range. This again is consistent with the hypothesis that the first fraction of homopolymer collects in the interphase and thus screens the A-B interaction, slightly reducing d.

Overall there seems much evidence that the localisation effect, the "bump" of solvent systems, also exists in copolymer-homopolymer blends. It is by no means an overt effect, but rather a subtle one. With sufficient precision, it is hoped that the experimental method of fluorescence decay measurements described in Section 5.1, or some other experimental methodology, might be able to detect this phenomenon.

The final area covered in this investigation, albeit more briefly, was the matter of phase behaviour. Like neat copolymer systems, copolymer-homopolymer blends can organise into several different ordered structures such as lamellae, cylinders in a hexagonal lattice, spheres in a *bcc* lattice, etc. Also, when none of these orderings are energetically favourable, the system may exist in a disorganised homogeneous state. The results of a comparison between the free energy of the organised lamellar structure and the disorganised homogeneous state were plotted in the phase diagram found in Figure 4.1.

In the low-f_H limit the homogeneous state became preferable when $\overline{\phi}_C \chi r_C$ dropped below 10.5, just as would be expected in the good solvent limit where the dilution approximation would be valid. As f_H increased, the ordered state would persist to lower values of $\overline{\phi}_C$ for a given χr_C. By extrapolation, there is some indication that there may exist finite, realistic values of f_H where the system may remain ordered to very small values of $\overline{\phi}_C$. However, since the phase behaviour has only been conclusively probed down to $\overline{\phi}_C = 0.1$ to 0.3, it is quite possible that there are unforeseen deviances in the phase boundary. At any rate, as $\overline{\phi}_C \to 0$, we enter the semi-dilute regime where the SCF approach would cease to apply.

At the very least, it does seem that the ordered structures other than the lamellar morphology may become energetically preferable in the low-$\overline{\phi}_C$ limit. From the model

for the high-f_H system described above, we find that, despite $f_A = f_B$, the relative subdomain thicknesses are very disparate with $d_B/d = \overline{\phi}_C{}^2 f_B$. With this high asymmetry, the cylindrical and spherical phases might be the more economic geometry since they are optimal when one sumdomain is of significantly smaller volume than the other. [1]

Indeed, using the "unit cell approximation" (UCA) [31] to obtain the NSCF equations in the cylindrical symmetry, we find that in an extreme corner of our data set with high χr_C and f_H and low $\overline{\phi}_C$ (namely, $\chi r_C = 50$, $f_H = 0.25$, and $\overline{\phi}_C = 0.3$) the cylindrical morphology *was* found to be energetically preferable to the lamellar structure. This is interesting as, in the neat copolymer case, $f_A = f_B = \frac{1}{2}$ as here would result in the lamellar morphology being the exclusive ordered structure. [1] The introduction of cylindrical and possibly spherical morphologies in blends with $f_A = f_B = \frac{1}{2}$ would thus seem to be a consequence of the asymmetries induced in the cell due to the presence of homopolymer.

In the neat copolymer case, when there is an asymmetry between the volume fraction of species A and species B the system will pass through a cylindrical and spherical equilibrium microphase when descending through values of χr_C toward the MST. [1] In our blends, since the homopolymer is of species A and the copolymer is configurationally symmetric, we have a similar inbalance between the total volume fraction of species A and species B in the system. Thus, one might expect that very near MST, cylinders or spheres might be the equilibrium state. Nonetheless, in the neat case, these non-lamellar morphologies are stable over a very narrow range of parameters, except when $\overline{\phi}_B$ is much different than $\frac{1}{2}$.

So, while the majority of the data collected in this investigation would seem to represent systems in which the lamellar structure is legitimately the most stable, this exception would seem to indicate that a more thorough exploration of microphase behaviour might be warranted.

The new standard in the study of phase behaviour is to consider the proper hexagonal or *bcc* unit cell by solving the mean field equations in two or three dimensions. [31] This is not something easily done within the present numerical implementation, as the number of calculations and rate of convergence of the NSCF equations in the present method when considered in 3-D are both prohibitively slow. [18] The proper course of action would seem to be the adaptation of Matsen and Schick's UCA-free approach to the solution of the copolymer-homopolymer blend NSCF formalism, [11] particularly so that one might explore the gyroidal phase. [6]

Recently, Drolet and Fredrickson did attempt to explore equilibrium morphologies in neat triblock copolymers in 2-D using a NSCF theory with a modest discretisation grid. [36] The technique showed promise in its ability to generate spontaneously, without inforced symmetries, various known morphologies in 2-D in addition to some previously unreported ones. However, in order to keep the computations on a realistic scale, a sacrifice in resolution had to be made. The NSCF were solved in a 128x128 box with length and width each roughly 10 times the size of a typical unit cell. Thus, there was insufficient resolution to obtain anything beyond a qualitative result. Furthermore, the investigation would have to be restricted to the weak segregation regime in order to minimise numerical error in the discrete spacial derivatives of the NSCF.

Unfortunately, a similarly-qualitative exploration that included 3-D phases such as spheres would be two orders of magnitude more demanding, computationally. Exploration in 3-D would be necessary in order to encompass all the standard morphologies. Quantitative exploration would require even greater computational power, perhaps as much as 10^3 on top of the demands of a 3-D NSCF solution.

Section 4.2 gave a glimpse at what the macrophase separation of our targeted systems may be like. However, the required resolution of free energy vs. $\overline{\phi}_C$ for each choice of f_H and χr_C would result in the need for a prohibitively large number of unique NSCF

calculations. And so, the phase boundaries determined here for each choice of χr_C and f_H were rough at best. Three trends were observed that were believed qualitatively correct, however:

1. Macrophase transition boundaries appeared primarily at large f_H. This would seem likely to be a natural progression of the strong isolation of homopolymer from the copolymer interphase in high-f_H scenarios – namely $f_H \gtrsim 2/\chi r_C$.

2. The lower and upper extremes on $\overline{\phi}_C$ of macrophase separation for a given χr_C and $\overline{\phi}_C$ seemed to grow wider with increase of χr_C.

3. The aforementioned widening appeared primarily as a result of a shift of the upper bound on $\overline{\phi}_C$ while the lower bound was much less affected.

As with the issue of stability of other microphase structures such as cylinders and spheres, a further investigation of macrophase separation using NSCF would seem warranted, if the requisite computing power becomes feasible.

Overall, this investigation has provided many insights into the characteristic behaviour of copolymer-homopolymer blends, particularly in idealised extremes. It has also suggested several avenues of further investigation – both theoretical and experimental.

In theory, the study of competing microphase morphologies and also of macrophase separation would seem warranted. A further improvement on the mean field formalism itself may also be of interest. The mean field approximation leads one to treat the mean density profiles, $< \hat{\rho}_\kappa(\boldsymbol{r}) >$ in Eq. 2.28, as equivalent to the most probable density profile, $\rho_\kappa^{(peak)}(\boldsymbol{r})$. An improvement on this would be to expand Eq. 2.28 functionally about this most probable configuration and from there determine the lowest-order correction term to the approximation $< \hat{\rho}_\kappa(\boldsymbol{r}) > \simeq \rho_\kappa^{(peak)}(\boldsymbol{r})$.

On the experimental frontier, the investigation of homopolymer localisation at the interphase should continue. The NSCF suggests specific trends in homopolymer localisation which could be investigated through the use of fluorescence decay experiments.

And so, like most scientific investigations, the self-consistent mean field theory of copolymer-homopolymer blends enlightens certain aspects of our system of interest, but in revealing its results, suggests directions of further investigation.

Bibliography

[1] J. D. Vavasour and M. D. Whitmore. Self-consistent mean field theory of the microphases of diblock copolymers. *Macromolecules*, 25:5477–5486, 1992.

[2] M. D. Whitmore and J. Noolandi. Self-consistent theory of block copolymer blends: Neutral solvent. *J. Chem. Phys.*, 93:2946–2955, 1990.

[3] M. Banaszak and M. D. Whitmore. Mean field theory of the lamellar structure of block copolymer/homopolymer blends in the weak segregation regime. *Macromolecules*, 25:2757–2770, 1992.

[4] A. E. Woodward. *Atlas of Polymer Morphology.* Oxford University Press, Don Mills, Ontario, 1988.

[5] P. J. Flory. *Principles of Polymer Chemistry.* Cornell University Press, Ithaca, N.Y., 1953.

[6] D. A. Hajduk, P. E. Harper, S. M. Gruner, C. C. Honeker, E. L. Thomas, and L. J. Fetters. A re-evaluation of bicontinuous cubic phases in starblock copolymers. *Macromolecules*, 25:2570–2573, 1995.

[7] E. Helfand and Z. R. Wasserman. Microdomain structure and the interface in block copolymers. In I. Goodman, editor, *Developments in Block Copolymers*, volume 1, pages 99–125. Elsevier, New York, 1982.

[8] L. Leibler. Theory of microphase separation in block copolymers. *Macromolecules*, 13:1602–1617, 1980.

[9] M. D. Whitmore and J. D. Vavasour. Self-consistent mean field theory of the microphase diagram of block copolymer/neutral solvent blends. *Macromolecules*, 25:2041–2045, 1992.

[10] M. Banaszak and M. D. Whitmore. Self-consistent theory of block copolymer blends: Selective solvent. *Macromolecules*, 25:3406–3412, 1992.

[11] M. W. Matsen and M. Schick. Microphases of diblock copolymers with conformational asymmetry. *Macromolecules*, 27:4014–4015, 1994.

[12] C. Kittel. *Introduction to Solid State Physics*. Wiley, New York, 6th. edition, 1986.

[13] M. W. Matsen. Stabilizing new morphologies by blending homopolymer with block copolymer. *Phys. Rev. Lett.*, 74:4225–4228, 1995.

[14] M. D. Whitmore and J. D. Vavasour. Self-consistent field theory of block copolymers and block copolymer blends. *Acta Polymer.*, 46:341–360, 1995.

[15] F. Reif. *Fundamentals of Statistical and Thermal Physics*. McGraw-Hill, New York, 1965.

[16] M. Doi and S. F. Edwards. *The Theory of Polymer Dynamics*. Oxford Science Publications, Oxford, 1986.

[17] K. F. Freed. *Renormalization Group Theory of Macromolecules*. Wiley-Interscience, New York, 1987.

[18] J. D. Vavasour. *Self-Consistent Mean Field Theory of the Microphases of Neat Diblock Copolymers*. BSc Thesis, Memorial University of Newfoundland, 1992.

[19] M. Banaszak. *Microphase and Macrophase Separation in Binary and Ternary Block Copolymer Blends*. PhD thesis, Memorial University of Newfoundland, 1991.

[20] J. D. Whitmore and M. D. Vavasour. Self-consistent field theory of block copolymers with conformational asymmetry. *Macromolecules*, 26:7070–7075, 1993.

[21] L. Fox, editor. *Numerical Solution of Ordinary and Partial Differential Equations*. Addison-Wesley, Reading, Mass., 1962.

[22] W. H. Press, S. A. Teukolsky, W. T. Vetterling, and B. P. Flannery. *Numerical Recipes in C: The Art of Scientific Computing*. Cambridge University Press, New York, 2nd. edition, 1993.

[23] K. M. Hong and J. Noolandi. Theory of phase equilibria in systems containing block copolymers. *Macromolecules*, 16:1083–1093, 1983.

[24] M. D. Whitmore and J. Noolandi. Theory of phase equilibria in block copolymer-homopolymer blends. *Macromolecules*, 18:2486–2497, 1985.

[25] K. I. Winey, E. L. Thomas, and L. J. Fetters. Swelling a lamellar diblock copolymer with homopolymer: influence of homopolymer concentration and molecular weight. *Macromolecules*, 24:6182–6188, 1991.

[26] T. Hashimoto, T. Tanaka, and H. Hasegawa. Ordered structure in mixtures of a block copolymer and homopolymers. 2. effects of molecular weights of homopolymers. *Macromolecules*, 23:4378–4386, 1990.

[27] P.-G. de Gennes. *Scaling Concepts in Polymer Physics*. Cornell University Press, Ithaca, N.Y., 1979.

[28] E. Helfand and Y. Tagami. Theory of the interface between immiscible polymers. II. *J. Chem. Phys.*, 56:3592–3601, 1972.

[29] G. H. Fredrickson and L. Leibler. Theory of block copolymer solutions: Nonselective good solvents. *Macromolecules*, 22:1238–1250, 1989.

[30] M. Banaszak and M. D. Whitmore. Mean field theory of the phase behavior of ternary block copolymer-hompolymer blends. *Macromolecules*, 25:249–260, 1992.

[31] M. W. Matsen and M. D. Whitmore. Accurate diblock copolymer phase boundaries at strong segregations. *J. Chem. Phys.*, 105:9698–9701, 1996.

[32] M. A. Winnik, J. G. Spiro, and R. Yahya. (private communication).

[33] A. Yekta, J. Duhamel, and M. A. Winnik. Dipole-dipole energy transfer. fluorescence decay functions for arbitrary distributions of donors and acceptors: systems with planar geometry. *Chem. Phys. Lett.*, 235:119–125, 1995.

[34] A. Yekta, J. G. Spiro, and M. A. Winnik. A critical evaluation of direct energy transfer as a tool for analysis of nanoscale morphologies in polymers. Application to block copolymer interfaces. *J. Chem. Phys.*, 102:7960–7970, 1998.

[35] M. Inokuti and F. Hirayama. Influence of energy transfer by the exchange mechanism on donor luminescene. *J. Chem. Phys.*, 43:1978–1989, 1965.

[36] F. Drolet and G. H. Fredrickson. Combinatorial screening of complex block copolymer assembly with self-consistent field theory. *Phys. Rev. Lett.*, 83:4317–4320, 1999.

Appendix A

Program Listing

```
/*

  Copolymer-homopolymer blends

  Assumes homopolymer and block A are same species

*/

#include <stdio.h>
#include <io.h>
#include <fcntl.h>
#include <sys\stat.h>
#include <math.h>

// Constants

#define GRID 101        // Number of spacial steps for all functions
#define STEPS 41        // Number of time steps to record in diffusion solution
#define FINE_STEPS 10   // Number of sub-steps in time for diffusion solver

#define pi 3.14159265358979

// Dependent constants

#define R_END (GRID-1.)
#define T_END (STEPS-1)

// Variables

double phiA0,           // mean block A density
       phiB0,           // mean block B density
```

```
        phiH0,          // mean homopolymer density
        phiC0,          // mean copolymer density
        fA,             // block A copolymer fraction
        fB,             // block B copolymer fraction
        fH,             // homopolymer-to-copolymer volume ratio
        chirc,          // interaction coefficient
        epsilon,        // coil parameter
        beta,           // Diffusion parameter
        energy,         // Free energy
        lastEnergy,     // Previous free energy for comparison
        R,              // Initial lattice parameter
        Rstep,          // Lattice parameter step
        Rres;           // Smallest order of lattice parameter step

double phiA[GRID],      // block A density profile
        phiB[GRID],     // block B density profile
        phiH[GRID],     // homopolymer density profile
        omegaA[GRID],   // block A potential
        omegaB[GRID],   // block B potential
        newA[GRID],     // new block A potential
        newB[GRID],     // new block B potential
        qA[GRID][STEPS], // block A propagator
        qB[GRID][STEPS], // block B propagator
        qH[GRID][STEPS], // homopolymer propagator
        qAp[GRID][STEPS],// block A reverse propagator
        qBp[GRID][STEPS],// block B reverse propagator
        alpha[GRID],    // integrator (d3r = dr, 2*pi*r*dr, or 4*pi*r*r*dr)
        QC,             // copolymer modes
        QH,             // homopolymer modes
        conv,           // target self-consistent error limit
        error,          // current self-consistent error limit
        ratio,          // Used to extrapolate next trial potential
        x, y;           // generic variable

int preload,            // non-zero if potentials preloaded
    core,               // +1 if A in core, -1 if B in core
    dim,                // dimensions
    iterations,         // number of iterations before aborting
    count,              // counts iterations on this pass
```

```
    found_bottom = 0,   // goes true when energy went down after a step
    first_pass = 1,     // goes false when one data point collected
    reset = 1,          // non-zero to restore defaults
    i, j, k, l,         // generic variables
    last;               // record # of next entry to process in params.dat

char entry[5],          // Number for this data set
     prefile[5],        // Number of file containing first-guess potential
     file[256];         // Temp string for building file names

// Math operation macros

#define VECTOR(x) for (i = 0; i < GRID; i++) {x};

#define INTEGRATE_R(x, y) \
    i = 0; x = (y)*17./48.*alpha[0]; \
    i = 1; x += (y)*59./48.*alpha[1]; \
    i = 2; x += (y)*43./48.*alpha[2]; \
    i = 3; x += (y)*49./48.*alpha[3]; \
    for (i = 4; i < GRID - 4; i++) x += (y)*alpha[i]; \
    i = GRID - 4; x += (y)*49./48.*alpha[GRID - 4]; \
    i = GRID - 3; x += (y)*43./48.*alpha[GRID - 3]; \
    i = GRID - 2; x += (y)*59./48.*alpha[GRID - 2]; \
    i = GRID - 1; x += (y)*17./48.*alpha[GRID - 1];

#define INTEGRATE_T(x, y) \
    j = 0; x = (y)*17./48./T_END; \
    j = 1; x += (y)*59./48./T_END; \
    j = 2; x += (y)*43./48./T_END; \
    j = 3; x += (y)*49./48./T_END; \
    for (j = 4; j < STEPS - 4; j++) x += (y)/T_END; \
    j = STEPS - 4; x += (y)*49./48./T_END; \
    j = STEPS - 3; x += (y)*43./48./T_END; \
    j = STEPS - 2; x += (y)*59./48./T_END; \
    j = STEPS - 1; x += (y)*17./48./T_END;

// Math operation functions

void Diffusion(double q[GRID][STEPS], double, double *, double);
```

```
void Oracle(void);

// File I/O functions

int OpenParameters(void);
void CloseParameters(void);
int GetParameters(void);
void WriteData(void);

// Program

void main(void) {
    int handle, file_action;
    char output[256];

    OpenParameters();

    while (1) {

        // Load fundamental parameters:
        //   fA, phiC0, chirc, epsilon, R, core, preload, conv, iterations, Rstep
        //   Rres, ratio;
        while ((i = GetParameters()) == 2); // find next unlocked data set
        if (!i) {
            CloseParameters();
            return;
        }

        // Initialise

        lastEnergy = 0;
        first_pass = 1;
        found_bottom = 0;

        // Calculate frequently-used constants

        fB = 1. - fA;
        phiA0 = fA*phiC0;
        phiB0 = fB*phiC0;
```

```
        phiH0 = 1. - phiC0;

        // If were not preloading the potential, calculate one for a starting point

        if (!preload) {
            VECTOR(
                phiA[i] = phiA0*(1+core*cos(i*pi/R_END));
                phiB[i] = phiB0*(1-core*cos(i*pi/R_END));
                phiH[i] = phiH0;
                omegaA[i] = chirc*(phiB[i] - phiB0);
                omegaB[i] = chirc*(phiA[i] - phiA0);
            );
        } else {
            sprintf(file, "data\\omeg%s.dat", prefile);
            handle = open(file, O_BINARY|O_RDONLY);
            read(handle, omegaA, sizeof(omegaA));
            read(handle, omegaB, sizeof(omegaB));
            close(handle);
        }

        // First write to ENER????.DAT file should clear file

        file_action = O_TRUNC;

        // Initialise t=0 step of qA, qB, and qH

        VECTOR(
            qA[i][0] = 1.;
            qB[i][0] = 1.;
            qH[i][0] = 1.;
        )

        // Initialise integrator

        switch (dim) {
default:
            VECTOR(
                alpha[i] = 1./R_END;
            )
```

```
    break;
case 2:
    x = 2./R_END/R_END;
    VECTOR(
        alpha[i] = x*i;
    )
    break;
case 3:
    x = 3./R_END/R_END/R_END;
    VECTOR(
        alpha[i] = x*i*i;
    )
    break;
}

// Loop until minimum found

lastEnergy = 0;
while (!found_bottom || Rstep > Rres || -Rstep > Rres) {

    // Loop until self-consistent error is within tolerence

    count = iterations;
    error = conv;
    while (error >= conv && --count) {

        // Solve diffusion equations for forward propagators

        beta = 1./(6.*R*R);
        Diffusion(qA, beta, omegaA, fA);
        Diffusion(qB, beta*epsilon, omegaB, fB);
        Diffusion(qH, beta, omegaA, fH);

        // Set initial conditions for reverse propagator

        VECTOR(
            qAp[i][0] = qB[i][T_END];
            qBp[i][0] = qA[i][T_END];
        );
```

```
// Solve diffusion equation for reverse propagators

Diffusion(qAp, beta, omegaA, fA);
Diffusion(qBp, beta*epsilon, omegaB, fB);

// Calculate normalisation constants

INTEGRATE_R(QC, qA[i][T_END]*qB[i][T_END]);
INTEGRATE_R(QH, qH[i][T_END]);

// Calculate density profiles

VECTOR(
    INTEGRATE_T(phiA[i], qA[i][j]*qAp[i][T_END-j]);
    INTEGRATE_T(phiB[i], qB[i][j]*qBp[i][T_END-j]);
    INTEGRATE_T(phiH[i], qH[i][j]*qH[i][T_END-j]);
    phiA[i] *= phiA0/QC;
    phiB[i] *= phiB0/QC;
    phiH[i] *= phiH0/QH;
);

// Potentials

y = phiA0 + phiH0;

VECTOR(
    x = (omegaA[i] + omegaB[i]) / 2;
    newA[i] = chirc*(phiB[i] - phiB0) + x;
    newB[i] = chirc*(phiA[i] + phiH[i] - y) + x;
);

// Calculate error from last iteration

error = 0.;
VECTOR(
    x = newA[i] - omegaA[i];
    if (x < 0) x = -x;
    if (x > error) error = x;
```

```
        x = newB[i] - omegaB[i];
        if (x < 0) x = -x;
        if (x > error) error = x;
    );

    printf("Iteration #%d: error = %f   \x0D", iterations-count, error);

    // Calculate new potential

    Oracle();
}

// Calculate free energy

INTEGRATE_R(energy, (phiA[i]+phiH[i])*(chirc*phiB[i] - omegaA[i])
    - omegaB[i]*phiB[i]);
energy -= chirc*(phiA0+phiH0)*phiB0 + phiC0*log(QC) + phiH0*log(QH)/fH;

// Determine next step direction

if (energy > lastEnergy) {
    // If we've already passed bottom, go finer
    if (found_bottom) Rstep /= 10;
    // Reverse direction and try again
    Rstep = -Rstep;
} else {
    WriteData();
    // If energy going down after two samples, we're on its trail...
    if (!first_pass) found_bottom = 1;
}

// Add entry to energy vs. repeat distance log

if (count) {
    sprintf(output, "%f\t%f\n", R, energy);
} else {
    sprintf(output, "%f\t%f\tFAILED\t%f\n", R, energy, error);
}
```

```
            for (i = 0; output[i]; i++);
            sprintf(file, "data\\ener%s.dat", entry);
            handle = open(file, O_CREAT|O_RDWR|file_action, S_IWRITE|S_IREAD);
            write(handle, output, i);
            close(handle);

            // Subsequent writes to ENER????.DAT will append to file
            file_action = O_APPEND;

            R += Rstep;
            first_pass = 0;
            lastEnergy = energy;
        }
        printf("                                                                    \n");
    }
}

// Solve diffusion equation

void Diffusion (double q[GRID][STEPS], double D, double *w, double z) {
    double dt, f, g, g0, tf, b1[GRID], b2[GRID], a, b, c, d, r[GRID], a2[GRID],
           sp[GRID], sq[GRID];
    int l;

    dt=z/T_END/FINE_STEPS;
    f = D*dt/2.*R_END*R_END;
    g0 = f/2.*(dim-1);
    tf = 2.*f+dt*w[0]/2.;
    b2[0] = (tf-1.)/f;
    b1[0] = -(tf+1.)/f;
    c = 2.;
    r[0] = q[0][0];

// Decomposition of tridiagonal matrix

    for (i = 1; i < GRID; i++) {
        r[i] = q[i][0];
        g = g0/i;
        a = (f-g)/(f+g);
```

```
        a2[i] = a;
        sp[i] = c/b1[i-1];
        tf = 2.*f+dt*w[i]/2.;
        b = -(tf+1.)/(f+g);
        b1[i] = b-a*sp[i];
        b2[i] = (tf - 1.)/(f+g);
        c = 1.;
    }

// Correct final coefficient for boundary conditions
// (c=2 corrects initial point as a2(1)+1=2)

    a2[GRID-1] += 1;
    b1[GRID-1] -= sp[GRID-1];

// Time step loop: forward substitution

    for (j = 1; j < STEPS; j++) {
        for (l = 0; l < FINE_STEPS; l++) {
            sq[0] = (r[0]*b2[0]-2*r[1])/b1[0];
            for (i = 1; i < GRID-1; i++) {
                d = -a2[i]*r[i-1]+b2[i]*r[i]-r[i+1];
                sq[i] = (d-a2[i]*sq[i-1])/b1[i];
            }
            r[GRID-1] = (r[GRID-1]*b2[GRID-1] -
                a2[GRID-1]*(r[GRID-2]+sq[GRID-2]))/b1[GRID-1];


// Back substitution

            for (i = GRID-2; i >=0 ; i--) r[i] = sq[i] - sp[i+1]*r[i+1];
        }
        for (i = 0; i < GRID; i++) q[i][j] = r[i];
    }
}

// Extrapolate next potential

void Oracle(void) {
```

```
    for (i = 0; i < GRID; i++) {
        omegaA[i] += (newA[i] - omegaA[i]) * ratio;
        omegaB[i] += (newB[i] - omegaB[i]) * ratio;
    }
    return;
}

// Platform-specific file I/O

int phandle;                    // Handle for params.dat file when open

struct {                        // Record structure
    long dim;
    double fA;
    double fH;
    double phiC0;
    double chirc;
    double epsilon;
    double R;
    long core;
    long preload;
    char prefile[4];
    double conv;
    double Rstep;
    double Rres;
    double ratio;
    long iterations;
    char note[10];
} rec;

#define RECORD_SIZE sizeof(rec)

// Opens params.dat file and set start position according to last_set.dat

// If you want to use your own method of inputing parameters, simply insert a
// "return 1;" at the top of this function and modify GetParameters according
// to your needs

int OpenParameters(void) {
```

```
    int handle2, x;

    entry[0] = '0';
    entry[1] = '0';
    entry[2] = '0';
    entry[3] = '0' - 1;

    phandle = open("data\\params.dat", O_RDONLY|O_BINARY);
    // If file couldn't be opened, return
    if (phandle == -1) return 0;

    // See if we're starting other than at the first file set
    handle2 = open("data\\last_set.dat", O_RDONLY|O_BINARY);
    if (handle2 == -1) return 1;

    // Starting at other than beginning, so read position and move there
    read(handle2, &last, sizeof(last));
    lseek(phandle, RECORD_SIZE*last, 0);

    x = last;
    entry[3] += x % 10;
    x /= 10;
    entry[2] += x % 10;
    x /= 10;
    entry[1] += x % 10;
    x /= 10;
    entry[0] += x % 10;

    return 1;
}

// Close params.dat and update last_set.dat

void CloseParameters(void) {
    if (phandle == -1) return;
    close(phandle);
}

// Read a parameter set from the file and advance
```

```
// If you want to use your own method of inputting data, rewrite GetParameters
// to load up the "rec" structure yourself.  GetParameters should return a 1
// if a parameter set is available, 0 to exit the program, or a 2 to have the
// program discard the data set returned by GetParameters and then call
// GetParameters again for another one.

int GetParameters(void) {
    int handle;

    // Update last data set processed

    handle = open("data\\last_set.dat", O_RDWR|O_BINARY|O_CREAT|O_TRUNC,
        S_IREAD|S_IWRITE);
    write(handle, &last, sizeof(last));
    close(handle);

    // Advance entry pointers (better not go beyond 10000 files!)

    entry[3]++;
    if (entry[3] > '9') {
        entry[2]++;
        entry[3] = '0';
    }
    if (entry[2] > '9') {
        entry[1]++;
        entry[2] = '0';
    }
    if (entry[1] > '9') {
        entry[0]++;
        entry[1] = '0';
    }

    // If there was an error opening, return
    if (phandle == -1) return 0;

    // Read data if any left
    if (!read(phandle, &rec, sizeof(rec))) return 0;
```

```
    // Set parameters
    dim = rec.dim;
    fA = rec.fA;
    fH = rec.fH;
    phiC0 = rec.phiC0;
    chirc = rec.chirc;
    epsilon = rec.epsilon;
    R = rec.R;
    core = rec.core;
    preload = rec.preload;
    prefile[0] = rec.prefile[0];
    prefile[1] = rec.prefile[1];
    prefile[2] = rec.prefile[2];
    prefile[3] = rec.prefile[3];
    conv = rec.conv;
    Rstep = rec.Rstep;
    Rres = rec.Rres;
    ratio = rec.ratio;
    iterations = rec.iterations;

    last++;

    // If this one has the "locked" bit set, return the skip flag
    if (rec.note[0] & 128) return 2;

    printf("Data set %04d:\n", last-1);
    printf("  dim = %d, fA = %f, fH = %f,\n", dim, fA, fH);
    printf("  phiC0 = %f, chirc = %f, epsilon = %f\n", phiC0, chirc, epsilon);
    printf("\n");

    return 1;
}

void WriteData(void) {
    int handle;
    char output[256];

    if (count) {
        printf("R = %f, energy = %f, iterations = %d\n", R, energy, iterations - count);
```

```
    } else {
        printf("R = %f, energy = %f, CONVERGENCE FAILED! (error=%f)\n", R, energy, error);
    }

    sprintf(file, "data\\dens%s.dat", entry);
    handle = open(file, O_CREAT|O_TRUNC|O_RDWR, S_IWRITE|S_IREAD);
    VECTOR(
        sprintf(output, "%f\t%f\t%f\t%f\n", phiA[i], phiB[i], phiH[i], qA[i][T_END]*qB[i][T_END]/QC);
        for (j = 0; output[j]; j++);
        write(handle, output, j);
    );
    close(handle);

    sprintf(file, "data\\omeg%s.dat", entry);
    handle = open(file, O_CREAT|O_TRUNC|O_RDWR|O_BINARY, S_IWRITE|S_IREAD);
    write(handle, omegaA, sizeof(omegaA));
    write(handle, omegaB, sizeof(omegaB));
    close(handle);
}
```